Dissertation
submitted to the
Combined Faculties for the Natural Sciences
and for Mathematics
of the
Ruperto-Carola University of Heidelberg, Germany
for the degree of
Doctor of Natural Sciences

presented by

Dipl.-Phys. Kai Schwenzer
born in Heilbronn, Germany

Oral examination: 29.10.2003

Ground state and thermal dynamics of strong interaction

Referees: Prof. Dr. Hans-Jürgen Pirner
Dr. habil. Jürgen Berges

Zusammenfassung

Grundzustand und thermische Dynamik der starken Wechselwirkung

Wir untersuchen den Grundzustand der starken Wechselwirkung wie auch ihr Verhalten bei endlicher Temperatur und Dichte innerhalb einer effektiven Niederenergie-Beschreibung. Dies geschieht mittels einer lokalen, chiralen 4-Fermion Wechselwirkung beschrieben durch das Nambu−Jona-Lasinio Modell bei einer Skala von etwa 1 GeV. Um die nichtperturbative Dynamik zu behandeln, stellen wir Renormierungsgruppen-Flussgleichungen in nächstführender Ordnung in der Ableitungsentwicklung auf, die über die führenden Kopplungen hinausgehen und die volle bosonische Feldabhängigkeit der Flußvariablen berücksichtigen. Wir untersuchen diese Flußgleichungen sowohl in ihrer allgemeinen Form, die Korrekturen in $1/N_c$ beinhaltet, als auch in der Näherung einer großen Anzahl von Farbfreiheitsgraden N_c, um eine Verbindung zu bisherigen Arbeiten herzustellen. Als Anwendung des Modells im Vakuumsektor berechnen wir das Spektrum des Diracoperators. Unter Verwendung der Flußgleichungen bei endlicher Temperatur und Dichte untersuchen wir das chirale Phasendiagramm und die Zustandsgleichung der Quarkmaterie und vergleichen unsere Ergebnisse mit Gittersimulationen. Weiterhin diskutieren wir die dem Renormierungsgruppen Formalismus inhärente Skalenabhängigkeit im Kontext einer skalenabhängigen Quarkmasse die aus Gitterresultaten für Stom-Strom-Korrelatoren abgeleitet wird.

Abstract

Groundstate and thermal dynamics of strong interaction

We analyze both the groundstate of strong interaction and its behavior at finite temperature and density within an effective low-energy description of strong interaction. This is done in terms of quarks which interact by a local chiral four-fermion NJL-interaction at a scale of order 1 GeV. To address the non-perturbative dynamics, we derive renormalization group flow equations in next to leading order in the derivative expansion that go beyond the leading renormalizable couplings and include the entire bosonic field dependence. We examine these flow equations both in there general form that includes corrections in $1/N_c$ and in large N_c approximation in order to make contact to previous work on the NJL-model. As an application of the model in the vacuum sector, we compute the spectrum of the Dirac operator. The flow equations are generalized to finite temperatures and densities via the Matsubara formalism. Within this scheme, we analyze the chiral phase diagram and the equation of state of quark matter and compare our results to recent lattice simulations. In addition we study the scale dependence inherent in the RG method in the different context of scale dependent quark masses derived from lattice results on current-current correlators.

Contents

Chapter 1

Introduction

The quest for understanding the structure of matter in nature has been one of the great challenges of natural philosophy since its beginning. It has invoked various different pictures with growing degree of refinement - especially since it has been addressed by physics in a scientific manner. By the middle of the last century it became clear that the main characteristics which identify matter cannot be ascribed to an enduring, massive entity but originate from a dynamic, interacting process. Even beyond, all this dynamics is already present in vacuum, since due to the relativistic quantum nature of our world virtual particles are created and destroyed continuously. This is pictured by Feynman's path integral description where all processes that are allowed within a given theory indeed contribute simultaneously to the values of physical observables. From this point of view matter is merely given the role of slight disturbances in a brewing vacuum, caused by particles with a tiny but conserved[1] quantum number - the baryon number.

The respective interaction which causes all this dynamics is aptly named *strong interaction*. There is a wealth of evidence that the rich variety of physics governed by strong interaction ranging from elementary particles and nuclei to objects as large as neutron stars is described by the surprisingly simple Lagrangian of *quantum chromodynamics* (QCD) in terms of a non-Abelian gauge symmetry. Despite the large number of phenomena described, QCD is somewhat intransparent. First of all, the elementary *quarks and gluons* which appear in the QCD action and carry the *color* gauge charge are not observed at all as asymptotic states in nature, but color is *confined* to the interior of composite, colorless excitations named *hadrons*. Secondly, there is a mass gap in the particle spectrum, nearly all of these hadronic excitations have very large masses compared to the primary degrees of freedom of QCD. In addition there are also no indications of a parity degeneracy of hadron spectra as required by another approximate symmetry of the massless QCD action - the *chiral symmetry*. This can

[1] However, according to the current physical picture there are baryon number violating processes that created the matter surrounding us within a highly non-equilibrium state in the early universe.

be explained if one assumes that chiral symmetry is broken dynamically in the ground state, leaving the light hadrons as approximate Goldstone bosons and giving the other hadrons large dynamically generated masses.

Unfortunately, none of these basic properties of the complicated ground state of strong interaction - namely dynamical chiral symmetry breaking and confinement - has been entirely understood so far from the point of view of the primary underlying dynamics. Accordingly, QCD hardly would have become the generally accepted theory of strong interaction without another crucial ingredient - its *asymptotic freedom*. At large momentum scales the gauge coupling becomes small and permits a perturbative expansion which enabled to compute rates and cross sections for a huge variety of processes in favorably agreement with the experimental results gathered in accelerator experiments around the world over the last decades[2]. Furthermore, the advent of sufficiently fast computers over the last years has enabled first principle computations even at low energies by direct solution of the discretized QCD action on finite lattices. Despite various problems and limitations these simulations qualitatively approved the above picture and could in some cases even make quantitative contact to experimental observations. Nevertheless, the lattice method has equally failed so far in one crucial point: to extract out of the complicated dynamics a simplified dynamical mechanism for the two basic properties of strong interaction.

A transparent method to account for strong dynamics is the *renormalization group*. It is a very successful tool to include quantum fluctuations by exploiting the self-similar nature of all possible processes in order to integrate fluctuations on different scales one after the other. A discretized version of the renormalization group idea could be visualized by a jigsaw in which small pieces are combined by simple rules to larger pieces that are the building blocks at an even larger scale, until finally the whole picture emerges. The main difficulty in integrating out these quantum fluctuations is that they are coupled on all scales. Inherently, the renormalization group method directly includes the effect of fluctuations on small spatial scales into fluctuations on larger scales. In contrast, the influence of large scale fluctuations on smaller ones[3] is encoded in the momentum dependence of physical couplings which is by far harder to capture. Though, in strong coupling theories like QCD, this momentum dependence becomes important, as it induces *collective behavior* by which whole lumps of primary particles can propagate collectively and transport conserved quantum numbers. The renormalization group forms a framework in which such collective excitations can arise or freeze out again during the integration process.

It is known experimentally that the color charge is confined to small spatial regions of the order 1 fm, forming the observed collective hadronic states. Thereby the approximately *natural*, i.e. scale-free[4] theory of QCD has to generate dynamically a momentum scale $\Lambda_{QCD} \approx$ 200 MeV. Just this scale is indeed signalized in QCD by the divergence of its running coupling α_s within a perturbative renormalization group treatment. However, this result only shows that the colored degrees of freedom become inappropriate to describe the system effectively

[2]The fact that what is finally observed in the detectors are still hadronic excitations or their decay products, nevertheless, dramatically complicates the respective analyses. However, there are many reactions and measuring quantities that do not depend on the details of the complicated hadronization process.

[3]In the jigsaw picture this would be the unaccustomed influence of the placement of the pieces on large scales on the form of these pieces - or even more visual, the pieces themselves are changed in order to make the jigsaw "fit" on large scales.

[4]Actually, QCD involves explicit quark masses which, however, have only small impact on the ground state and the low-energy spectrum of the theory.

at lower scales, since they involve too complicated dynamics - but unfortunately, it neither gives any hint on the effective degrees of freedom at low energies nor on how they arise as collective states out of the underlying dynamics.

However, indications for the nature of the effective low-energy dynamics arise from less rigorous approaches. First of all, in a quasi-classical approximation of the gauge dynamics one finds that the dynamics is dominantly mediated by topological *instanton* excitations. At low energies, they couple the matter fields in a chirality breaking local interaction that involves all fermion species present in the theory. Furthermore, the integration of quantum fluctuations in QCD down to some scale of the order 1 GeV via renormalization group methods should result in an effective theory containing respective fermionic interaction terms. The simplest form of such a purely fermionic interaction in accordance with the symmetries is described by the Nambu−Jona-Lasinio model which will be discussed in this work. In the discussed context, the aim is especially to examine to what extent such a simplified description can account for bulk properties of the groundstate of strong interaction if the dynamics is covered adequately.

Since the ground state of strong interaction is such intricate, it would surely be most welcome to be able to examine its form in a more simplified setting where the interaction is weaker and the fundamental degrees of freedom are allowed to propagate over larger distances - or even to be able to observe the transition to such a state by changing some bulk property of the system. Fortunately, in theory there are indeed parameters that allow to do this, namely the *temperature* and the *density* of an equilibrium system. As can be inferred directly from the QCD action, at asymptotically large temperature the system should be in a plasma phase where both confinement is absent and chiral symmetry is restored[5]. According to the current cosmological picture of a hot big bang such a plasma phase was present in the first microsecond - but probably never since, because all presently known astrophysical processes can account for not a quarter the required energy densities. From various different approaches including semi-perturbative QCD, lattice QCD, random matrix theory, chiral perturbation theory and effective models it is known that in the idealized case of massless quarks the respective phase transition occurs at the huge temperature $T_c \approx 160$ MeV. However, in nature with massive quarks a mere crossover is more likely (cf. Fig. 1.1).

Whereas under normal conditions matter stabilizes in the already rather dense form of nuclei, at even higher baryon density further unaccustomed states of matter are expected. Compared to ordinary quark matter where the quarks form a Fermi sea, the slightest attractive interaction can destabilize this Fermi sea at sufficiently high densities and lead to a color superconducting state of matter. According to the current physical picture which is much less assured at finite density due to difficulties of lattice simulations caused by a complex measure which prevents a direct probabilistic treatment, there is a first order phase transition from ordinary matter to a state with a restored chiral symmetry[6]. Due to the complex non-perturbative interaction there is a whole range of possible phases at high density which include color flavor locking, disoriented chiral condensates or even the formation of crystalline structures. According to the phase structure at either finite temperature or finite density only, in the regime where both temperature and density are present, there should be a critical

[5]Naively, this follows from the fact that the mean momentum scale in the system is large and thereby the coupling becomes weak due to the asymptotic freedom of QCD.

[6]However, at very high densities chiral symmetry may be broken again by a locking of color and flavor degrees of freedom.

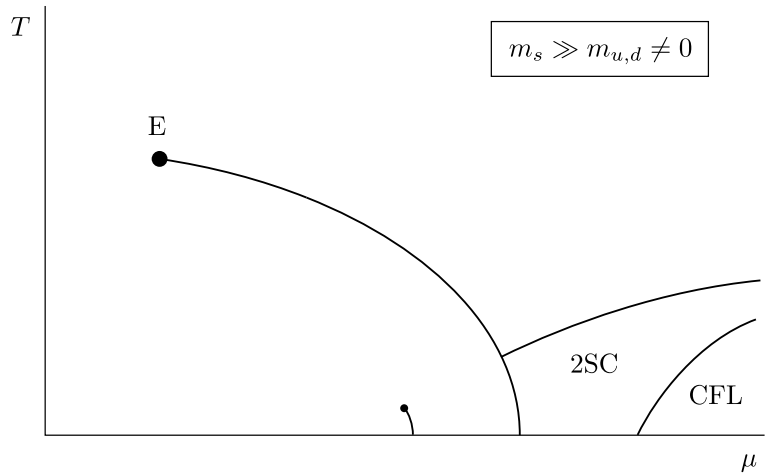

Figure 1.1: The current picture on the phase diagram of strong interaction in a schematic form taken from [1].

point in the phase diagram where large fluctuations are present and which probably could be detected in an experimental analysis.

As a matter of course, experimentally it is neither possible to statically heat or compress a considered system nor to observe the produced state directly. Instead, the only way to deposit the necessary enormous amount of energy in a sufficiently small volume is the collision of relativistic heavy ions. This results in a gigantic explosion where the system goes through various complicated non-perturbative stages far from equilibrium and produces hundreds to thousands of hadronic particles in the final state. Therefore, to analyze such a reaction in order to trace back the properties of the initial state is similarly complicated and indirect as the nontrivial ground state itself (cf. Fig. 1.2).

This explains why despite the extensive search at several facilities - most prominently the Super Proton Synchrotron (SPS) - and various proposed signatures no fully conclusive sign for a new phase of matter has been found so far. However, there are other promising facilities like the currently running Relativistic Heavy Ion Collider (RHIC) in Brookhaven, the forthcoming Large Hadron Collider (LHC) at CERN in Geneva and the planned upgrade of the accelerator of the Gesellschaft für Schwerionenforschung (GSI) in Darmstadt. The first two machines operate at very high energies of the order of several hundred GeV per nucleon and should produce a hot but rather dilute plasma, whereas the latter will operate at lower energies but high luminosity and therefore would allow to study the interesting case of cold dense matter. Additional information on dense matter can also be obtained from astrophysical observations of compact stars whose core densities could exceed those of atomic nuclei by a multiple.

Although the experimentally accessible system is nonuniform and far from equilibrium, the desired new phases of matter are just described by a uniform thermal system. Furthermore, a homogeneous system is all that can be analyzed in an approximately realistic way so far. But even beyond that there are serious indications that the system could be at least partially thermalized[7]. On the basis of this incentive, in this work the behavior of strong interaction at

[7]In particular, such a thermal system could be present in a local co-moving frame.

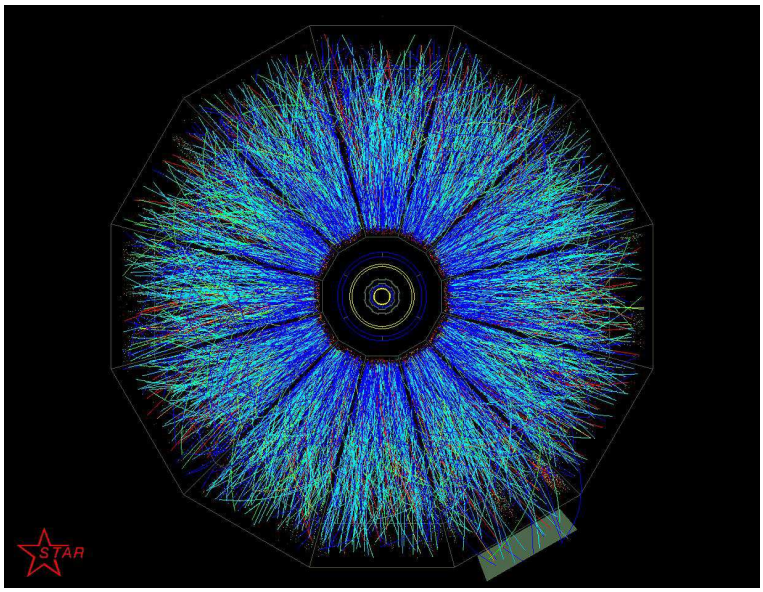

Figure 1.2: Exemplary picture of an Au-Au-collision at 100 GeV/A from the tracking chamber of the STAR detector at the RHIC collider.

finite temperature and baryon density is analyzed within the same model as its groundstate. This is achieved by taking into account both quantum and thermal fluctuations within the same renormalization group scheme. Within this framework, various thermal aspects as the phase structure and the equation of state are examined.

Overview

The second introductory chapter motivates the work in the subsequent chapters. It presents the basic formalism and techniques used in a coherent way in order to resort to it in the remainder of the work. It focuses on the effective field theory method within the framework of the renormalization group to describe the low energy behavior of strong interaction both in vacuum and at finite temperature and density.

The third chapter covers the ground state properties of strong interaction. One of the main results of this work is the effective action for the generalized linear σ-model that includes arbitrarily many couplings and derivative couplings by an extension of the Yukawa coupling and of the wave function renormalization factors of the standard linear σ-model to field dependent quantities analogous to its bosonic potential. This generalized effective action is subsequently used to derive renormalization group improved flow equations for the NJL model in next to leading order in the derivative expansion within the proper time scheme. Thereby, the individual contributions in these flow equations can be uniquely attributed to generating 1-loop Feynman diagrams which themselves represent infinitely many diagrams. Further the connection to the standard self-consistent approach of the NJL model is discussed and it is shown that it is equivalent to the renormalization group approach in the large N_c limit.

Due to the inclusion of the full field dependence and the leading momentum dependence the approximation is capable to describe the non-perturbative behavior of the theory. This is demonstrated by the analysis of various vacuum properties which agree with bulk properties of the strong interaction ground state in nature. It confirms the main results obtained in the large N_c approximation and improves the response of the system to an explicit chiral symmetry breaking by a finite current quark mass. The chapter is closed by an analysis of the spectrum of the Dirac operator which generalizes previous results at small eigenvalues to higher scales and recovers level repulsion as the dominating feature in this regime.

Chapter four discusses thermal aspects of strong interaction. For this task a thermal flow equation is derived in local potential approximation which is characterized by its simple analytic form. This is possible due to the introduction of a different set of cutoff functions than in previous analyses. Again, the large N_c limit provides the simplest possible solution scheme and yields an analytic solution at vanishing temperature and finite density. Within the large N_c approximation scheme the equation of state and the phase diagram are computed and are compared to previous analyses. In addition the change of the equation of state with chemical potential is examined which has been considered in lattice simulations, recently. The inclusion of mesonic dynamics is so far considered in the local potential approximation. Thereby, the pionic fluctuations enhance the low temperature region of the equation of state, whereas the high temperature region can be included by a free gas of quarks and gluons. Furthermore, the phase diagram is examined in the renormalization group scheme and gives so far a description at finite temperature and moderate densities.

In order explore the feasibility of exploiting the scale structure inherent in the renormalization group flow, the momentum dependence of correlation functions is studied in Chapter five. In particular it is examined to what extend the momentum dependence can be parametrized within an momentum dependent quark mass. Therefore, data on current-current-correlation functions in different mesonic channels obtained in lattice simulations is analyzed in order to extract the momentum dependence of the quark mass.

Chapter 2

Effective field theory and the renormalization group

2.1 Symmetries of strong interaction

Symmetries play a central role in physics since they encode the physical principles which are abstracted from nature and are required for a theory in order to describe physics. Moreover, at the classical level physical theories are often uniquely described by their symmetry structure[1], and its elementary excitations are given as representations of the respective symmetry group. At the quantum level, however, the situation is much more intricate, since symmetries can be broken by strong dynamics and totally different collective degrees of freedom can emerge. Nevertheless, the classical symmetries are important even in this case, since they provide the *maximal* Fock space, which is subsequently restricted by the dynamics and eventually cut down to some subspace that can be parametrized by another - possibly nonlinear - basis of excitations. Another crucial aspect of symmetries in physics is their direct connection to conserved quantities which are indispensable for any deterministic description of nature. In particular according to Noether's theorem, every unbroken, continuous symmetry provides a conserved current which guarantees the conservation of the associated charge.

At the bottom of any quantum field theory is the relativistic spacetime symmetry, which governs how particles propagate in space and time according to special relativity. The respective symmetry group is given by a $SL(2,\mathbb{C})/Z_2$ [2]. The generalized rotation group $SL(2,\mathbb{C})$ thereby reflects the indefinite metric of Minkowski space-time and contains as subgroups the

[1] This is mostly the case when the respective theories are simplified approximations of nature which only rely on basic physical principles, but does not hold e.g. for the standard model with its roughly 20 free parameters. Nevertheless, from a philosophic point of view this property is highly desirable for a unified theory of nature, since it guarantees that the respective theory relies only on rational physical principles, like the principle of relativity or the gauge principle.

boosts and the ordinary rotations. On the other hand, the Z_2 part of the factor group is of topological origin and it is effectively the reason that there is something as matter at all. It effects that the possible representations, which are specified by their internal spin degree of freedom, fall into two distinct classes with integer and half integer spin respectively. Together with the spin-statistic theorem, this simple fact yields for half integer spin particles all the familiar properties - like Pauli's exclusion principle and conserved quantum numbers - that characterize matter, whereas elementary particles of integer spin merely play the role of spurious exchange particles[2].

Since $SL(2,\mathbb{C})/Z_2$ is locally isomorphic to $SU(2)_L \otimes SU(2)_R$ the physical spectrum in field theory is given by representations (a,b), $2a, 2b \in \mathbb{N}$ of this group[3], with spin $s = a+b$. However, so far the important discrete symmetries of space inversion and time reversal have not been considered. Namely, the above free fields for massive particles change under space inversion $\mathcal{P}$ by an interchange of their components $\mathcal{P}(a,b) = (b,a)$. Therefore to construct a representation that transforms under the full Poincarè group one has to combine the above representations in the form $(a,b) \oplus (b,a)$. The observed particles in nature correspond to the lowest representations. According to the standard model of particle physics which includes QCD, there are only massive fermionic particles ψ which transform according to the Dirac representation $(\frac{1}{2},0) \oplus (0,\frac{1}{2})$, whereas the fundamental bosons A_μ are initially massless[4] and transform according to the vector representation $(\frac{1}{2},\frac{1}{2})$. Both of these representations of the Poincaré group have two internal degrees of freedom given by the spin in the massive and polarization in the massless case.

Since the self interactions of the matter fields are all non renormalizable and therefore not acceptable from the viewpoint of a fundamental theory[5] as discussed in Section 2.5, matter has to couple to bosonic fields. Because scalar fields are likewise inappropriate[6], the only possible renormalizable interaction is the coupling to a vector field A_μ in the representation $(\frac{1}{2},\frac{1}{2})$[7]. However, strictly speaking there is no quantum field, that transforms as a massless vector under Lorentz transformations. Nevertheless, a vector field gives rise to an anti-symmetric tensor quantum field of the form $F_{\mu\nu} = \partial_\mu A_\nu - \partial_\nu A_\mu$. Therefore, in the more general context of *gauge invariance* a Poincare invariant theory can be constructed which has an additional invariance under local coordinate transformations of both the fermionic and bosonic fields.

Generally these gauge transformations form a local $SU(N)$ symmetry group. Whereas in quantum electrodynamics (QED) the group which parametrizes the gauge freedom is just the minimal $U_E(1)$, in case of QCD the symmetry group is the non-Abelian $SU_C(3)$ color group. Quarks and gluons transform as a triplet and an octet [3] under $SU_C(3)$, i.e. the gluons themselves carry color charge and are subject to nonlinear self interactions. This is basically the reason why strong interaction is that strong, since the self interaction allows for pronounced non-uniformity in order to form very strong fields just in-between present

[2]Bosonic collective degrees of freedom on the other hand can very well carry conserved charges, like e.g. the charged currents in electroweak theory or mesonic excitations.

[3]This is still a space time symmetry and should not be confused with the internal chiral $SU_L(N_f) \otimes SU_R(N_f)$ flavor symmetries discussed in the following.

[4]Due to spontaneous symmetry breaking however the mediators of weak interaction acquire a mass.

[5]Or at least for a theory with a large range of applicability, i.e. a large cutoff. However. as an effective theory with a restricted range of applicability they are perfectly applicable, as will be exploited in this work.

[6]Unless they arise as Goldstone bosons, scalar fields are not prevented from acquiring a mass, which is not acceptable for a fundamental theory since it restricts its range of applicability.

[7]Compared to a spinor-tensor-interaction, this interaction has the advantage that it can describe long range interactions as found in nature.

charges. In addition, the gauge group $SU_C(3)$ has the center group Z_3, which is of special importance since it encodes the minimal gauge freedom and therefore the presence of this global symmetry can be exploited as a signature for confinement in pure gauge theory.

The existence of different colored fields grouped in $SU_C(3)$-multiplets does not follow from space-time symmetries but is an additional property that has not been explained so far from fundamental underlying principles. Moreover, it is known experimentally that the quarks come in six different flavors which behave equal under strong interaction but are strongly distinguished by their different masses[8] ranging from a few MeV to more than hundred GeV. This spoils the above picture of physics governed by symmetries and points out that something important is missing so far in the current description of nature.

Though, strong interaction is more symmetric, than the above analysis suggests. Just as the high momentum region of strong interaction can be described successfully in terms of colored degrees of freedom which are not directly observed experimentally, the low energy regime is successfully described by an additional chiral symmetry which is hidden and spontaneously broken in the ground state. The symmetry comes about if the current masses of the light quarks are small compared to the inherent scale of strong interaction, so that they can be approximately regarded as massless. This does not only imply that from the point of view of strong interaction they are invariant under flavor rotations, but also brings up an important difference in the Lorentz transformation property of massless and massive spin-$\frac{1}{2}$ fields. Massless matter fields ψ_L and ψ_R transform corresponding to the individual left- and right handed Weyl spinor representations $(\frac{1}{2},0)$ and $(0,\frac{1}{2})$ which do *not* mix under parity. Therefore in the limit of N_f massless quarks, the classical action is invariant under independent left- and right handed flavor rotations of the chiral symmetry group $U_L(N_f)\otimes U_R(N_f)$, which can be decomposed into $SU_L(N_f)\otimes SU_R(N_f)\otimes U_V(1)\otimes U_A(1)$[9].

Chiral symmetry is however multiply broken. First of all it is explicitly broken by the finite current quark masses[10], so the concept of chiral symmetry only makes sense for current quark masses $m_c < \Lambda_{QCD} \approx 200$ MeV, i.e. at most for three flavors and only at low energies $\lesssim 1$ GeV. Whereas the three flavor symmetry is rather strongly broken, the two flavor symmetry is only slightly affected by the quark masses and holds at the percent level. The spontaneous breaking of chiral symmetry reduces the symmetry of the ground state to the vector part $SU_V(N_f)$ of $SU_L(N_f)\otimes SU_R(N_f)$. Finally the axial $U_A(1)$ part of chiral symmetry is also broken by anomalous quantum processes. This manifests itself in the non-conservation of the axial vector current[11] [4]. To the present knowledge, the $U_V(1)$ part on the other hand remains unbroken and leads to baryon number conservation[12].

The above discussion is summarized in the Lagrangian of QCD with the approximate classical symmetry structure $SL(2,\mathbb{C})/Z_2\otimes Z_2\otimes SU_C(3)\otimes SU_L(N_f)\otimes SU_R(N_f)\otimes U_V(1)\otimes$

[8] In addition, they are also distinguished by the electroweak interaction, which however has hardly an influence on the properties of sub-nuclear strongly interacting systems due to its weakness.

[9] Thereby, the $SU_L(N_f)\otimes SU_R(N_f)$ part contains the electromagnetic local $U_E(1)$ symmetry if QED is additionally considered.

[10] Furthermore, the finite current quark masses also break the scale invariance of the theory, which gives rise to the trace anomaly of the energy momentum tensor.

[11] Still, it is an approximate symmetry as exploited in the theory of a partial conserved axial vector current (PCAC) [2].

[12] Although the vector current is protected against spontaneous symmetry breaking [5], an extremely small anomalous breaking is not fully ruled out yet [6].

$U_A(1)$, which reads in Minkowski space[13]

$$\mathcal{L}_{\text{QCD}} = \bar{q}(i\not{D} - m)q - \tfrac{1}{4}F^a_{\mu\nu}F^{a,\mu\nu} \,. \tag{2.1}$$

2.2 EFFECTIVE FIELD THEORY FOR CHIRAL SYMMETRY

Since the gluonic dynamics becomes too complicated at low energies, the predictive power of QCD is limited to the lattice method in this regime, which is only constrictive applicable. This arouses the need for an *effective field theory* that describes the same physical content within a mathematically manageable language. However, in this case it is just the absence of symmetry which provides such an effective field theory - more precisely the spontaneous breakdown of chiral symmetry in vacuum. According to Goldstone's theorem this implies for each broken global symmetry the existence of one massless boson of zero spin with the same parity as the current of the broken symmetry. Such (pseudo) Goldstone bosons are given by the extraordinary light pions in the case of the approximate chiral symmetry[14] for $N_f = 2$. These nearly massless excitations, totally dominate low energy processes and give rise to an effective description, since their dynamics is almost entirely determined by chiral symmetry, whose breakdown gave rise to them.

Therefore, it was known before the advent QCD, that low energy processes can be described, up to some low energy constants, by the concept of spontaneously broken chiral symmetry in terms of its group structure and the dominating Goldstone bosons. This was discovered first in the context of current algebra but was later conveniently formalized in the framework of effective field theory via the use of effective Lagrangians. In particular, this allowed a controlled expansion in external momenta and the current quark masses within *chiral perturbation theory*[15] [7] as the unique low energy effective field theory of strong interaction physics. Whereas to lowest order there are only two low energy constants, which are not provided by symmetry principles, namely the pion decay constant F and the chiral quark condensate, their number rises fast with the order of the chiral expansion.

Since in the groundstate of strong interaction, chiral symmetry is broken to its vector subgroup, it follows from group theoretical considerations, that the Goldstone boson fields are isomorphic to the factor group $(SU_L(N_f) \otimes SU_R(N_f))\,/SU_V(N_f)$ [8]. This defines the transformation properties of the Goldstone boson fields, which furnish a "nonlinear representation"[16] of chiral symmetry. In the case $N_f = 2$ discussed in this work, this representation can be parametrized by three bosonic fields in the form[17]

$$U(x) = \exp\left(\frac{i\vec{\tau}\cdot\vec{\phi}(x)}{F}\right) \,, \quad \text{where} \quad U(x) \to U'(x) = LU(x)R^\dagger \tag{2.2}$$

specifies the behavior under chiral transformations. The groundstate given by $\phi(x) = 0 \Leftrightarrow U(x) = \mathbb{I}$ is invariant under the $SU_V(2)$ subgroup only. Due to $UU^\dagger = \mathbb{I}$, the effective Lagrangian that can be built out of the fields U contains only derivative couplings or explicit symmetry breaking terms, as described by the nonlinear σ model.

[13] Here, the covariant derivative and the anti-symmetric field strength tensor are given by $\not{D} \equiv \gamma_\mu(\partial^\mu + igt^j A^j_\mu)$ and $F^a_{\mu\nu} \equiv \partial_\mu A^a_\nu - \partial_\nu A^a_\mu + f^{abc}A^b_\nu A^c_\mu$.

[14] Additional pseudo Goldstone bosons for $N_f = 3$ are the kaons, which are already rather heavy.

[15] An extensive introductory review is given in [8].

[16] From the mathematical point of view a representation is only defined to be linear.

[17] Here ϕ_i are the three Goldstone fields, τ_i are Pauli matrices and L/R are elements of $SU_{L/R}(2)$.

At energies much larger than the pion mass, the assumption that the pions are the only effective degrees of freedom looses its justification and chiral perturbation theory becomes inappropriate. In this regime also the quark dynamics contributes. However, the effect of the gauge degrees of freedom can approximately be absorbed into the dynamics of effective constituent quarks. Like the current quarks which appear in the action of QCD these quasi particles furnish a linear representation of chiral symmetry. In the case $N_f = 2$ the transformation property under independent left- and right-handed flavor rotations reads explicitly

$$q_{L/R} \to q'_{L/R} = \exp\left(-i\vec{\theta}_{L/R} \cdot \vec{\tau}\right) q_{L/R} \ , \tag{2.3}$$

where the chiral components of the Dirac spinor are given by $q_{L/R} \equiv (1 \mp \gamma_5)q$. In order to build an effective model[18] from these degrees of freedom, one has to consider bilinears to combine them to an effective Lagrangian. As can be seen from the above transformation properties, the minimal effective interaction which is invariant under chiral transformations is given by

$$(\bar{q}q)^2 + (\bar{q}i\gamma_5\vec{\tau}q)^2 \ . \tag{2.4}$$

Correspondingly, the simplest linear chiral representation of bosonic fields in the two flavor case, which can be invariantly coupled to the matter fields is given by four chiral fields in the combination $\Sigma = \sigma + i\vec{\pi} \cdot \vec{\tau}\gamma_5$. In order to be chiral invariant, all self interactions of these fields have to be constructed from the quantity $\Sigma\Sigma^\dagger = \sigma^2 + \vec{\pi}^2 \equiv \Phi^2$ where $\Phi = (\sigma, \vec{\pi})$. Consequently, a purely bosonic theory constructed out of these chiral fields depends only on the radial variable Φ^2 and is invariant under the rotation group $O(4)$, which is locally isomorphic to $SU_L(2) \otimes SU_R(2)$.

2.3 EUCLIDEAN AND THERMAL FIELD THEORY

The macroscopic world is entirely dominated by the distinction of space and time. Although both concepts have been combined in the formulation of relativity, their distinction is still prominently reflected in the indefinite metric of Minkowskian space. From the point of view of field theory, this distinction complicates the description dramatically since it involves the concept of causality, i.e. a deterministic connection between an initial state and some final configuration. However, as long as only "static" properties of the vacuum or some other system in equilibrium are regarded, the signalized role of time has no bearing. Instead such systems, are only the scene where time-depended, causal events can happen. Nevertheless, the knowledge about such systems is already a good deal in a relativistic quantum theory, since its properties can be altered dramatically compared to the classical situation by the incessant fluctuations of the system - which are not restricted by causality.

In this line of thought, the fundamental object in field theory, which contains all information about the dynamics of the system is the vacuum-vacuum amplitude

$$\mathcal{Z} = \langle 0| \, e^{-\frac{i}{\hbar}\int dt \int d^3x \, \mathcal{H}(\chi)} \, |0\rangle \ . \tag{2.5}$$

[18]This intermediate energy theory is less rigorous than the low energy description provided by chiral perturbation theory. However it can be set on a much firmer basis within the context of the renormalization group, as discussed in Section 2.5.

It can be probed by appropriate sources in order to compute from it any desired correlation function. Furthermore, it has an instructive path integral representation

$$\mathcal{Z} = \int_{\chi(t_i,\vec{x})=\chi_i(\vec{x})}^{\chi(t_f,\vec{x})=\chi_f(\vec{x})} D\chi \, \exp\left(i \int d^4x \, \mathcal{L}_M(\chi) \right) , \tag{2.6}$$

where the integral extends over field configurations[19] in Minkowski space. The weight factor is thereby a highly oscillating quantity, whose period is determined by the characteristic wavelength of the system - e.g. the de Broglie wavelength of the excitations for weakly coupled systems. This makes the evaluation of Eq. (2.6) a very complicated task for strongly coupled systems, where the path integral is not solely dominated by a saddle point[20].

On the other hand the thermodynamic grand canonical partition function for equilibrium systems is given by

$$Z = \mathrm{Tr}\, \mathrm{e}^{-\beta(H-\sum_i \mu_i N_i)} = \sum_r \langle r| \, \mathrm{e}^{-\beta(H-\sum_i \mu_i N_i)} \, |r\rangle \ , \tag{2.7}$$

where the sum over r extends over all possible states of the system. Due to the formal analogy of the weight factors in the two expressions Eqs. (2.5) and (2.7) it is possible to express the thermodynamic partition function in path integral form [9]. However, the "time" variable should be imaginary in this case in order to reproduce the minus sign in the exponent of Eq. (2.7). Furthermore the trace enforces the path integral to be periodic respectively anti-periodic in this Euclidean time variable corresponding to whether the integral extends over bosonic or fermionic fields[21]

$$Z = \int_{\chi(0,\vec{x})=\pm\chi(\beta,\vec{x})} D\chi \, \exp\left(- \int_0^\beta d\tau \int d^3x \, \left(\mathcal{L}_E(\chi) - \sum_i \mu_i n_i(\chi) \right) \right) . \tag{2.8}$$

The appearing functional $\mathcal{L}_E(\chi)$ is the Euclidean Lagrangian which directly follows from its Minkowski analog[22]. As in the Minkowski case, derivatives with respect to appropriately chosen currents yield all desired thermal correlation functions. Especially if one is able to solve the above functional integral[23] in the limit $T \to 0$ one obtains vacuum to vacuum amplitudes and therefore important non-perturbative information on the ground state of the theory. These correlation functions however include Euclidean fields and do not provide any information on causal time-evolution as for instance required for transition amplitudes and cross sections.

The above expression Eq. (2.8) is the basis of the lattice regularization approach [10] to field theory. By discretizing spacetime and representing the derivatives appearing in the Lagrangian by finite differences, it is possible to perform the integral by standard Monte

[19] Here, χ is an abbreviation that includes the complete field content of the considered theory.

[20] When a saddle point dominates, the contributions in the vicinity of the saddle point saturate the integral, since contributions from other paths interfere destructively and cancel. This corresponds to the classical solution of the problem described by the respective Euler-Lagrange equations.

[21] Here, the n_i denote the densities associated with the conserved charges N_i that are present in the system due to non vanishing chemical potentials μ_i.

[22] In the remainder of the work we will work in Euclidean space and will not show the index E explicitly.

[23] That means first of all to find an appropriate regularization scheme and a definition for the measure in order to give meaning to the diverging expression.

Carlo methods due to the exponential decay of the weight factor. Despite its various restrictions[24] this method provides a significant number of predictions[25], that mostly compare well with experiment. The realm of applicability ranges from vacuum properties like correlation functions [11], mass spectra or heavy quark potentials to thermal physics [12, 13, 14], which inherently forms the most direct area of application of the lattice method since it relies to a lesser extend on extrapolations.

2.4 Effective action and derivative expansion

The vacuum of a relativistic quantum theory is the crucial system that has to be determined and understood before any physical process can be analyzed. This is especially the case, when the groundstate is nontrivial due to the breakdown of classical symmetries, as it is the case in QCD. The only possible source of knowledge about the vacuum and likewise about thermal systems are correlation functions of appropriate operators. There is a certain class, namely local operators, which is of special importance in this respect, since they lend themselves to actual computations and provide a simple picture of the involved dynamics. Nevertheless, in strong coupling situations nonlocal operators can become increasingly important.

If one is interested in the vacuum state of a given theory, the partition function Z is not the ideal quantity to consider, even though it contains all possible dynamics - actually it contains more dynamics than necessary. This is the case since it includes contributions from disconnected quantum fluctuations that do not enter in physical correlation functions. Therefore, it is reasonable to consider instead of the generating functional of correlation functions $Z[J_\chi]$, depending on appropriate source terms J_χ for the occurring fields χ

$$Z[J_\chi] = \int D\chi \exp\left(-\int d^4x\,(\mathcal{L} - J_\chi\chi)\right)\,, \tag{2.9}$$

the generating functional W of connected correlation function

$$W[J_\chi] \equiv \log Z[J_\chi]\,, \tag{2.10}$$

which directly provides the necessary normalization. Variations with respect to the sources provide the desired correlation functions, and especially a single functional derivative yields an averaged (av) field configuration $\chi_{\text{av}}(x)$

$$\frac{\delta W[J_\chi]}{\delta J_\chi(x)} = \frac{\int D\chi\,\chi(x)\exp\left(-\int d^4x\,(\mathcal{L} - J_\chi\chi)\right)}{\int D\chi\exp\left(-\int d^4x\,(\mathcal{L} - J_\chi\chi)\right)} = \langle\Omega\,|\chi(x)|\,\Omega\rangle_J \equiv \chi_{\text{av}}(x)\,. \tag{2.11}$$

The fields $\chi_{\text{av}}(x)$ are intentionally denoted averaged fields, since the measure $D\chi$ has not been specified yet and one could define it to incorporate not all possible field configurations.

[24] The main problem for lattice gauge theory are still the limited computational resources. This restricts current simulations to rather small lattices and large quark masses. To make contact to physics, delicate extrapolations to the continuum limit and the chiral limit are necessary. There have been strong improvements on the theoretical side by the introduction of perfect actions [10] or domain-wall fermions [4]. Nevertheless, there are still situations, e.g. at finite baryon chemical potential, where lattice theory is not directly applicable.

[25] For instance the mass of the lightest particle within a given channel can be obtained from the decay behavior of the two-point function. This also provides a method to connect the inherently dimensionless lattice units to physical scales - typically by a computation of the ρ-mass, since the ρ-resonance largely dominates the vector channel.

Correspondingly the path integral would sum only over a part of the Fock space - this is one crucial ingredient for the renormalization group method discussed in the next section. In case of an unrestricted measure, vanishing external currents and a homogeneous field configuration the above expression gives the usual vacuum expectation value χ_0. It is non-vanishing in case of the chiral broken groundstate reflecting the nontrivial vacuum structure.

The effective action Γ which represents the generating functional of one particle irreducible (1PI) correlation functions can be obtained from W by a Legendre transformation in order to exchange the arbitrary sources by the averaged field configurations in presence of these sources

$$\Gamma[\chi_{av}] \equiv -W[J_\chi] + \int d^4x\, J_\chi \chi_{\rm av} \tag{2.12}$$

Equivalently to (2.11) the derivative of the effective action with respect to the fields $\chi_{\rm av}$ gives

$$\frac{\delta\Gamma[\chi_{\rm av}]}{\delta\chi_{\rm av}(x)} = J_\chi(x)\,. \tag{2.13}$$

This relation points out the importance of the effective action Γ, since for vanishing sources it is minimized by the true vacuum quantum field configuration. For a homogeneous system, the vacuum state is determined by the global minimum of the effective potential

$$\Gamma[\chi_{\rm av}] = \int d^4x\, U[\chi_{\rm av}] + \mathcal{O}(\partial)\ , \tag{2.14}$$

which represents the lowest order in a derivative expansion, discussed in the next section.

Despite the far simpler form of the Euclidean path integral compared to the Minkowski case, it cannot be computed in full generality. Therefore, an expansion of the action appearing in the exponential in fluctuations (fl) around the groundstate represented by the averaged (av) field configuration $\chi = \chi_{\rm av} + \chi_{\rm fl}$ is necessary to obtain an approximate solution

$$S \approx S_{\rm av} + \int d^4x \left(\frac{\delta S}{\delta\chi(x)} - J_\chi(x)\right)_{\rm av} \chi_{\rm fl}(x) + \tfrac{1}{2}\int d^4x \int d^4y\, \chi_{\rm fl}(x)\, \left.\frac{\delta^2 S}{\delta\chi(y)\delta\chi(x)}\right|_{\rm av} \chi_{\rm fl}(y) \tag{2.15}$$

The linear contribution vanishes according to the definition of the fields $\chi_{\rm av}$. This is of particular importance for an explicit chiral symmetry breaking term, since it does not experience any quantum corrections [15]. The remaining Gaussian approximation to the path integral includes one loop fluctuations. It can be integrated out formally and results in a nonlocal functional determinant[26]

$$\Gamma[\chi_{\rm av}] = \tfrac{1}{2}\log \mathrm{Sdet}\left(\left.\frac{\delta^2 S}{\delta\chi(y)\delta\chi(x)}\right|_{\rm av}\right) \equiv \tfrac{1}{2}\,\mathrm{STr}\log\left(\left.\frac{\delta^2 S}{\delta\chi(y)\delta\chi(x)}\right|_{\rm av}\right) \tag{2.16}$$

where the right hand side is just the definition of the determinant of an operator. Thereby, the functional integral is transformed into a trace over the full eigenspace of the respective operator, which includes both an integration over external variables and a sum over the internal degrees of freedom of the fields.

[26] The super determinant and trace is just used for conciseness of the notion, reflecting the fact that the field χ can also include fermionic parts. In the following we will not rely on supersymmetric methods to evaluate these expressions.

In particular the external trace performed in momentum space yields an integration over the three momentum and a sum over the zeroth component of the Euclidean four momentum, due to the periodicity of the initial path integral

$$\Gamma[\chi_{\rm av}] = \tfrac{1}{2} T \sum_{n=-\infty}^{\infty} \int \frac{d^3p}{(2\pi)^3} \mathrm{Str}\, \log\left(\frac{\delta^2 S}{\delta\chi(y)\delta\chi(x)}\bigg|_{\rm av} \right) , \tag{2.17}$$

where the Euclidean energy is restricted to the Matsubara frequencies $\omega_n = 2n\pi T$ for bosonic and $\nu_n = (2n+1)\pi T$ in case of fermionic fields and the small (super) trace (Str) runs over the internal variables of the fields. In the vacuum limit of vanishing temperature the above external trace simplifies to an integration over the full Euclidean momentum space.

Since the one loop effective action Eq. (2.16) is still a very complicated nonlocal object, which includes all possible interaction terms that are allowed by the symmetries of the theory, one has to rely on further approximations. This can be done by an expansion in local operators. Especially if these local operators involve derivatives, and the regarded associated external momenta p are small compared to the inherent scale Λ of a given theory, they are suppressed by $\frac{p}{\Lambda}$. This is the idea of the derivative expansion [16, 17, 18], whereas it is a rather nontrivial task to set the above qualitative argument on a sound basis. In contrast, interaction terms that do not include derivatives are not suppressed, intrinsically. Although, the renormalization group provides such a suppression in perturbative regimes, the neglect of such terms is generally not justified in strong coupling theories as those discussed in this work - especially not the restriction to renormalizable couplings only.

2.5 THE RENORMALIZATION GROUP AND ITS PROPER TIME FORM

Physical phenomena are closely connected to intrinsic scales of a given theory. These scales are basically responsible for the formation of structure due to the fact that an interaction becomes strong enough to bind primary degrees of freedom[27]. This usually leads to new a regime where physics is described in a simpler way using different degrees of freedom. In massless QCD, which consists of pointlike particles[28] and does not include explicit scales, such scales have to be determined entirely by the dynamics. This strong dependence of physical systems on scales is implemented in the method of the *renormalization group*, which enables to link the physics at different scales.

Basically, the renormalization group (RG) is a method to actually perform the functional integrals discussed in the last section in a way that does not rely on a weak coupling expansion and so is also applicable in strong coupling regimes[29]. As already noted in the last section the integration measure in Eq. (2.9) or the respective expression for the effective action Eq, (2.13) does not have to extend over the whole Fock space. One can divide the full measure into two parts depending on whether the momentum scales in the corresponding fluctuations

[27] Examples range from the regime of hadronic excitations where the strong coupling constant rises drastically at a scale of $\approx 10^{-15}$ m, up to scales of $\gtrsim 10^6$ m where the self gravitation becomes strong enough to collapse dust of the observed density to form stars - which themselves form even much larger structures.

[28] Even if some possible underlying degrees of freedom, like e.g. strings, should have a finite extension, it would be negligibly small compared to the considered physical system.

[29] Although, surely also renormalization group computations are much easier performed in weak coupling situations, as know from high precision computations of running coupling constants in the perturbative regime of gauge theories like QED or QCD.

are above $\chi_>$ or below $\chi_<$ a given scale Λ

$$\int D\chi \exp\left(-S(\chi)\right) = \int D\chi_> D\chi_< \exp\left(-S(\chi)\right) = \int D\chi_< \exp\left(-S_\Lambda(\chi_{\rm av})\right) \tag{2.18}$$

Integrating out the high momentum fluctuations, yields an *effective low energy theory* at the scale Λ. Thereby, fluctuations at larger scales are encoded into the couplings of the low energy effective action.

The idea of the renormalization group [19, 20] is to perform the above integration process on the differential level by successively integrating out infinitesimal momentum slices $[\Lambda - \Delta\Lambda, \Lambda]$, $[\Lambda - 2\Delta\Lambda, \Lambda - \Delta\Lambda]$, $\cdots$. One such integration step defines a renormalization group transformation[30] and forms the continuum analog of a block spin transformation in statistical physics. The amazing point about the integration procedure performed by the renormalization group, is that it gives a formal expression for the full functional integral that relies only on one loop dynamics and does not require the hardly manageable higher order terms in Eq. (2.15) on the differential level. This is encoded in a functional differential flow equation [20], which describes the averaging of the action in the evolution from some ultraviolet (UV) to an infrared (IR) scale.

The hard separation of scales, as described above is not ideal for practical computations. However, there are also exact flow equations[31] that rely on a smooth cutoff function and describe the averaging of a 1PI effective action. In particular, the exact equation given in [21] provides a manageable method to cover realistic systems. It has been applied successfully to various theories [22] including especially low energy strong interaction physics, which has been examined both in vacuum [23, 24, 25, 26] and at finite temperatures and densities [27, 28, 29]. The Schwinger proper time (SPT) [33] RG flow equations [34, 35, 36] used in this work do not belong to the class of exact RG equations[32] [30]. Instead they are RG improved one loop equations. However, they inherently respect symmetries of the action, since the regulator does not act directly on the momentum integral. Previous analyses in the SPT scheme found comparable results to those obtained with exact flow equations [37, 38, 39].

The starting point to obtain the SPT flow equation is the effective action Eq. (2.16) with the divergent logarithm regularized in the Schwinger proper time scheme as discussed in Appendix C

$$\Gamma[\chi_{\rm av}, k] = -\tfrac{1}{2}\,\mathrm{STr}\int \frac{d\tau}{\tau} \exp\left(-\tau\left(\frac{\delta^2 S}{\delta\chi(y)\delta\chi(x)}\bigg|_{\rm av}\right)\right) f(\tau k^2) \tag{2.19}$$

where f is a smooth cutoff function depending on an IR scale parameter k. Taking derivatives on both sides of Eq. (2.19) with respect to the cutoff scale k yields a just a formulation of the above equation on the differential level. The RG improvement is achieved by the replacement of the UV action S by the effective action $\Gamma[k]$ at the scale k including quantum fluctuations

[30] Contrary to what the word suggests, these transformations do not form a group but only a half group, since the process of integrating out fluctuations is not invertible.

[31] For a comprehensive review of the exact renormalization group, see [22].

[32] However, in the case of the local potential approximation a one to one correspondence could be drawn between certain exact and SPT flows [31]. Furthermore, implicit correction terms have been given for the general case [32]. The inclusion of these terms relates the SPT flow to a generalized Callan-Symanzik flow which is exact. In this respect the SPT flow given in Eq. (2.20) can be viewed as an approximation of an exact flow.

on larger scales

$$\frac{\partial\Gamma[\chi,k]}{\partial k} = -\tfrac{1}{2}\,\mathrm{STr}\int\frac{d\tau}{\tau}\exp\left(-\tau\left(\frac{\delta^2\Gamma[\chi,k]}{\delta\chi(y)\delta\chi(x)}\right)\right)\frac{\partial f(\tau k^2)}{\partial k} \tag{2.20}$$

The justification for this improvement stems from the above picture of integrating out infinitesimal momentum slices successively, using after each integration step the partially integrated effective action as integration kernel for the next one. This leads to an integral equation, which can be transformed into the improved differential equation on the differential level. However, the soft cutoff involved in the SPT scheme prevents this procedure from being a rigid derivation. Nonetheless, the advantage of the proper time flow equations is their particular simple form compared to flow equations derived in other RG schemes.

The classic application for the RG method is the region around a second order phase transition. In this universal regime certain properties of a given model are only governed by the symmetry that is broken in the transition and therefore large universality classes of different models are already described by the simplest representative that includes the minimal realization of the respective symmetry [40]. This is the case, since the correlation length diverges at a second order phase transition corresponding to massless modes in the theory. Due to the absence of mass scales the renormalization group flow expressed in dimensionless variables shows scaling behavior and is governed by IR fix points, while loosing the information on the exact UV theory specified by the UV values of the parameters[33]. However, even in such a universal regime all quantities that involve scales themselves, like for instance the critical temperature, are not determined by the scaling solution but depend on the detailed UV physics and require a more detailed analysis.

By an expansion of the effective action in local operators as discussed in the previous section, the flow equation for the effective action can be transformed into a coupled set of flow equations for the respective couplings. Under the assumption that these couplings are small enough that the kinetic term dominates, one can consider the asymptotic behavior of these couplings λ at IR scales k much smaller than some UV scale Λ. According to such a dimensional analysis a coupling scales roughly according to its mass dimension δ_λ corresponding to [41, 40]

$$\sim \lambda\left(\frac{k}{\Lambda}\right)^{-\delta_\lambda}\,. \tag{2.21}$$

This divides the couplings into relevant ($\delta_\lambda > 0$), marginal ($\delta_\lambda = 0$) and irrelevant couplings ($\delta_\lambda < 0$) and leads to a partial fix point behavior since for $k << \Lambda$ only relevant and possibly marginal couplings should be important[34]. Although the above conclusion has been stated much more rigorously [42], it is strictly applicable only in weak coupling situations. However, when couplings are large and the IR scale is not very much lower than the UV scale, as in the case discussed in this work, higher order couplings are not obviously negligible. In particular, the RG flow generates all possible couplings compatible with the symmetries of the theory. Such higher order couplings can become large in strong couplings regimes and influence the flow of the relevant and marginal couplings. Therefore, a main objective of this work is to

[33] This exemplifies the property of the RG being only a half-group

[34] This singles out renormalizable theories like QCD or the standard model, which only contain such *renormalizable* couplings since their UV scale is assumed to be very large, so that irrelevant couplings do not enter in low-energy processes.

include the effect of higher order couplings into the flow, in order to examine non-universal regimes like the groundstate of strong interaction.

It seems very tempting to apply the renormalization group formalism to QCD in order to obtain a low energy effective theory by integrating out the gauge dynamics. In principle RG flow equations have been applied successfully to gauge theories [43, 44]. However, in case of QCD this task is especially complicated by the discussed strong coupling effects, which so far prevented a rigorous solution in the low-energy regime. In particular it raises the challenge of a change of the degrees of freedom during the flow, since the colored gauge degrees of freedom are not present at low energies. Nevertheless, there have been considerable efforts [45] which showed that both perturbative gluon exchange and instanton induced interactions [46, 47] can lead to local fermionic interactions. Moreover, aside from the technical difficulties, generally integrating out the gluonic dynamics of QCD as well as the quark dynamics down to a given scale, should lead to a fermionic theory with - possibly arbitrary many - purely fermionic interaction terms [45]. The hope is that only a few of them dominate and describe the IR physics reasonably.

2.6 NJL-MODEL AND BOSONIZATION

As just discussed it should at least in principle be possible to obtain fermionic self interactions as an effective low energy theory of QCD by integrating out the gauge interaction at large momenta. Although such a connection has not been established so far, it is interesting to consider a local fermionic theory as an effective model for strong interaction, since in principle this situation holds similarly for QCD itself[35]. Such a fermionic model that includes the lowest order chiral four fermion interaction is provided by the Nambu−Jona-Lasinio model.

The Nambu−Jona-Lasinio (NJL) model[36] [49] was proposed already 1961 as a theory of nucleons and their dynamical mass generation. Due to its non-renormalizable interaction term, it was understood already at that time, that it can hold only as the low energy limit of some primary interaction. This interaction has been found later described by the non-Abelian gauge interaction of QCD between the more fundamental quark degrees of freedom - which subsequently also replaced the nucleons in applications of the NJL model. The Euclidean Lagrangian of the NJL model with quarks is given by[37]

$$\mathcal{L}_{\mathrm{NJL}} = \bar{q}(\partial\!\!\!/ + m_{\mathrm{c}})q - g_{\mathrm{NJL}}\left((\bar{q}q)^2 + (\bar{q}i\vec{\tau}\gamma_5 q)^2\right) \ . \tag{2.22}$$

As has been discussed in Section 2.2, this form contains the minimal four fermion interactions in accordance with chiral $SU_L(2)\otimes SU_R(2)$ symmetry[38] - namely scalar and pseudoscalar color singlet channels. In the original article and various ensuing work it has been solved in a self-consistent framework of Schwinger-Dyson and Bethe-Salpeter type. Other non-perturbative

[35] QCD is also assumed to be only a low-energy limit of some underlying theory since it contains explicit mass terms and is therefore not natural [41], i.e. due to the RG arguments given in the last section these mass terms get small at large scales and require an unattractive fine tuning. Though, embedded in the standard model of particle physics these masses are generated by the Higgs mechanism, from the point of view of naturalness the problem is only shifted to the explicit mass of the Higgs boson [48, 2].

[36] There are several revue articles on this model which give an overview over its broad field of applications [50, 51].

[37] In this work we use a representation in which all Euclidean γ-matrices are Hermitian.

[38] Additionally one can introduce the current mass term m_c to account for a small explicit symmetry breaking.

solution schemes have been rarely applied to the NJL model. This holds especially for the RG method, which will be applied to this model in the remainder of this work.

The fact, that the NJL model includes colored quarks but only color singlet interactions directly shows that it cannot account for color confinement in fermionic states. However, it implements dynamical chiral symmetry breaking and thereby following the arguments given in the preceding sections one can in principle expect that it accounts for the low-energy physics. Since, it contains constituent quark degrees of freedom and is inherently defined around a scale of the order 1 GeV, the question that remains is whether this minimal representation is sufficient at this scale to describe the chiral physics of the groundstate[39].

In the chiral limit the NJL model has the four fermion coupling $g_{\rm NJL}$ as its only free parameter. Neglecting the momentum dependence and all higher order couplings the four fermion coupling $g_{\rm NJL}$ is renormalized by the one loop graph

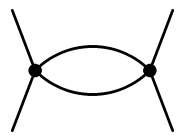

Because of the two 4-fermion couplings and the massless propagators, the respective Wilsonian flow equation can aside from a numerical factor c directly be inferred from the above diagram [53, 52]

$$k\frac{\partial g_{\rm NJL}}{\partial k} = -c\,k^2\,g_{\rm NJL}^2\,, \tag{2.23}$$

This equation can be integrated analytically starting at some UV-scale Λ leading to the result

$$g_{\rm NJL}(k) = \frac{g_{\rm NJL}(\Lambda)}{1-\frac{c}{2}(\Lambda^2-k^2)g_{\rm NJL}(\Lambda)} \tag{2.24}$$

In this simplified approximation for large enough $g_{\rm NJL}(\Lambda)$ the result has a Landau pole[40] at a finite scale k, where the coupling diverges. This is exactly the same behavior that occurs for the running coupling in QCD. It signals the formation of some bound state, when an attractive interaction becomes large enough. However, aside from the scale at which this happens and the critical coupling for which such a bound state forms, the above analysis does not provide any further information. In particular it does not give any hint on the precise properties of the groundstate of the theory.

To learn something about the vacuum state and the low-energy behavior it is necessary to go beyond the considered approximation. Since the above analysis suggests that bound states are formed, it seems promising to include these states explicitly into the theory. Compared to QCD, where it is not clear at all how such colorless bound states are connected to the underlying colored degrees of freedom, the situation is more transparent in the NJL model. Because the interaction rises dramatically in the considered colorless quark-antiquark channels, it is possible to give the system the chance to saturate these channels by the inclusion

[39] In principle even the lowest order four fermion interaction could be extended to various other channels. Namely, as far as the meson channels are considered there are also vector and axial vector and the remaining scalar channels [52]. Further one could also consider diquark or even color octet channels.

[40] This behavior is quite universal, as long as only massless propagators and at least two couplings are present in the respective graph. It applies for instance also to QCD and the theory of superconductors.

of respective states. Technically, this is done by a partial bosonization of the action through the introduction of auxiliary bosonic fields into the path integral using the identity [54]

$$e^{g_{\rm NJL}(\bar\psi\psi)^2} = \frac{\int D\sigma\, e^{-\frac{1}{4\,g_{\rm NJL}}\sigma^2 - \bar\psi\sigma\psi}}{\int D\sigma\, e^{-\frac{1}{4\,g_{\rm NJL}}\sigma^2}} \,. \tag{2.25}$$

These fields just act as constraints and are no dynamical degrees of freedom at the UV-scale. Nevertheless, they linearize the nonlinear fermionic coupling and therefore allow to include significantly more dynamics within a one loop computation. The bosonization procedure yields the partition function for the associated linear σ-model

$$Z = \int D\Phi \int D\bar q \int Dq \, \exp\left(-\int d^4x\, \mathcal{L}_{\rm L\sigma M}\right) \,, \tag{2.26}$$

with the Euclidean Lagrangian

$$\mathcal{L}^{\rm uv}_{\rm L\sigma M} = \bar q \left(\partial\!\!\!/ + g\tilde\Sigma\right) q + U_{\rm uv} \,. \tag{2.27}$$

Here, the quark mass term in the fermionic Lagrangian which breaks chiral symmetry explicitly can be either left unchanged, in which case it appears in the matrix $\tilde\Sigma$ leaving the bosonic potential in a symmetric form

$$\tilde\Sigma = \frac{m_{\rm c}}{g} + \Sigma \quad , \quad U_{\rm uv} = \frac{m^2_{\rm uv}}{2}\,\Phi^2 \,, \tag{2.28}$$

or can also be bosonized in which case the bosonic potential becomes asymmetric[41]

$$\tilde\Sigma = \Sigma \quad , \quad U_{\rm uv} = \frac{m^2_{\rm uv}}{2}\,\Phi^2 - \delta\,\sigma \,. \tag{2.29}$$

Finally, the respective couplings in the different representations are connected by

$$g_{\rm NJL} = \frac{g^2}{2\,m^2_{\rm uv}} \quad , \quad m_{\rm c} = \frac{g\,\delta}{m^2_{\rm uv}} \,. \tag{2.30}$$

The Lagrangian (2.27) obviously lacks kinetic terms for the bosonic fields at the UV scale, reflecting the fact that they are only auxiliary fields which could be integrated out immediately in order to retain back the original NJL model. However, as has been discussed in the previous section, during the RG flow all couplings compatible with the symmetries of the model are generated by the dynamics - including especially the kinetic terms of the bosonic fields. Thereby, collective mesonic degrees of freedom arise naturally from the RG evolution and become propagating excitations.

Correspondingly, the four fermion vertex which is removed at the UV scale by the bosonization procedure equally rises again during the evolution. This would lead to some sort of double counting, since mesons appear in the theory both as elementary and as composed degrees of freedom in the form of a quark chain. A method to evade these problems and include this effect by a continuous bosonization has been proposed recently [55]. There the additionally included contributions account for the fact, that the mesonic states have a bound state substructure.

[41] We will use the latter method to deal with explicit chiral symmetry breaking in this work.

Without a connection to a underlying fermionic theory, the linear σ-model [56] including propagating mesonic excitations has been proposed one year before the NJL-model

$$\mathcal{L}_{\mathrm{L}\sigma\mathrm{M}} = \bar{q}\,(\partial\!\!\!/ + g\Sigma)\,q + \tfrac{1}{2}(\partial_\mu\Phi)(\partial^\mu\Phi) + \tfrac{1}{2}m^2\Phi^2 + \tfrac{1}{4}\lambda\Phi^4\,. \tag{2.31}$$

On the perturbative level it is renormalizable [57] and can be solved in a simple mean field approximation. Compared to the NJL model it has more freedom since it contains aside from the Yukawa coupling g further couplings in the bosonic potential.

As a chiral theory the linear σ-model respects the necessary low energy theorems [2]. This includes first of all a version of the Goldberger–Treiman relation[42] on the constituent quark level

$$g_{\pi N} = g_a \frac{m_N}{f_\pi} \quad \rightarrow \quad m_q = g\, f_\pi \tag{2.32}$$

which relates the constituent quark mass m_q to the pion-decay constant f_π via the Yukawa couplings g. We will also apply the Gell-Mann–Oakes–Renner relation

$$m_\pi^2\, f_\pi^2 = m_c\, \langle \bar{q}q \rangle \tag{2.33}$$

which connects the pion mass m_π to the chiral quark condensate $\langle \bar{q}q \rangle$ and the current quark mass $m_c \equiv \frac{1}{2}(m_u + m_d)$. These relations are important to connect the model parameters to physical observables.

[42] The usual Goldberger Treiman relation on the hadron level involves the nucleon mass m_N, the pion-nucleon coupling $g_{\pi N}$ and the constant g_A measured in low energy nuclear beta decay.

Chapter 3

The strongly interacting vacuum

QCD as the theory of strong interaction is well established in the perturbative regime. Unfortunately, aside from lattice computations its predictive power is still limited in the non-perturbative regime. Although, within the framework of the renormalization group it should in principle be possible to obtain a low energy theory by integrating out the complicated gluonic dynamics. As discussed in the last chapter, this task could not been done yet in a rigorous manner due to various problems.

Nevertheless, an effective field theory should be able to describe physics at a considered scale, as long as the relevant degrees of freedom at the regarded scale and all dynamics consistent with the symmetries of the problem are included. However, the true advantage of a good effective field theory is that it is not necessary to include all dynamics in order to describe physics, but certain approximations are already sufficient. In this sense, QCD does not seem to have the appropriate degrees of freedom in order to describe physics efficiently at low energies. In the simplest picture, appropriate degrees of freedom in that region may be some dressed fermionic quasi-particles with a residual interaction. The physical restriction for an effective theory build out of such constituent quarks in the non-perturbative regime of strong interaction is, that it has to obey chiral symmetry and its spontaneous breaking in vacuum. From this point of view, the Nambu–Jona-Lasinio (NJL) model [49], we employ here, is the simplest nontrivial effective theory consistent with these requirements - and it is interesting to examine, to what extend such a simplified description works.

In order to check the real power of an effective theory, it is necessary to consider an adequate approximation scheme. Simple approximations often have enough free parameters to tune the model just to fit nature. This involves the loss of predictive power and in principle does not imply that a full solution of the theory will give a reasonable description of the physics. Therefore, one has to determine, if the approximation scheme converges and if more complex dynamics can be neglected, by going to more elaborate approximations. This work is understood as a first step in this direction.

3.1 EFFECTIVE ACTION OF THE GENERALIZED LINEAR σ-MODEL

We assume the NJL model described in Section 2.6 to be a reasonable description of nature at scales below ≈ 1 GeV. In this region the gluon degrees of freedom are supposed to be already frozen out and the quarks determine the action. The physics is governed by chiral symmetry, which is spontaneously broken in the infrared. The goal of our analysis is to give an improved solution for the scalar NJL model described by the Lagrangian Eq. (2.22). Since chiral symmetry is spontaneously broken in vacuum, the effective theory should at least contain pions, which represent the lowest lying excitations in the hadron spectrum. As discussed in Section 2.6, these Goldstone bosons are included into the description by a partial bosonization, through the introduction of auxiliary scalar fields π and their chiral partner σ. It leads to the associated linear σ-model with quarks which is equivalent to the NJL model at the UV scale $k_{\rm uv} \approx 1$ GeV given in Eq. (2.27) [54]. The bosonization procedure introduces two parameters, namely a dimensionless Yukawa coupling $g_{\rm uv}$ and a bosonic mass parameter $m_{\rm uv}$, instead of only one four fermion coupling $g_{\rm NJL}$. A full solution of the model should still depend on the ratio $\frac{g_{\rm uv}}{m_{\rm uv}}$ of these parameters and not on them individually. The NJL model in large N_c approximation is governed by the parameter $g_{\rm NJL} \cdot k_{\rm uv}^2$ where $k_{\rm uv}$ is the cutoff scale of the model. If this parameter is larger than a critical value one has chiral symmetry breaking. In the calculation with meson loops the effect of the quark pairing interaction is reduced. Therefore, it is interesting to examine whether also the groundstate preserves this behavior in our approximation.

According to the general discussion in Section 2.4, at zero temperature in Euclidean space the partition function of the linear σ-model with appropriate source terms $\bar{\eta}$, η and J is given by

$$Z[J,\bar{\eta},\eta] = e^{-W[J,\bar{\eta},\eta]} = \int \mathcal{D}q\mathcal{D}\bar{q}\mathcal{D}\Phi \exp\left(-S[\bar{q},q,\Phi] + \int d^4x\,(J\Phi + \bar{\eta}q + \bar{q}\eta)\right) . \tag{3.1}$$

To solve this functional integral, we will apply the renormalization group techniques presented in Section 2.5, in order to successively integrate out infinitesimal scale slices, starting from a UV scale $k_{\rm uv}$ down to the IR. According to the discussion in that section, all possible higher order couplings compatible with the symmetry of the theory are generated during the renormalization group flow and influence the flow of the relevant operators remaining in the IR. To include this effect the action from which the one loop corrections for a renormalization group step are computed, must already include all these couplings to provide the necessary freedom for the renormalization group flow. Therefore, we will compute one loop fluctuations from the following parametrization[1] for the Euclidian action of the generalized linear σ-model

$$S[\bar{q},q,\Phi] = \int d^4x \left(Z_q(\Phi^2)\bar{q}\partial\!\!\!/ q + \tfrac{1}{2}Z_\Phi^{ab}(\Phi)(\partial_\mu\Phi^a)(\partial^\mu\Phi^b) + G(\Phi^2)\bar{q}\Sigma q + U(\Phi^2)\right) \tag{3.2}$$

The effective wavefunction renormalization factors $Z_\Phi^{ab}(\Phi)$, $Z_q(\Phi^2)$ as well as the effective Yukawa coupling $G(\Phi^2)$ in this general action are functions of the bosonic fields Φ and thereby include arbitrary many "elementary" couplings - in full analogy to the effective potential $U(\Phi^2)$. Furthermore, the effective bosonic wavefunction factor $Z_\Phi^{ab}(\Phi)$ has the general form

[1] Within this work we denote field-dependent, effective masses and couplings by capital letters, whereas the respective small characters are used for their physical values at the vacuum expectation value of the fields.

compatible with chiral symmetry given by a matrix in $O(4)$-space. The quark- and meson-fields $\bar{q}, q, \Phi, \Sigma$ are bare fields, where $\Sigma = \sigma + i\vec{\tau}\vec{\pi}\gamma_5$ is the chiral $SU(2)_L \otimes SU(2)_R$-representation and $\Phi = (\sigma, \vec{\pi})$ is the $O(4)$-representation of the meson fields discussed in Section 2.2.

Note, that we have neglected higher powers of fermionic bilinears like the initial four fermion interaction[2]. As mentioned in Section 2.6 these additional dynamics can be included into the flow of higher order bosonic interactions encoded by additional terms in the flow equation for the Yukawa coupling G [55]. Since these additional terms reflect the bound state substructure of the collective mesonic states, they should be relevant for the physics of the σ-mode of the chiral field. Although in nature the situation is much more complicated e.g. due the tolerably light strange quark mass, experimentally the hardly resolvable resonance in the isoscalar 0^{++} "σ-channel" is know to be exceptionally broad [58, 59]. However, in the IR the pions can - as far as only strong interaction is considered - in good approximation be considered as elementary particles due to there Goldstone boson nature. Therefore, we have so far neglected these effects in our calculation[3].

The 1PI effective action introduced in Section 2.4 reads in the considered case

$$\Gamma[\bar{q}, q, \Phi] = -W[J] + \int d^4x \; (J\Phi + \bar{\eta}q + \bar{q}\eta) \tag{3.3}$$

We calculate Γ within a saddle point expansion corresponding to a one loop approximation. Since the Yukawa term in Eq. (3.2) contains both quark and meson fields, one has to shift the quark fields, before they can be integrated out. The result is an additional term[4] in the meson determinant, which generates corrections to the Yukawa coupling and the wavefunction renormalization of the quark fields [15]. Suppressing spacetime integrations, we find for the effective action in one loop ($1L$) approximation

$$\Gamma^{1L}[\Phi, \bar{q}, q] = S[\Phi, \bar{q}, q] - \mathrm{Tr}\,\log S_{\bar{q}q} + \tfrac{1}{2}\mathrm{Tr}\,\log\left(S_{\Phi^i\Phi^j} - 2\, S_{\Phi^i q} S^{-1}_{\bar{q}q} S_{\bar{q}\Phi^j}\right) , \tag{3.4}$$

where

$$S_{\bar{q}q}(x,y) = \left.\frac{\delta^2 S[\Phi, \bar{q}, q]}{\delta\bar{q}(x)\delta q(y)}\right|_{av} \quad , \quad S_{\bar{\Phi}^i\Phi^j}(x,y) = \left.\frac{\delta^2 S[\Phi, \bar{q}, q]}{\delta\Phi^i(x)\delta\Phi^j(y)}\right|_{av} \quad , \quad \cdots \quad . \tag{3.5}$$

and functional derivatives are understood to act from left and right respectively. The first logarithm results from fermion loop fluctuations, whereas the two terms in the second logarithm are the contributions of the bosonic and of mixed loops respectively, which can formally be represented in graphical form[5]

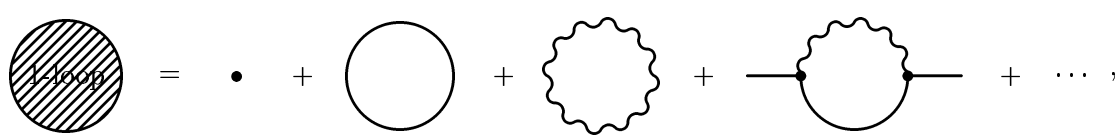

[2]Generally, instead of the Yukawa coupling $G(\Phi^2)$ and the bosonic potential $U(\Phi^2)$ there should be a generalized chiral symmetric potential $V(\Sigma, \bar{q}, q)$, as the lowest term in the derivative expansion.

[3]For a future improvement of the considered approximation the inclusion of these effects would be very interesting since it would allow a complete solution of the NJL model to a given order in the derivative expansion.

[4]Within a supersymmetric solution method for the Gaussian functional integration [22], the supertrace would run over a non-diagonal supermatrix and the additional term would arise from the required diagonalization.

[5]Fermions are represented by straight and bosons by wavy lines.

i.e. each proper vertex is renormalized by the appropriate one loop graphs[6]. The functional derivatives of S can be computed by a careful analysis of the differential operators in coordinate space representation and read in matrix notation

$$S_{\bar{q}q} = Z_q \partial\!\!\!/ + G\Sigma \equiv D \tag{3.6}$$

$$S_{\Phi^i\Phi^j} = -Z_\Phi \partial^2 + U'' + A - B_\mu \partial_\mu + C \tag{3.7}$$

$$S_{\Phi^i q} = \bar{q}\left(Ge^i + \frac{\delta G}{\delta \Phi^i}\Sigma + \frac{\delta Z_q}{\delta \Phi^i}\partial\!\!\!/\right) \tag{3.8}$$

$$S_{\bar{q}\Phi^j} = \left(Ge^j + \frac{\delta G}{\delta \Phi^j}\Sigma + \frac{\delta Z_q}{\delta \Phi^j}\partial\!\!\!/\right) q \tag{3.9}$$

where D is the Dirac operator and in addition the following abbreviations have been used

$$e \equiv (1, i\vec{\tau}\gamma_5) \tag{3.10}$$

$$(U'')^{ij} \equiv \frac{\delta U}{\delta \Phi^i \delta \Phi^j} \tag{3.11}$$

$$A^{ij} \equiv \frac{1}{2}\left(\frac{\delta^2 Z_\Phi^{ab}}{\delta \Phi^i \delta \Phi^j}\left(\partial_\mu \Phi^a\right)\left(\partial_\mu \Phi^b\right) - \partial_\mu\left(\left(\frac{\delta Z_\Phi^{ib}}{\delta \Phi^j} + \frac{\delta Z_\Phi^{bi}}{\delta \Phi^j}\right)\left(\partial_\mu \Phi^b\right)\right)\right) \tag{3.12}$$

$$B_\mu^{ij} \equiv \frac{1}{2}\left(\frac{\delta Z_\Phi^{ij}}{\delta \Phi^b} + \frac{\delta Z_\Phi^{ji}}{\delta \Phi^b} - \frac{\delta Z_\Phi^{bj}}{\delta \Phi^i} - \frac{\delta Z_\Phi^{jb}}{\delta \Phi^i} + \frac{\delta Z_\Phi^{ib}}{\delta \Phi^j} + \frac{\delta Z_\Phi^{bi}}{\delta \Phi^j}\right)\left(\partial_\mu \Phi^b\right) \tag{3.13}$$

$$C^{ij} \equiv \bar{q}\left(\frac{\delta^2 G}{\delta \Phi^i \delta \Phi^j}\Sigma + \frac{\delta G}{\delta \Phi^j}e^i + \frac{\delta G}{\delta \Phi^i}e^j + \frac{\delta^2 Z_q}{\delta \Phi^i \delta \Phi^j}\partial\!\!\!/\right) q \tag{3.14}$$

The purely bosonic part of this expression has been obtained earlier in [60], where it was used for a perturbative two-loop expansion of the effective action.

In principle the obtained logarithms contain terms with arbitrary many fields and derivatives. However, in order to compute them one has to perform a suitable truncation. The truncation we use in this work is to consider the parametrization for the action of the generalized linear σ-model Eq. (3.2) also for the effective action. This corresponds to a derivative expansion up to next to leading order (NLO), without an additional truncation in bosonic fields on which previous approaches [23, 37] relied. Thereby it goes beyond the perturbative result given in [60] which makes it possible to consider this generalized parametrization during the entire RG evolution and include all effects of higher bosonic couplings within the flow.

Furthermore, the appearing traces over the logarithms are generally divergent and need regularization. We will perform this regularization in the Schwinger proper time regularization scheme [33] presented in Appendix C. The logarithm of the Dirac operator Eq. (3.6) cannot be regularized completely in the SPT scheme. However, regularization is possible for its physically dominant[7] real part given by

$$\begin{aligned}\mathrm{Re}\left(-\mathrm{Tr}\log\left(D\right)\right) &= -\tfrac{1}{2}\mathrm{Tr}\log\left(DD^\dagger\right)\\ &= -\tfrac{1}{2}\mathrm{Tr}\log\left(-Z_q^2\partial^2 - Z_q\left(\partial\!\!\!/ Z_q\right)\partial\!\!\!/ + Z_q\left(\partial\!\!\!/\left(G\Sigma^\dagger\right)\right) + G^2\Sigma\Sigma^\dagger\right)\end{aligned} \tag{3.15}$$

[6]Here, the first two loops contribute to vertices with bosonic external lines only, whereas the last loop renormalizes vertices which include external fermionic legs. It is the first representative of a series of loops with alternating bosonic and fermionic propagators and the corresponding number of external fermionic legs.

[7]The imaginary part is responsible for anomalous processes and contributes only in higher order, cf. [54]. Since we are mainly concerned with bulk properties of the strongly interacting groundstate, we will neglect these effects here.

Moreover, the fermionic propagator D^{-1} appearing in the bosonic logarithm of Eq. (3.4) can cause divergences and has to be incorporated in the regularization procedure. Consequently, this part likewise cannot be regularized entirely in the SPT scheme. However, as we will show, a regularization is possible for the considered truncation Eq. (3.2). For this purpose, it is necessary to decompose the respective logarithm

$$\begin{aligned}\Gamma^{1L} \approx & S - \tfrac{1}{2}\,\mathrm{Tr}\,\log\left(-Z_q^2\partial^2 - Z_q\left(\partial\!\!\!/ Z_q\right)\partial\!\!\!/ + Z_q\left(\partial\!\!\!/\left(G\Sigma^\dagger\right)\right) + G^2\Phi^2\right)\\ & + \tfrac{1}{2}\,\mathrm{Tr}\,\log\left(-Z_\Phi\partial^2 + U'' + A - B_\mu\partial_\mu\right)\\ & + \tfrac{1}{2}\,\mathrm{Tr}\,\log\left(1 + \left(-Z_\Phi\partial^2 + U'' + A - B_\mu\partial_\mu\right)^{-1}\left(C - 2\,S_{\bar q\Phi^i}D^{-1}S_{\Phi^j q}\right)\right)\,, \end{aligned} \tag{3.16}$$

where we have neglected all non-commuting parts, since they do not contribute in the considered truncation Eq. (3.2).

Since the appearing operators are neither coordinate nor momentum eigenstates, the coordinate space part of the functional trace (Tr) can be transformed into an integration over the full phase space by the introduction of a complete set of momentum eigenstates[8] (cf. [36]), leaving only a trace (tr) over the internal degrees of freedom of the fields

$$\begin{aligned}\Gamma^{1L} &\approx S + \Delta\Gamma_F + \Delta\Gamma_B + \Delta\Gamma_M\\ &\equiv S - \tfrac{1}{2}\int d^4x\int\frac{d^4p}{(2\pi)^4}\,\mathrm{tr}\,\log\big(Z_q^2\left(p^2 - 2ip_\mu\partial_\mu - \partial^2\right)\\ &\qquad\qquad - Z_q\left(\partial\!\!\!/ Z_q\right)\left(ip\!\!\!/ + \partial\!\!\!/\right) + Z_q\left(\partial\!\!\!/\left(G\Sigma^\dagger\right)\right) + G^2\Phi^2\big)\\ &\quad + \tfrac{1}{2}\int d^4x\int\frac{d^4p}{(2\pi)^4}\,\mathrm{tr}\,\log\left(Z_\Phi\left(p^2 - 2ip_\mu\partial_\mu - \partial^2\right) + U'' + A - iB_\mu p_\mu - B_\mu\partial_\mu\right)\\ &\quad + \tfrac{1}{2}\int d^4x\int\frac{d^4p}{(2\pi)^4}\,\mathrm{tr}\,\log\Big(1 + \left(Z_\Phi\left(p^2 - 2ip_\mu\partial_\mu - \partial^2\right) + U''\right)^{-1}\\ &\qquad\qquad \cdot\left(C - 2\,S_{\bar q\Phi^i}D^{-1}S_{\Phi^j q}\right)\big|_{\partial\!\!\!/\to\partial\!\!\!/+ip\!\!\!/}\Big)\,. \end{aligned} \tag{3.17}$$

Here, corresponding to our truncation Eq. (3.2) we already dropped terms which contain both fermions and derivatives on bosonic fields.

While the logarithms in the fermionic and bosonic contributions $\Delta\Gamma_F$ and $\Delta\Gamma_B$ in Eq. (3.17) could be transformed directly into proper time form, the last contribution $\Delta\Gamma_M$ which contains both bosonic and mixed fluctuations needs a more careful treatment in order to properly regularize its full momentum dependence. The corresponding computation which includes an expansion of the logarithm to first order is sketched in Appendix A and yields

$$\begin{aligned}\Delta\Gamma_M \approx \int d^4x\int\frac{d^4p}{(2\pi)^4}\,\bar q\,\mathrm{tr}\Bigg[&\frac{1}{p^2+M_\Phi^2}E_G + \tfrac{1}{2}\left(\frac{1}{p^2+M_\Phi^2} + \frac{M_\Phi^2}{(p^2+M_\Phi^2)^2}\right)E_{Z_q}\\ &+ \frac{1}{M_q^2 - M_\Phi^2}\left(\frac{1}{p^2+M_\Phi^2} - \frac{1}{p^2+M_q^2}\right)F_G\\ &+\tfrac{1}{2}\frac{1}{M_q^2 - M_\Phi^2}\left(\frac{1}{p^2+M_\Phi^2} - \frac{1}{p^2+M_q^2} + \frac{M_\Phi^2}{(p^2+M_\Phi^2)^2} - \frac{M_q^2}{(p^2+M_q^2)^2}\right)F_{Z_q}\Bigg]\,q\,, \end{aligned} \tag{3.18}$$

[8] This yields additional terms accompanied by the respective momenta due to the commutation relation: $f(\partial_\mu)e^{ipx} = e^{ipx}f(\partial_\mu + ip_\mu)$.

where $M_\Phi^2 = Z_\Phi^{-1}U''$ is the squared effective bosonic mass matrix in $O(4)$-space, $M_q^2 = Z_q^{-2}G^2\Phi^2$ is the squared effective quark mass which is diagonal in $O(4)$-space and the $O(4)$-matrices E_G, E_{Z_q} and F_G, F_{Z_q} are given in Eq. (A.4) and contain contributions from bosonic and mixed fluctuations to the Yukawa coupling G and the quark wavefunction renormalization factor Z_q respectively.

In the above form the partially truncated effective action can be transformed to proper time integrals using the expressions for the logarithms and inverse powers Eqs. (C.1, C.3). For the moment we implicitly assume analogous to Eq. (C.1) an IR regulator κ and an UV regulator Λ in the proper time integral to ensure proper regularization of the effective action, which thereby takes the form

$$\begin{aligned}\Gamma^{1L} \approx & S + \tfrac{1}{2}\int d^4x \int \frac{d^4p}{(2\pi)^4}\int\frac{d\tau}{\tau}\,\mathrm{tr}\left[e^{-\tau\left(Z_q^2\left(p^2-2ip_\mu\partial_\mu-\partial^2\right)-Z_q\left(\not\partial Z_q\right)\left(i\not p+\not\partial\right)+Z_q\left(\not\partial\left(G\Sigma^\dagger\right)\right)+G^2\Phi^2\right)}\right] \\ & - \tfrac{1}{2}\int d^4x \int \frac{d^4p}{(2\pi)^4}\int\frac{d\tau}{\tau}\,\mathrm{tr}\left[e^{-\tau\left(Z_\Phi\left(p^2-2ip_\mu\partial_\mu-\partial^2\right)+U''+A-B_\mu\partial_\mu-iB_\mu p_\mu\right)}\right] \\ & + \int d^4x \int \frac{d^4p}{(2\pi)^4}\int d\tau\,\bar q\,\mathrm{tr}\left[e^{-\tau(p^2+M_\Phi^2)}E_G + \tfrac{1}{2}\left(1+\tau M_\Phi^2\right)e^{-\tau(p^2+M_\Phi^2)}E_{Z_q}\right. \\ & \qquad + \left(e^{-\tau(p^2+M_\Phi^2)} - e^{-\tau(p^2+M_q^2)}\right)\frac{F_G}{M_q^2-M_\Phi^2} \\ & \qquad \left. + \tfrac{1}{2}\left(\left(1+\tau M_\Phi^2\right)e^{-\tau(p^2+M_\Phi^2)} - \left(1+\tau M_q^2\right)e^{-\tau(p^2+M_q^2)}\right)\frac{F_{Z_q}}{M_q^2-M_\Phi^2}\right] q\,. \end{aligned} \tag{3.19}$$

This general expression for the one loop effective action of the linear σ-model cannot be evaluated in closed form. In the spirit of a derivative expansion discussed in Section 2.4, at low energies only terms with a minimal number of derivatives should be important. Therefore, we expand the effective action in next to leading order in derivatives given by our parametrization (3.2). In order to perform this expansion it is convenient to decompose the $O(4)$ matrix[9]

$$Z_\Phi^{ij} = Z_\sigma(\Phi^2)X_\sigma^{ij} + Z_\pi(\Phi^2)X_\pi^{ij}\,, \tag{3.20}$$

by the use of $O(4)$ projectors on the radial and spherical parts of the Φ-field, which correspond to the σ- and π-fields in the vicinity of the vacuum state[10]

$$X_\sigma^{ij} = \frac{\Phi^i\Phi^j}{\Phi^2}\quad,\quad X_\pi^{ij} = \delta^{ij} - \frac{\Phi^i\Phi^j}{\Phi^2}\quad,\quad X_\sigma^2 = X_\sigma\,,\ X_\pi^2 = X_\pi\,,\ X_\sigma X_\pi = X_\pi X_\sigma = 0\,. \tag{3.21}$$

Therefore, the truncated 1-loop ($T1L$) effective action contains different kinetic terms for the bosonic modes in NLO derivative expansion

$$\begin{aligned}\Gamma^{T1L} = \int d^dx \Bigg[& U(\Phi^2) + G(\Phi^2)\,\bar q\Sigma q \\ & + \frac{Z_\pi(\Phi^2)}{2}\left((\partial_\mu\Phi)^2 - \frac{(\Phi\partial_\mu\Phi)^2}{\Phi^2}\right) + \frac{Z_\sigma(\Phi^2)}{2}\frac{(\Phi\partial_\mu\Phi)^2}{\Phi^2} + Z_q(\Phi^2)\,\bar q\not\partial q\Bigg]\,,\end{aligned} \tag{3.22}$$

[9]Note, that the required inverse Z_Φ^{-1} is then simply given by $\left(Z_\Phi^{-1}\right)^{ij} = Z_\sigma^{-1}(\Phi^2)X_\sigma^{ij} + Z_\pi^{-1}(\Phi^2)X_\pi^{ij}$.

[10]This spherical basis for the $O(4)$-fields should in principle enable the system to evolve to the "chiral circle" where only the spherical pion mode is present and fluctuations in the radial sigma direction are suppressed at the groundstate $\Phi = \Phi_0$ if both bosonic Z-factors are considered.

In the following, we will restrict ourselves to the kinetic term $Z_\phi(\Phi^2) \equiv Z_\pi(\Phi^2)$ of the spherical mode, which is often referred to as a uniform wavefunction approximation since it corresponds to the limit $Z_\pi = Z_\sigma$. This approximation is justified, since the wavefunction renormalization factor for the radial mode should vanish in the IR, reflecting that the σ-meson is no physical excitation in the low energy spectrum, as confirmed by the applicability of the nonlinear σ-model and by chiral perturbation theory in this regime. Since the mass of the σ-meson becomes large anyhow the σ-dynamics is strongly suppressed in this regime and the approximation has only a minor impact on physical observables[11]. Nevertheless, it would be very interesting to examine this evolution of the system from a linear to a nonlinear representation of the chiral fields explicitly in an improved approximation that contains different wavefunction renormalization factors for the chiral modes.

The actual derivative expansion of Eq. (3.17) is performed by an expansion of the exponentials in powers of the proper time variable τ, discarding all terms not present in the parametrization Eq. (3.22). The result is a lengthy expression Eqs. (B.1, B.2) given in Appendix B. The main difficulty is to resum the derivative expansion, in order to obtain the full field dependence - without relying on truncations in fields as well. This computation is sketched in the remainder of Appendix B and it is satisfying to obtain a closed expression for the effective action in the considered truncation. A similar calculation has been carried out for ϕ^4-theory [34, 35] and for $O(N)$-models [39].

By comparing the form of Eq. (3.22) with the resummed expression of the derivative expansion of the truncated effective action Γ^{T1L} one obtains, as the result of the computation, expressions for the one loop corrections to the Φ-dependent parameters of the model. These expressions for the effective potential $U(\Phi^2)$, the Yukawa coupling $G(\Phi^2)$ and the wave function renormalization factors $Z_\phi(\Phi^2)$ and $Z_q(\Phi^2)$ are given by

$$U(\Phi^2) = U^{\rm uv} + \frac{1}{32\pi^2}\int \frac{d\tau}{\tau^3}\left[4N_c N_f\, e^{-\tau M_q^2} - \left(3\, e^{-\tau M_\pi^2} + e^{-\tau M_\sigma^2}\right)\right] \tag{3.23}$$

$$\begin{aligned} Z_\phi(\Phi^2) = Z_\phi^{\rm uv} + \frac{Z_\phi}{32\pi^2}\int \frac{d\tau}{\tau^2}\Bigg[&4N_c N_f\, G_\pi^2\, e^{-\tau M_q^2} \\ &+8\, F_\pi^2\, \Lambda^2 \left(\frac{e^{-\tau M_\pi^2} + e^{-\tau M_\sigma^2}}{(M_\sigma^2 - M_\pi^2)^2} - \frac{2}{\tau}\,\frac{e^{-\tau M_\pi^2} - e^{-\tau M_\sigma^2}}{(M_\sigma^2 - M_\pi^2)^3}\right)\Bigg] \end{aligned} \tag{3.24}$$

$$\begin{aligned} G(\Phi^2) = G^{\rm uv} + \frac{1}{16\pi^2}\int \frac{d\tau}{\tau^2}\Bigg[&3\, G\, G_\pi^2\, \frac{e^{-\tau M_\pi^2} - e^{-\tau M_q^2}}{M_q^2 - M_\pi^2} - G\, G_\sigma^2\, \frac{e^{-\tau M_\sigma^2} - e^{-\tau M_q^2}}{M_q^2 - M_\sigma^2} \\ &+ 3\sqrt{Z_\phi}\, Z_q\, G_\pi^{(5)}\, e^{-\tau M_\pi^2} + \sqrt{Z_\phi}\, Z_q\, G_\sigma^{(5)}\, e^{-\tau M_\sigma^2}\Bigg] \end{aligned} \tag{3.25}$$

[11] In the far IR regime $k \lesssim m_\pi$, the effective potential evolves to a convex form. Thereby, for $k \to 0$ also the σ-mass and the four boson coupling λ vanish in the chiral limit. However, this has no impact on other observable quantities like the pion decay constant or the masses of the physical low energy excitations, whose evolution has already ceased in this region.

$$Z_q(\Phi^2) = Z_q^{\rm uv} + \frac{Z_q}{32\pi^2}\int\frac{d\tau}{\tau^2}\Bigg[3\,G_\pi^2\,\frac{\left(1+\tau M_\pi^2\right)e^{-\tau M_\pi^2}-\left(1+\tau M_q^2\right)e^{-\tau M_q^2}}{M_q^2-M_\pi^2} + G_\sigma^2\,\frac{\left(1+\tau M_\sigma^2\right)e^{-\tau M_\sigma^2}-\left(1+\tau M_q^2\right)e^{-\tau M_q^2}}{M_q^2-M_\sigma^2} + 3\,G_\pi^{(4)}\left(1+\tau M_\pi^2\right)e^{-\tau M_\pi^2}+G_\sigma^{(4)}\left(1+\tau M_\sigma^2\right)e^{-\tau M_\sigma^2}\Bigg] \quad (3.26)$$

All masses and couplings appearing in this general action are *effective* Φ*-dependent quantities* - i.e. "potentials" in Φ^2 - representing the renormalization of infinitely many couplings. Explicitly, these quantities include the effective quark mass $M_q(\Phi^2)$ and the effective pion- and sigma-mass $M_\pi(\Phi^2)$ and $M_\sigma(\Phi^2)$, given by

$$M_q^2 = \frac{G^2}{Z_q^2}\,\Phi^2 \quad (3.27)$$

$$M_\sigma^2 = \frac{2}{Z_\phi}\left(\frac{\partial U}{\partial\Phi^2}+2\,\frac{\partial^2 U}{(\partial\Phi^2)^2}\,\Phi^2\right) \quad (3.28)$$

$$M_\pi^2 = \frac{2}{Z_\phi}\,\frac{\partial U}{\partial\Phi^2}\,, \quad (3.29)$$

the effective pion decay constant $F_\pi(\Phi^2)$

$$F_\pi^2 = Z_\phi\,\Phi^2\,, \quad (3.30)$$

and the effective 4-boson coupling $\Lambda(\Phi^2)$ and Yukawa couplings $G_\pi(\Phi^2)$ and $G_\sigma(\Phi^2)$

$$\Lambda \equiv \frac{2}{Z_\phi^2}\,\frac{\delta^2 U}{(\delta\Phi^2)^2}\,, \quad (3.31)$$

$$G_\pi \equiv \frac{G}{\sqrt{Z_\phi}\,Z_q}\,, \quad (3.32)$$

$$G_\sigma \equiv \frac{1}{\sqrt{Z_\phi}\,Z_q}\left(G+2\,\frac{\delta G}{\delta\Phi^2}\,\Phi^2-2\,\frac{G}{Z_q}\,\frac{\delta Z_q}{\delta\Phi^2}\,\Phi^2\right) = \frac{Z_q}{\sqrt{Z_\phi}\,G}\,\frac{\delta M_q^2}{\delta\Phi^2}\,. \quad (3.33)$$

Further this generalized effective action contains higher order couplings of a quark-antiquark pair to two $G_\pi^{(4)}(\Phi^2)$, $G_\sigma^{(4)}(\Phi^2)$ or three bosons $G_\pi^{(5)}(\Phi^2)$, $G_\sigma^{(5)}(\Phi^2)$, given by

$$G_\pi^{(4)} = \frac{1}{Z_\phi\,Z_q}\,\frac{\delta Z_q}{\delta\Phi^2} \quad (3.34)$$

$$G_\sigma^{(4)} = \frac{1}{Z_\phi\,Z_q}\left(\frac{\delta Z_q}{\delta\Phi^2}+2\,\frac{\delta^2 Z_q}{(\delta\Phi^2)^2}\,\Phi^2-4\,\frac{1}{Z_q}\left(\frac{\delta Z_q}{\delta\Phi^2}\right)^2\Phi^2\right) \quad (3.35)$$

$$G_\pi^{(5)} = \frac{1}{Z_\phi^{3/2}\,Z_q}\,\frac{\delta G}{\delta\Phi^2} \quad (3.36)$$

$$G_\sigma^{(5)} = \frac{1}{Z_\phi^{3/2}\,Z_q}\left(3\,\frac{\delta G}{\delta\Phi^2}+2\frac{\delta^2 G}{(\delta\Phi^2)^2}\Phi^2-4\,\frac{G}{Z_q}\frac{\delta Z_q}{\delta\Phi^2}-8\,\frac{\Phi^2}{Z_q}\frac{\delta G}{\delta\Phi^2}\frac{\delta Z_q}{\delta\Phi^2}+4\,\frac{G\,\Phi^2}{Z_q^2}\left(\frac{\delta Z_q}{\delta\Phi^2}\right)^2\right) \quad (3.37)$$

All these effective expressions are partially[12] renormalized quantities which reduce to their physical renormalized values m_q, m_π, m_σ, f_π, λ, g_π, g_σ, $g_\pi^{(4)}$, $g_\sigma^{(4)}$, $g_\pi^{(5)}$ and $g_\sigma^{(5)}$ in the vacuum state, i.e. for $\Phi = \Phi_0 \equiv \langle 0 \,|\Phi|\, 0\rangle$. For instance the renormalized physical masses are given by

$$m_q = M_q(\Phi^2)\big|_{\Phi=\Phi_0} \quad , \quad m_\pi = M_\pi(\Phi^2)\big|_{\Phi=\Phi_0} \quad , \quad m_\sigma = M_\sigma(\Phi^2)\big|_{\Phi=\Phi_0} \quad , \quad \cdots \quad . \tag{3.38}$$

Due to our improved approximation the broken chiral symmetry manifests itself not only in a chiral condensate and different masses for the chiral modes as in simpler approximations, but also in different dynamics of the massless Goldstone bosons and the massive σ-field. As will be seen below from the evolution, this difference becomes especially important in the IR regime.

Although all other effective couplings defined above are renormalized quantities, G is still a bare quantity, that does not contain the appropriate wavefunction renormalization. This is reflected in the appearance of explicit wavefunction renormalization factors where there is no other bare coupling on the right hand side of Eq. 3.25. We already note that from the N_c counting rules [61, 62] of QCD it follows that compared to the terms resulting from fermionic fluctuations, accompanied by an explicit N_c factor from the fermionic trace, all other terms from bosonic and mixed fluctuations are of order $1/N_c$. Hence, in large N_c approximation which will be studied in Section 3.4 only the fermionic dynamics contributes.

As will be discussed in Section 3.3, from the couplings and the propagator structure, a *generating* 1-loop graph associated with a given term in the 1-loop effective action can be determined unequivocally. Since the propagator structure is somewhat hidden in the exponents of the proper time representation in Eqs. (3.23-3.26) we will give the explicit connection after we have derived the flow equations which explicitly include this propagator structure. These 1-loop graphs represent infinitely many elementary graphs which can be generated from them by the attachment of bosonic legs. The effective couplings on the other hand are connected to respective tree level diagrams, which are equally identified with their correct symmetry factors. Therefore, if there is such a simple connection to certain generating graphs, after the event the effective action Eqs. (3.23-3.26) in principle could have been obtained from the translation of the graphical representation. However, the complexity of the respective contributions shows that it is a rather difficult task to consider all contributions with their correct symmetry factors. Therefore, the operator formalism is an advantageous tool, since its mathematical rigidity fully restricts the form of the expressions, whose physical meaning can be checked afterwards by the comparison to the graphical representation.

Finally, because of the great importance of the $O(N)$-model for various applications, we give the general form Eqs. (B.18, B.19) of the $O(N)$-symmetric bosonic part, valid for a theory in d dimensions with a N dimensional scalar field in Appendix B.

3.2 FLOW EQUATIONS OF THE BOSONIZED NJL MODEL

The expression for the effective action computed in the last section is a perturbative one loop result and cannot be expected to hold in the strong coupling regime. In order to deal with strong coupling effects, we apply RG techniques to derive non-perturbative flow equations within the Schwinger proper time scheme presented in Section 2.5. To set up the SPT flow equations of the generalized linear σ-model in the given truncation Eqs. (3.22-3.26)

[12] These effective quantities are only partially renormalized, since they still depend on bare fields Φ.

we introduce a smooth cutoff function $f(k^2\tau)$ depending on the infrared cutoff scale k in the τ-integrals. A general set of functions, that satisfies the necessary requirements stated in Appendix C is given there. For our computations in the vacuum sector, we choose as common cutoff function f for the effective action the function $f^{(2)}$ given by

$$f^{(2)}(k^2\tau) = \left(1 + k^2\tau + \frac{1}{2}(k^2\tau)^2\right) \mathrm{e}^{-k^2\tau} , \tag{3.39}$$

which has been used in several analyses so far [37, 38, 39]. However we will check the dependence on the cutoff function later on. The heat kernel cutoff functions f suppress fluctuations with momenta below the cutoff scale k. Going to $k \to 0$ means to include more and more infrared modes. Finally all modes are included, because of the limiting behavior $f_k \to 1$. The ultraviolet region is left undisturbed due to the extra τ and τ^2 terms in front of the exponential. Therefore now we can extend the τ-integration to the interval $[0, \infty]$[13]. As pointed out in [35], in order to obtain the effect of a Pauli-Villars-cutoff within the proper time scheme, one would need different cutoff functions for different orders in the derivative expansion. On the other hand, as shown in [63], where the influence of the special form of the cutoff on the renormalization group flow has been studied systematically, using the regulator Eq. (3.39) already for the lowest order improves the convergence.

Note further, that since the expression for the effective action can be expressed entirely by renormalized couplings and fields, this cutoff function does not involve any wavefunction renormalization factors (cf. Appendix B). With the cutoff function f, all terms in the effective action become functions of the cutoff scale k

$$\Gamma^{T1L} = \int d^dx \left[U(\Phi^2, k) + \tfrac{1}{2} Z_\phi(\Phi^2, k) \left(\partial_\mu \Phi\right)^2 + G(\Phi^2, k)\, \bar{q}\Sigma q + Z_q(\Phi^2, k)\, \bar{q}\partial\!\!\!/ q\right] . \tag{3.40}$$

For instance the cutoff dependent effective potential reads

$$U(\Phi^2, k) = U^{\mathrm{uv}} + \frac{1}{32\pi^2} \int_0^\infty \frac{d\tau}{\tau^3} f(k^2\tau) \left(4N_f N_c\, e^{-\tau M_q^2} - \left(3\, e^{-\tau M_\pi^2} + e^{-\tau M_\sigma^2}\right)\right) . \tag{3.41}$$

It is easy to find the flow equation for U by taking the derivative with respect to the cutoff parameter k

$$k\frac{\partial U}{\partial k} = \frac{1}{32\pi^2} \int \frac{d\tau}{\tau^3}\, k \frac{\partial f(k^2\tau)}{\partial k} \left(4N_f N_c\, e^{-\tau M_q^2} - \left(3\, e^{-\tau M_\pi^2} + e^{-\tau M_\sigma^2}\right)\right) . \tag{3.42}$$

Corresponding to the general discussion in Section 2.5 the RG improvement is obtained by the replacement of the masses and couplings of the classical action which appear in the exponents in Eqs. (3.41, 3.42) by the masses and couplings of the *effective* action Γ^{T1L}. Thereby the masses and couplings on the right hand side of Eq. (3.42) also become scale dependent, e.g. $M_\pi^2(\Phi) \to M_\pi^2(\Phi, k)$ and the differential equation (3.42) becomes a closed equation, since all masses are calculated from $U(\Phi, k)$. This replacement turns the one loop equation into a renormalization group improved flow equation, which goes beyond the standard one loop renormalization group running and includes higher loop terms successively into the proper time integral. Therefore it is capable to include non-perturbative physics in the strong coupling region.

[13] Due to the extra τ terms in front of the exponential the integral diverges in the UV region only through an additional term $\sim \log \Lambda^2$.

Finally we can analytically perform the τ integration using the set of integrals from Eq. (C.3) which gives back the characteristic propagator structure of the one loop fluctuations. Performing the analog replacement and integration procedure for all coefficients of the derivative expansion Eqs. (3.23-3.26) one obtains the flow equations for the other Φ^2-dependent model parameters G, Z_q and Z_ϕ, which altogether form a coupled system of four nonlinear partial differential equations[14]

$$k\frac{\partial U}{\partial k} = -\frac{1}{32\pi^2}\left(4N_cN_f\,\frac{k^6}{k^2+M_q^2} - 3\,\frac{k^6}{k^2+M_\pi^2} - \frac{k^6}{k^2+M_\sigma^2}\right) \tag{3.43}$$

$$k\frac{\partial Z_\phi}{\partial k} = -\frac{Z_\phi}{16\pi^2}\left(4N_cN_f\,G_\pi^2\,\frac{k^6}{\left(k^2+M_q^2\right)^3} + 4\,\Lambda^2\frac{k^6F_\pi^2}{\left(k^2+M_\sigma^2\right)^2\left(k^2+M_\pi^2\right)^2}\right) \tag{3.44}$$

$$\begin{aligned} k\frac{\partial G}{\partial k} = -\frac{1}{16\pi^2}\Bigg(&3\,G\,G_\pi^2\frac{k^6\left(2k^2+M_q^2+M_\pi^2\right)}{\left(k^2+M_q^2\right)^2\left(k^2+M_\pi^2\right)^2} - G\,G_\sigma^2\frac{k^6\left(2k^2+M_q^2+M_\sigma^2\right)}{\left(k^2+M_q^2\right)^2\left(k^2+M_\sigma^2\right)^2} \\ &+ 3\sqrt{Z_\phi}Z_qG_\pi^{(5)}\frac{k^6}{\left(k^2+M_\pi^2\right)^2} + \sqrt{Z_\phi}Z_qG_\sigma^{(5)}\frac{k^6}{\left(k^2+M_\sigma^2\right)^2}\Bigg) \end{aligned} \tag{3.45}$$

$$\begin{aligned} k\frac{\partial Z_q}{\partial k} = -\frac{Z_q}{32\pi^2}\Bigg(&3\,G_\pi^2\left(3\frac{k^6\left(M_q^2+M_\pi^2\right)}{\left(k^2+M_q^2\right)^2\left(k^2+M_\pi^2\right)^2} - 2\frac{k^8\left(M_q^2-M_\pi^2\right)^2}{\left(k^2+M_q^2\right)^3\left(k^2+M_\pi^2\right)^3}\right) \\ &+ G_\sigma^2\left(3\frac{k^6\left(M_q^2+M_\sigma^2\right)}{\left(k^2+M_q^2\right)^2\left(k^2+M_\sigma^2\right)^2} - 2\frac{k^8\left(M_q^2-M_\sigma^2\right)^2}{\left(k^2+M_q^2\right)^3\left(k^2+M_\sigma^2\right)^3}\right) \\ &+ 3\,G_\pi^{(4)}\frac{k^6\left(k^2+3M_\pi^2\right)}{\left(k^2+M_\pi^2\right)^3} + G_\sigma^{(4)}\frac{k^6\left(k^2+3M_\sigma^2\right)}{\left(k^2+M_\sigma^2\right)^3}\Bigg) \end{aligned} \tag{3.46}$$

In this set of equations all the masses and couplings are functions of the bare $O(4)$ invariant Φ^2 and the scale k. The heat kernel method gives these equations in a very simple form. All contributions to the flow consist of a dimensionless numerical factor, the couplings and a threshold function which compares the effective masses with the cutoff scale. Since the IR parameter k acts as a mass cutoff the propagator structure of the different loop contributions is still recognizable. The exact connection to the respective one loop graphs will be given in Section 3.3. Furthermore, due to the extra terms in the cutoff function $f(k^2\tau)$ the sensitivity to the ultraviolet is avoided and the differential equations above contain all information about the ultraviolet physics in the initial conditions.

To lowest order where G, Z_ϕ and Z_q are ϕ-independent the flow equations Eqs. (3.44-3.46) simplify considerably, since in this case the effective couplings reduce to[15]

$$G \approx g \quad , \quad G_\pi \approx G_\sigma \approx g_\pi \quad , \quad G_\pi^{(4)} \approx G_\sigma^{(4)} \approx G_\pi^{(5)} \approx G_\sigma^{(5)} \approx 0\,. \tag{3.47}$$

Again, the Yukawa coupling G is a bare quantity that does not include wavefunction renormalization. By the introduction of appropriate anomalous dimensions η_ϕ and η_q

$$\eta_\phi \equiv -\frac{k}{Z_\phi}\frac{\delta Z_\phi}{\delta k} \quad , \quad \eta_q \equiv -\frac{k}{Z_q}\frac{\delta Z_q}{\delta k} \tag{3.48}$$

[14]Note that the respective flow equation for the fermionic wavefunction renormalization factor previously given in [70] for Φ-independent Z_q was incomplete, which resulted in a different threshold function.

[15]Here, $g_\pi \equiv g_R$ is just the renormalized version of the common field independent Yukawa coupling g for both chiral modes.

an equation for the renormalized Yukawa coupling G_π can be given[16]

$$k\frac{\delta G_\pi}{\delta k} = \frac{1}{\sqrt{Z_\phi}\, Z_q} k\frac{\delta G}{\delta k} + \tfrac{1}{2}\eta_\phi\, G_\pi + \eta_q\, G_\pi\,. \tag{3.49}$$

However, in the expressions for the masses and the other couplings appearing on the right hand sides of the flow equations, the wavefunction renormalization constants themselves still enter. Thereby, compared to simpler approximations, where only the lowest order couplings are present, the number of differential equations is not reduced due to the fact that Z-factors enter the other equations only in the form of their anomalous dimension, which are given analytically. The flow for only renormalized couplings does complicate the flow equations since also equations for the other appearing couplings, like G_σ (cf. Eq. 3.31), have to be introduced. Therefore, the above form seems to be the simplest way to give the flow in the considered approximation.

Due to the renormalization group improvement every vertex in an effective averaged theory, obtained by integrating out part of the quantum fluctuations, has a substructure on a smaller spacetime or larger momentum scale. Thereby graphs of arbitrary loop order, containing loops at different scales, are generated in the flow and induce very complex dynamics. Since each mesonic and mixed loop is suppressed by a factor of $1/N_c$ (cf Section 3.4), the averaged effective action contains contributions of arbitrary orders in $1/N_c$, in strong contrast to the unimproved flow.

We should mention again, that compared with other approaches, the method of an renormalization group improvement does not lead to an exact flow equation in the case of the proper time regularization [30], because it involves already a truncated effective action. However, since exact flow equations just as well have to rely on truncations in the end, they may not always give better results in a given approximation. Especially, as SPT flow equations are often mathematically simpler. Furthermore, since the regularization of the effective action effects only the momentum structure, possible discrepancies from the exact result due to the proper time regularization scheme can appear only in the threshold functions of the flow equations[17]. However, there is a large freedom in the choice of these threshold functions also in exact RG approaches[18].

An additional flow equation which determines the chiral condensate can be obtained by differentiation of the partition function Z (Eq. (3.1)) with respect to an appropriately introduced source term $\Delta\bar{q}q$ which probes the chiral condensate

$$\langle\bar{q}q\rangle = \frac{\partial}{\partial\Delta}\log Z(\Delta)\bigg|_{\Delta=0}\,. \tag{3.50}$$

This flow equation is derived analogously to the other flow equations by introduction of the Schwinger proper time cutoff and reads

$$k\frac{\partial\langle\bar{q}q\rangle}{\partial k} = \frac{N_f N_c}{4\pi^2}\frac{k^6\, M_q}{(k^2+M_q^2)^2}\,. \tag{3.51}$$

[16]Here, the additional wavefunction renormalization factors in front of $k\frac{\delta G}{\delta k}$ just give the right hand side of Eq. (3.45) in terms of renormalized quantities only.

[17]Therefore, it should be possible to transfer the results obtained in this work to the exact RG formalism, by replacing the "elementary" couplings in the exact RG flow equations by the effective couplings given above.

[18]In particular the application of different threshold functions leads to different results as long as approximations are involved.

However, it is only driven by the flow of the other equations but does not couple back and influence the flow - as should be the case for a derived quantity.

As addressed in Appendix D the system of coupled partial differential equations (3.43)-(3.46) is hard to solve, even numerically. Discretizing the Φ^2-parameter on a grid transforms the system of partial differential equations for the variables $U(\Phi^2,k), g(\Phi^2,k),\ldots$ into a system of ordinary differential equations of variables $U_i(k), g_i(k),\ldots$. Even for a small grid such a discretization yields a system with a large number of coupled equations. For the treatment of quark matter at finite temperature and or density, as discussed in the next chapter, this procedure is necessary in order to deal with a possible first order phase transition where the effective potential exhibits two minima [28, 38]. However, in vacuum it is much less demanding to expand the variables at every evolution step in a Taylor series around the respective vacuum expectation value $\Phi_0^2(k)$, leaving the possibility to treat different variables in each case with the necessary approximation. Corresponding to the general discussion in Appendix D where also the form of the equations for the expansion coefficients is discussed, the Φ^2-dependent model parameters are expanded to a given order $p_{\max}$ suggested by the mass dimension of the respective terms. Since the effective potential evolves under renormalization group flow from a trivial to a nontrivial form, we consider two truncations in this case, given by

$$U(\Phi^2,k) = \sum_{i=1}^{p_{\max}} v_i(k)\,\Phi^{2i} \tag{3.52}$$

for $k > k_{\chi\mathrm{SB}}$ and

$$U(\Phi^2,k) = \sum_{i=2}^{p_{\max}} v_i(k)\,(\Phi^2-\Phi_0^2(k))^i \tag{3.53}$$

for $k < k_{\chi\mathrm{SB}}$, where $k_{\chi\mathrm{SB}}$ is the scale at which the evolution enters the chiral broken regime, characterized by the fact that v_1 becomes negative and the potential takes a nontrivial minimum Φ_0. We do not include the constant vacuum energy v_0, because we are only interested in vacuum properties of strong interaction in this work, but not in its influence on gravitation or its thermal aspects[19]. Since the other parameters of the model are accompanied by terms of mass dimension four (cf. Eq. (3.22)) they are correspondingly expanded up to order $p_{\max}-2$

$$G(\Phi^2,k) = \sum_{i=0}^{p_{\max}-2} \gamma_i(k)\,(\Phi^2-\Phi_0^2(k))^i\ ,\ Z_\pi(\Phi^2,k) = \sum_{i=0}^{p_{\max}-2} \zeta_i^\pi(k)\,(\Phi^2-\Phi_0^2(k))^i\ ,\quad \cdots\ . \tag{3.54}$$

Although the full flow is posed for bare quantities[20], in order to obtain renormalized physical quantities one has to express the theory by renormalized fields q_{R} and Φ_{R}. This is done by rescaling the fields to absorb the wavefunction renormalization factors in front of the kinetic terms. The renormalized quark and meson fields are related to the bare fields as

$$q_{\mathrm{R}} = \sqrt{Z_q}\,q\ , \tag{3.55}$$

$$\Phi_{\mathrm{R}} = \sqrt{Z_\phi}\,\Phi\ . \tag{3.56}$$

[19] In opposition, in case of thermal systems this constant part is the crucial quantity, since it represents the negative pressure.

[20] The corresponding bare quantities are the effective potential $U(\Phi^2)$ and the Yukawa coupling $G(\Phi^2)$ where bare means here that they are functions of bare fields and do not incorporate the appropriate wavefunction renormalization. Nevertheless the right hand sides of the flow equations have already been expressed - as far as possible - in terms of renormalized effective quantities.

Thereby one obtains the renormalized effective potential $U_{\rm R}(\Phi_{\rm R}^2)$ and the renormalized effective Yukawa coupling $G_{\rm R}(\Phi_{\rm R}^2)$ which contain the complete physical content of the model in the regarded approximation

$$U_{\rm R}(\Phi_{\rm R}^2) \equiv U(\Phi^2) \ , \tag{3.57}$$

$$G_{\rm R}(\Phi_{\rm R}^2) \equiv \frac{1}{\sqrt{Z_\phi}\, Z_q} G(\Phi^2) \ . \tag{3.58}$$

The most important quantities that can be obtained out of these functions are however already given in Eqs. (3.27-3.34) as they enter in the dynamics. Note, especially that from the above definitions it follows that $g_{\rm R} = G_{\rm R}(f_\pi^2) = g_\pi$.

Although the above equations Eqs. (3.43)-(3.46) describe the generic case of the generalized linear σ-model, we will use them in this work in order to examine the NJL model presented in Section 2.6. The NJL model is non-renormalizable and therefore includes an explicit UV cutoff scale $k_{\rm uv}$ at which the model is approximately assumed to hold classically. The effect of quantum fluctuations at larger scales is assumed to be included into the couplings at the UV scale[21]. The requirement that the flow Eqs. (3.43)-(3.46) should correspond to that of a bosonized version of the NJL model fixes nearly the complete freedom in the choice of the initial conditions. Therefore, we consider the action Eq. (3.22) to be preserved during the evolution and choose the UV starting values fixed by the bosonization procedure[22]

$$Z_\phi^{\rm uv} = 0 \quad , \quad Z_q^{\rm uv} = 1 \quad , \quad G_{\rm uv} = 1 \ , \tag{3.59}$$

and the UV potential

$$U_{\rm uv} = \frac{m_{\rm uv}^2}{2}\,\Phi^2 - \delta\,\sigma \ , \tag{3.60}$$

in order to obtain Eq. (2.27) as UV lagrangian.

At this point, we find it instructive to give explicitly the flow equations which follow from Eq. (3.43) if one assumes the simplest possible case of a quartic potential in local potential approximation (LPA)[23]. This case has been considered in [37]. The flow of the mesonic mass $m^2 = 2v_1$ and of the four meson coupling $\lambda = 4v_2$ in the symmetric regime is given by

$$k\frac{\partial m^2}{\partial k} = -\frac{3k^2}{8\pi^2}\frac{\lambda}{(1+m^2/k^2)^2} + \frac{N_f N_c k^2}{4\pi^2}\,g^2 \ , \tag{3.61}$$

$$k\frac{\partial \lambda}{\partial k} = \frac{3}{2\pi^2}\frac{\lambda^2}{(1+m^2/k^2)^3} - \frac{N_f N_c}{2\pi^2}g^4 \ , \tag{3.62}$$

and in the broken regime one finds

$$k\frac{\partial \Phi_0^2}{\partial k} = \frac{3k^2}{16\pi^2}\left[1 + \frac{1}{\left(1+2\lambda\Phi_0^2/k^2\right)^2}\right] - \frac{N_c N_f}{4\pi^2}\frac{k^2 g^2}{\lambda}\left[\frac{1}{\left(1+g^2\Phi_0^2/k^2\right)^2}\right] \ , \tag{3.63}$$

$$k\frac{\partial \lambda}{\partial k} = \frac{3}{8\pi^2}\left[\lambda^2 + \frac{3\lambda^2}{\left(1+2\lambda\Phi_0^2/k^2\right)^3}\right] - \frac{N_c N_f}{2\pi^2}g^4\left[\frac{1}{\left(1+g^2\Phi_0^2/k^2\right)^3}\right] \ . \tag{3.64}$$

[21] We would like to stress again that this is only a crude approximation for the physics at that scale, which could be governed by other more complicated interactions. However, the aim of the present work is to examine to what extend this simplification is reasonable.

[22] The specific choice of the UV value for the Yukawa coupling G will be discussed in the context of a numeric solution in Section 3.5.

[23] In the LPA approximation, the Yukawa coupling as well as the wavefunction renormalization factors do not evolve. Thereby g is a fixed constant and $Z_\phi = Z_q = 1$ during the entire flow.

In more general cases it is hardly possible to give the respective equations explicitly due to their sheer extend. We derive these equations by means of a computer algebra system [64] from the general ones Eqs. (3.43-3.46) whereby the resulting expressions fill tens of pages.

It is worth noting, that although the LPA is a valid approximation scheme for the linear σ-model, this is not the case for the NJL model, since it does not fulfill the correct initial condition[24] $Z_\phi = 0$. In this sense the linear σ-model is more general than the NJL model. However, this generality comes along with the drawback of arbitrariness, since there are more free unknown parameters in the theory, that cannot be specified by experimental input. For instance in a quartic LPA approximation [37] one has to fix the three free parameters m^2, λ and g. This culminates in a mean field solution to the linear σ model, where *all* free parameters have to be fitted[25].

3.3 Diagrammatic classification of the dynamics

Although it contains arbitrary many couplings, the 1-loop contributions to the effective action can be classified by a small set of generating 1-loop Feynman diagrams[26]. These graphs are uniquely associated with respective terms in the effective action (cf. Eqs. (3.43-3.46)) and themselves represent infinitely many elementary graphs. This is achieved by the introduction of the effective masses and couplings Eqs. (3.27-3.34), which are directly related to respective tree level diagrams.

The effective potential U has the most simple graphical representation, since it has no external legs and is therefore given by the fermionic and the bosonic loop, corresponding to the propagators in Eq. (3.23).

Due to the symmetry which only involves Φ^2, derivatives of the effective action with respect to Φ^2 yield the one loop corrections to bosonic masses and couplings which are represented by attaching an even number of bosonic legs to these loops[27]. In the case of σ-lines, one of the two legs can also couple to the condensate, denoted by a cross. Exemplary, a graph generated from the fermionic loop could take the following form

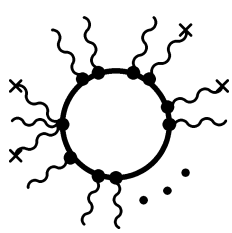

[24]The same holds for a leading order derivative expansion approximation, where both the effective potential and the Yukawa coupling evolve.

[25]More precisely, the complete potential U must be specified, whereas it is generated from the dynamics in the other approximation schemes.

[26]In the following we will represent quarks by straight lines, whereas both bosonic modes are represented by wavy lines.

[27]If there is a small explicit symmetry breaking in addition diagrams involving single external σ-legs are possible.

Here, all possible higher order couplings can be involved, as for instance the shown coupling of three bosons to a quark bilinear. In the case of a fermionic line vertices usually come in pairs, since attaching bosonic lines by derivation with respect to Φ^2 involves always two vertices[28]. On the other hand, if all lines at a vertex couple to the condensate this vertex contributes to the mass of the particle. So the infinite sum of couplings to the condensate Φ_0 just shifts the meson masses and quark masses to their respective values in the broken vacuum. This is represented for instance in the case of the meson propagator by the modified propagator

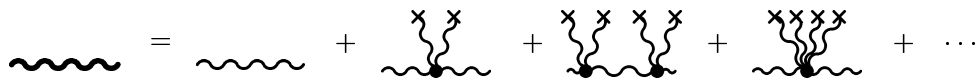

This generating nature of the one loop graphs as shown for the contributions to the effective potential holds for all other graphs discussed in the following.
The diagrams contributing to the Yukawa-coupling G in Eq. (3.45) have three external legs: a quark, an anti-quark and a bosonic one. The main contribution comes from the mixed loop[29] with a bosonic and a fermionic propagator, but the purely bosonic loop also adds a correction. The associated two diagrams are given by the one loop graphs

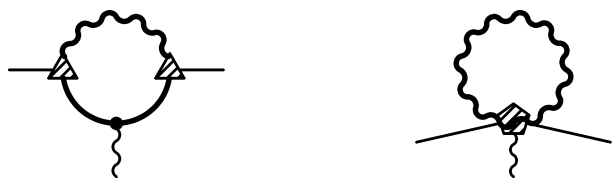

Note, that the power of the propagators in the flow equations results from the regularization and is not connected to the actual number of propagators in the respective diagrams [32]. Since the σ-mode condenses in vacuum, the respective Yukawa coupling for this mode is not simply the Yukawa coupling appearing in the UV-action, but an effective coupling represented by tree level graphs. Explicitly the renormalized effective Yukawa couplings G_π and G_σ read

$$G_\pi \equiv \frac{g}{\sqrt{Z_\pi}\, Z_q} \quad ,$$

$$G_\sigma \equiv \frac{g}{\sqrt{Z_\sigma}\, Z_q} + \frac{2\,\Phi^2}{\sqrt{Z_\sigma}\, Z_q}\frac{\delta g}{\delta \Phi^2} - \frac{2\,g\,\Phi^2}{\sqrt{Z_\sigma}\, Z_q}\frac{\delta Z_q^2}{\delta \Phi^2} = \frac{Z_q}{\sqrt{Z_\sigma}\, g}\frac{\delta M_q^2}{\delta \Phi^2} \quad ,$$

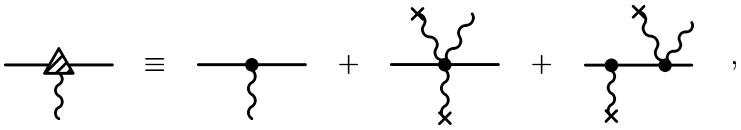

where the formal expressions for the parts of the renormalized couplings in the respective columns are represented by the tree level diagrams in the line below[30]. The 5 particle effec-

[28] This is represented by the grouping of vertices in the previous graph.

[29] The reason that in the respective graph two different kind of Yukawa couplings appear is that it renormalizes the bare effective Yukawa coupling G represented by a simple dot, whereas the two other effective couplings are partly renormalized ones.

[30] Explicitly, the first diagram can involve both π- and σ-lines, whereas the two following ones involve condensates and are restricted to an external σ-line.

tive coupling[31] occurring in the bosonic contribution is given by the following tree level graphs

$$G_\pi^{(5)} \equiv \frac{1}{\sqrt{Z_\pi^3}Z_q}\frac{\delta g}{\delta\Phi^2} \ ,$$

$$G_\sigma^{(5)} \equiv \frac{3}{\sqrt{Z_\sigma^3}Z_q}\frac{\delta g}{\delta\Phi^2} + \frac{2\,\Phi^2}{\sqrt{Z_\sigma^3}Z_q}\frac{\delta^2 g}{(\delta\Phi^2)^2} - \frac{4}{\sqrt{Z_\sigma^3}\,Z_q^2}g\frac{\delta Z_q^2}{\delta\Phi^2} - \frac{8\,\Phi^2}{\sqrt{Z_\sigma^3}Z_q^2}\frac{\delta g}{\delta\Phi^2}\frac{\delta Z_q}{\delta\Phi^2} + \frac{4\,\Phi^2}{\sqrt{Z_\sigma^3}Z_q^3}\,g\left(\frac{\delta Z_q}{\delta\Phi^2}\right)^2,$$

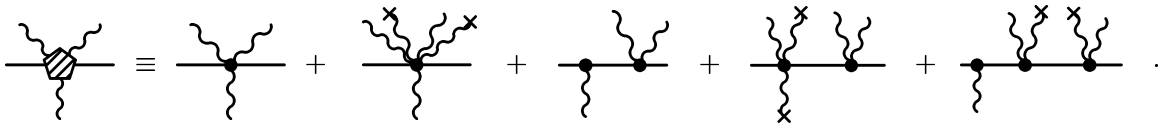

According to the propagator structure and the couplings in Eq. (3.44), the bosonic wave function renormalization factor Z_ϕ receives one loop corrections represented by the following two graphs involving a fermionic and a bosonic loop

The effective 4 boson coupling is simply obtained by differentiation of the effective potential

$$\Lambda \equiv \frac{2}{Z_\phi^2}\frac{\delta^2 U}{(\delta\Phi^2)^2} \ ,$$

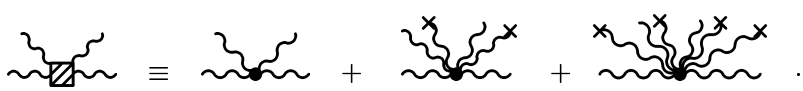

Finally, the diagrams contributing to the fermionic wavefunction renormalization factor Z_q in Eq. (3.46) have two external fermionic legs and resemble the graphs for the Yukawa coupling. Again the renormalization comes from the mixed loop with a minor correction from the bosonic loop

where the effective 4 particle coupling in this case is depicted by the following graphs

[31] The subscript corresponds to the two bosonic lines which are attached to the loop and not to the third line, which can be either of the mesons.

$$G_\pi^{(4)} \equiv \frac{1}{\sqrt{Z_\pi}\, Z_q^2} \frac{\delta Z_q}{\delta \Phi^2} \quad ,$$

$$G_\sigma^{(4)} \equiv \frac{1}{\sqrt{Z_\sigma}\, Z_q^2} \frac{\delta Z_q}{\delta \Phi^2} + \frac{2\,\Phi^2}{\sqrt{Z_\sigma}\, Z_q^2} \frac{\delta^2 Z_q}{(\delta \Phi^2)^2} - \frac{4\,\Phi^2}{\sqrt{Z_\sigma}\, Z_q^2} \left(\frac{\delta Z_q^2}{\delta \Phi^2} \right)^2 ,$$

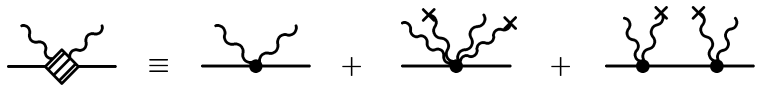

Within the renormalization group all these graphs are only the one loop corrections in an infinitesimal renormalization group step. Thereby, each vertex at a given scale includes corrections from the whole previous evolution which can contain arbitrary complex graphs that are built from these basic building blocks given above. This creates a very sophisticated dynamics that enables to treat non-perturbative regimes like the groundstate of strong interaction.

3.4 THE NJL-MODEL IN LARGE N_c

Since the number of colors N_c is the only accessible expansion parameter of the QCD action [61, 62] in the general case, an expansion in powers of $1/N_c$ is promising even though the physical number of colors $N_c = 3$ is not really a large number. Especially, in the case of the NJL model this approximation scheme has been extremely successful [50, 51] and the model chiefly owes the importance that it has in low energy physics to this method. Of particular relevance in this respect is the lowest expansion order given by the large N_c approximation which enabled to make revisable physical predictions already in the original work [49] within a self consistent solution scheme. During the last decades, work on the NJL model in the large N_c approximation, has been extensive [50, 51].

Although the derived flow equations (3.43-3.46) contain considerably more dynamics, than the large N_c approximation it is useful to consider the renormalization group approach in this standard approximation scheme which provides the simplest solution of the model. On the one hand to establish a connection to previous analyses and on the other hand to be able to compare the results obtained with the solution of the complete set of equations (3.43-3.46) discussed in the next section. Moreover, the main aim of this section is to clarify the connection between the self-consistent solution method of the NJL model via gap equations and the RG flow equations for the associated linear σ-model in large N_c approximation.

RG in large N_c and NJL gap-equation

In the large N_c limit only the fermion loop is relevant. Since the NJL effective action involves a trace over quark fields it is proportional to N_c and therefore the NJL coupling g_{NJL} is proportional to $1/N_c$. This also has to hold in the bosonized case Eq. (2.27). Assuming that the meson masses are independent of N_c, one obtains from Eq. (2.30) that the Yukawa coupling g behaves $\propto 1/\sqrt{N_c}$, in the same way as the QCD coupling constant. This implies that the meson fields Φ scale as $\mathcal{O}(\sqrt{N_c})$, which in turn means that the effective 4-meson coupling λ should be proportional to $1/N_c$.

Due to the large N_c behavior, the quark contribution in the flow equation of the potential U Eq. (3.43) is of order N_c, whereas the meson loop term is of order one and can be neglected. Also, for Z_ϕ Eq. (3.44) the second term can be dropped since it is of order $1/N_c$ compared to

the first one which is of order one. The bare Yukawa-coupling G (Eq. (3.45)) and the wave function renormalization factor Z_q (Eq. (3.46)) do not evolve at all, since the right hand sides of the evolution equations are of higher order in $1/N_c$ than the left hand sides, which reflects that the corresponding fluctuations are given by mixed loops.

Therefore, the large N_c flow equations read ($Z_q = g = 1$)

$$k\frac{\partial U}{\partial k} = -\frac{N_f N_c}{8\pi^2}\frac{k^6}{k^2+M_q^2}\,, \tag{3.65}$$

$$k\frac{\partial Z_\phi}{\partial k} = -\frac{N_f N_c}{4\pi^2}\frac{k^6}{(k^2+M_q^2)^3}\,. \tag{3.66}$$

The right hand sides of these equations only depend on the quark mass Eq. (3.27), but not on the potential U or the wave function renormalization factor Z_ϕ, therefore they completely decouple and can be integrated analytically[32]. In particular, these equations do not contain a RG improvement. Note that in the large N_c limit we have $M_q^2 = \Phi^2$ and the integrals read

$$\int_{U_{\rm uv}}^{U(k)} dU = -\frac{N_f N_c}{8\pi^2}\int_{k_{\rm uv}}^{k}\frac{\kappa^5}{\kappa^2+\Phi^2}d\kappa\,, \tag{3.67}$$

$$\int_{Z_\phi^{\rm uv}}^{Z_\phi(k)} dZ_\Phi = -\frac{N_f N_c}{4\pi^2}\int_{k_{\rm uv}}^{k}\frac{\kappa^5}{(\kappa^2+\Phi^2)^3}d\kappa\,. \tag{3.68}$$

Neglecting Φ-independent terms, the integral for the potential U yields

$$U(\Phi,k) = U_{\rm uv}(\Phi) + \frac{N_f N_c}{16\pi^2}\left(\Phi^4\log\left(\frac{k_{\rm uv}^2+\Phi^2}{k^2+\Phi^2}\right) - \Phi^2(k_{\rm uv}^2-k^2)\right)\,, \tag{3.69}$$

where the UV potential is given by Eq. (3.60). For comparison with the standard NJL approximation we will work in the following in the chiral limit $m_c = \delta = 0$, but since the term linear in σ does not get renormalized [15], the following computation is also valid for explicit symmetry breaking, which will be discussed subsequently.

Using $Z_\phi^{\rm uv} = 0$ as starting value, the equation for Z_ϕ can be integrated in the same way giving a slightly longer expression

$$Z_\phi(\Phi,k) = \frac{3}{8\pi^2}\left(2\,\log\left(\frac{k_{\rm uv}^2+\Phi^2}{k^2+\Phi^2}\right) - \frac{\left(k_{\rm uv}^2-k^2\right)\,\Phi^2\,\left(4\,k^2\,k_{\rm uv}^2+3\,\left(k^2+k_{\rm uv}^2\right)\,\Phi^2+2\,\Phi^4\right)}{\left(k^2+\Phi^2\right)^2\left(k_{\rm uv}^2+\Phi^2\right)^2}\right)\,. \tag{3.70}$$

Eqs. (3.69, 3.70) are the exact analytic solution of the large N_c flow equations for a given scale k. To obtain the physical vacuum expectation value Φ_0 of the field at the IR scale $k=0$, the potential has to be minimized with respect to Φ:

$$\left.\frac{\delta U(\Phi,k)}{\delta\Phi^2}\right|_{\Phi=\Phi_0} = \frac{m_{\rm uv}^2}{2} + \frac{N_f N_c}{16\pi^2}\left(2\Phi_0^2\log\left(\frac{k_{\rm uv}^2+\Phi_0^2}{\Phi_0^2}\right) - \frac{k_{\rm uv}^2(k_{\rm uv}^2+2\Phi_0^2)}{k_{\rm uv}^2+\Phi_0^2}\right) = 0\,. \tag{3.71}$$

[32] Such an analytic solution is possible also in other theories within the large N approximation [22].

This equation cannot be solved analytically due to the non algebraic logarithmic term. As we will show, it corresponds to the self consistent NJL gap equation[33], determining the physical quark mass $m_q = \Phi_0(k=0)$ as the minimum of the potential Eq. (3.69). The full potential provides more information than the NJL gap equation, since it gives arbitrary higher order moments of Φ besides its vacuum expectation value. This allows to compute for instance the spectrum of the Dirac operator [65] which will be presented in Section 3.6.

The NJL model in large N_c approximation is usually considered in a self consistent approach which leads to the NJL gap equation [49, 50, 54]. This equation determines the constituent quark mass and is usually regularized by a hard cutoff. Furthermore, to make contact with chiral degrees of freedom there is an additional equation that determines the mesonic wave function renormalization factor Z_ϕ, once the constituent quark mass is known [54].

To compare with our flow equations we regularize these equations in a Schwinger proper time scheme using the heat kernel cutoff. Since the heat kernel cutoff $f^{(n)}(k^2\tau)$ acts like a IR cutoff function, the desired UV regulation is given by the function $(1 - f^{(n)}(k_{\rm uv}^2\tau))$, which cuts off momenta larger than $k_{\rm uv}$. The gap equation and the determining equation for Z_ϕ read

$$1 = 8GN_cN_f \int_0^\infty d\tau \int \frac{d^4p}{(2\pi)^4} \; e^{-\tau(p^2+m_q^2)}(1 - f^{(n)}(k_{\rm uv}^2\tau)) \; , \tag{3.72}$$

$$Z_\phi = 2N_cN_f \int_0^\infty \tau d\tau \int \frac{d^4p}{(2\pi)^4} \; e^{-\tau(p^2+m_q^2)}(1 - f^{(n)}(k_{\rm uv}^2\tau)) \; . \tag{3.73}$$

The integrals appearing in these equations can be integrated analytically. With Eq. (2.30) the NJL coupling G is connected to the UV meson mass $m_{\rm uv}^2$. For the cutoff $f^{(2)}$ the integrated form of the gap equation Eq. (3.72) is analytically equal to Eq. (3.71). Similarly, the determining equation for Z_ϕ Eq. (3.73) yields Eq. (3.70) evaluated at $\Phi^2 = \Phi_0^2$ after integration. This connection between the equations in the RG scheme and the equations in the self consistent NJL approach holds for all cutoff functions $f^{(n)}$ Eq. (C.9), provided both schemes are regularized with the same cutoff. This shows that the RG flow result is *exactly identical* to the standard NJL approach in large N_c approximation.

Although the vacuum has to be computed numerically, there are two quantities, that allow an analytic solution. The first one is the scale $k_{\chi SB}$, where the system evolving from the UV enters the chiral broken regime, which is given as the solution of the equation

$$\left.\frac{\delta U(\Phi,k)}{\delta\Phi^2}\right|_{\Phi^2=0} = 0 \; , \tag{3.74}$$

and takes the simple form

$$k_{\chi\rm SB} = \sqrt{k_{\rm uv}^2 - \frac{8\pi^2}{N_cN_f} m_{\rm uv}^2} \; . \tag{3.75}$$

The other one is the ratio m_σ/m_q, which results from Eqs. (3.27, 3.38) using the analytic expressions for U and Z_ϕ at $k = 0$ and $\Phi = \Phi_0$. It is exactly 2 in large N_c, as known from the standard NJL approach [54, 66]. This implies that the same holds for the ratio of the couplings $\frac{\lambda}{g^2} = 2$.

[33] However it is not directly equivalent to a mean field approximation, since in a mean field approximation the complete IR potential has to be specified, whereas the characteristic logarithmic term in Eq. (3.69) arises out of the quark dynamics and it is impossible to fit it by a parametrization of the potential with a finite number of local couplings.

Numerical solution

Although the physical number of three colors is not really large it is known from standard NJL computations, that the large N_c limit gives a reasonable approximation. For a numerical solution, we adjust the UV parameters to reproduce standard values used in the self consistent NJL approach [54] of $m_q = 320$ MeV and $f_\pi = 93$ MeV in the case of an explicit chiral symmetry breaking. This case of explicitly broken chiral symmetry will be discussed subsequently. The corresponding initial parameters for the RG evolution read

$$\begin{aligned} k_{\rm uv} &= 1037 \text{ MeV} , \\ m_{\rm uv} &= 228.0 \text{ MeV} , \\ Z_\phi^{\rm uv} &= 0 , \end{aligned} \tag{3.76}$$

and $Z_q = g = 1 = \text{const}$. This corresponds to a four fermion coupling of $g_{\rm NJL} = 9.62$ GeV^{-2}. With these initial values we calculate the effective potential from Eq. (3.69) and the wave function renormalization from the corresponding expression for Z_ϕ. The result is the renormalized effective potential $U_{\rm R}$, which is shown in Fig. 3.1 in the chiral limit as a function of the field $\Phi_{\rm R}$ and the scale k. From this potential we compute the scale dependent expectation value of the chiral field, which corresponds to the pion decay constant on account of the Goldberger-Treiman relation Eq. (2.32). This scale dependent pion decay constant $f_\pi(k)$ is shown as white curve in Fig. 3.1.
The evolution[34] of the pion decay constant is also shown in Fig. 3.2 together with the chiral quark condensate $\langle \bar{q}q \rangle(k)$ which is obtained from the solution of Eq. (3.51) as evaluated at the vacuum expectation value Φ_0. These two quantities are order parameters of the chiral phase transition discussed in the next chapter. In the chiral symmetric regime for scales $k > k_{\chi SB} = 626$ MeV (cf. Eq. (3.75)) both quantities vanish in the chiral limit. Below that scale they become non-vanishing and approach their physical values at $k = 0$ as shown by the dashed curves. Thereby, the rise of the chiral condensate just below $k_{\chi SB}$ is quite drastic.

The flow of the quark mass and meson masses which are given from Eq. (3.27) is plotted in Fig. 3.3. In the chiral symmetric regime both meson masses are identical, while the quark mass is zero in the chiral limit. Below the symmetry breaking scale the pions become massless while the σ-meson mass rises again. Due to the nontrivial vacuum of the effective potential, the quarks acquire a finite mass. In the IR limit $k = 0$ we find the values for the physical parameters which simplify in the large N_c case compared to the general expressions given in Section 3.1. The quark mass is given by $m_q = \Phi_0(k=0)$ and the σ-meson mass by the previous expression Eqs. (3.27, 3.38). The Yukawa coupling is given by $g_{\rm R} = Z_\phi^{-1/2}(k=0)$ and the pion decay constant is $f_\pi = Z_\phi^{1/2}(k=0)\,\Phi_0(k=0)$. The IR values are summarized in Table 3.1 (second column). We next compare our model with the physical case of an explicit chiral symmetry breaking due to a finite current quark mass m_c. The value of the mean current quark mass $m_c = \frac{m_u + m_d}{2} = 7$ MeV is taken from chiral perturbation theory [67], which has been performed at our UV scale of 1 GeV, although there is some uncertainty because of the different regularization schemes. From Eq. (2.30) the parameter δ can be computed resulting

[34] The cutoff scale k is no real physical scale, since it is only a parameter in a smooth cutoff function. Therefore, only the limit $k \to 0$ leads to an effective action that is connected to physical observables. Nevertheless, the respective plots give an instructive simplified picture of the scale dependence of the theory. We will examine a possible connection between the scale k and a physical accessible scale parameter in more detail in Chapter 5 in order to exploit the scale information inherent in the RG approach.

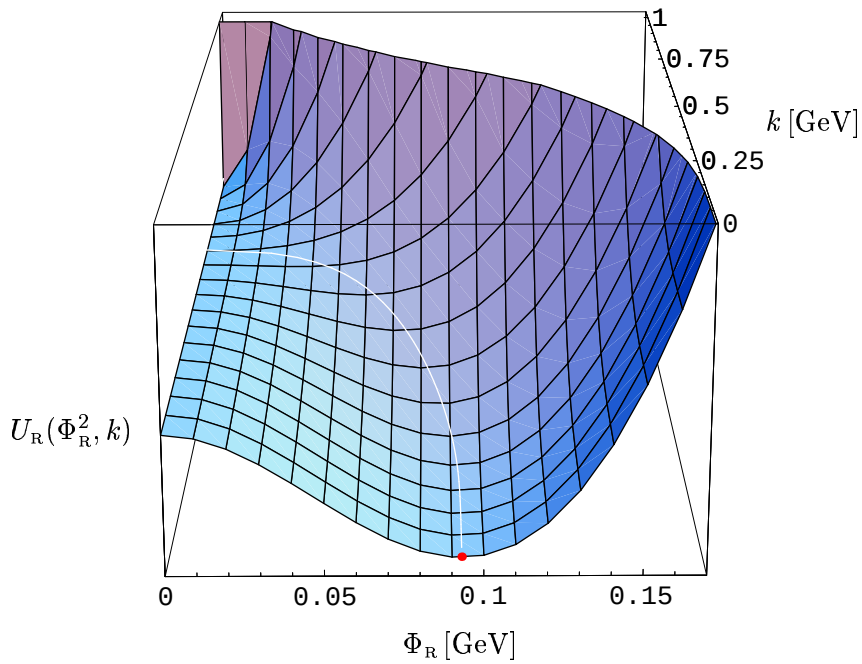

Figure 3.1: The evolution for the renormalized meson potential in large N_c approximation. In the UV the renormalized potential is infinite for all $\Phi_{\rm R}$ due to the vanishing wave function renormalization constant. The quadratic potential, which arises when Z_ϕ gets finite, evolves to a potential with broken symmetry in the IR. The white curve shows the evolution of the vacuum expectation value, which corresponds to $f_\pi = 92$ MeV at $k = 0$, denoted by the endpoint.

in $\delta = 3.64 \cdot 10^{-4}(\text{GeV})^3$. As already discussed, the solution Eq. (3.69) obtains in the case of explicit symmetry breaking, with a term linear in σ in the UV potential Eq. (3.60). The vacuum expectation value is now given by minimization with respect to σ.

The evolution of the renormalized physical masses is shown as solid curves in Fig. 3.3, which exhibits a very reasonable splitting of the mass scales. There is a continuous transition in the k evolution from the current quark to the constituent quark regime, since the system is in a nontrivial vacuum right from the beginning of the evolution. The quark mass assumes its current quark mass in the UV and the pion looses its role as an exact Goldstone boson and acquires a small finite mass in the IR.

The IR values of the physical quantities are shown in the first column of Table 3.1, The effect of the explicit chiral symmetry breaking is a minor change in the other parameters and a finite pion mass of 116 MeV which is reasonable close to the physical value. For the the chiral quark condensate we obtain an infrared value $\langle \bar{q}q \rangle_{RG}^{\frac{1}{3}} = 253.6$ MeV, which compares well to the value obtained from the Gell-Mann–Oakes–Renner relation $\langle \bar{q}q \rangle_{GOR}^{\frac{1}{3}} = 255.2$ MeV (cf. Eq. 2.33). This result is not surprising (cf. [54]) since the initial conditions of the flow equations have been adjusted to reproduce the correct IR values.

The change of the pion decay constant compared to the chiral limit amounts only to 1 MeV and is rather small in large N_c approximation compared to chiral perturbation theory

		$m_c = 7$MeV	χ-limit	Φ^4-truncation
f_π	[MeV]	93.0	92.0	105
$\langle\bar{q}q\rangle^{\frac{1}{3}}$	[MeV]	-254	-254	-
$m_q = \Phi_0$	[MeV]	320	309	285
m_σ	[MeV]	650	618	570
m_π	[MeV]	116	0	0
λ		23.6	22.6	14.9
$g_{\mathrm{R}} = Z_\phi^{-1/2}(\Phi_0^2)$		3.44	3.36	2.73

Table 3.1: The IR values for different approximations are shown. All computations are done with the UV initial conditions $k_{\mathrm{uv}} = 1037$ MeV, $m_{\mathrm{uv}} = 228.0$ MeV and $Z_\phi^{\mathrm{uv}} = 0$. The first column shows the analytic RG result with explicit chiral symmetry breaking due to a finite current quark mass of 7 MeV. In the second column the analytic RG result in the chiral limit is given, which is equal to the result of the NJL gap-equation regularized with the proper time regulator. In the last column the results of a simple quartic truncation of the potential are shown.

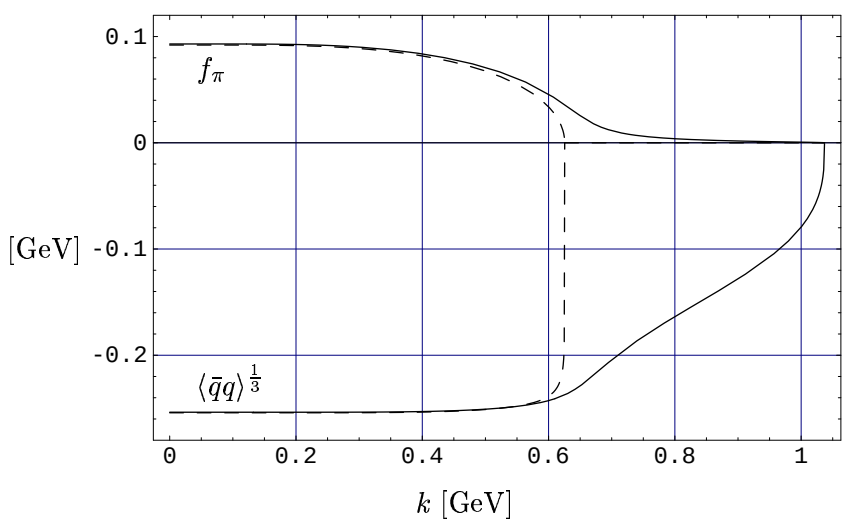

Figure 3.2: The evolution of the order parameters of chiral symmetry, namely the pion decay constant and the chiral quark condensate, as a function of the renormalization scale k. The dashed curves show the case of the chiral limit, whereas the solid curves represent the physical case with an explicit symmetry breaking due to a current quark mass of $m_q = 7$ MeV.

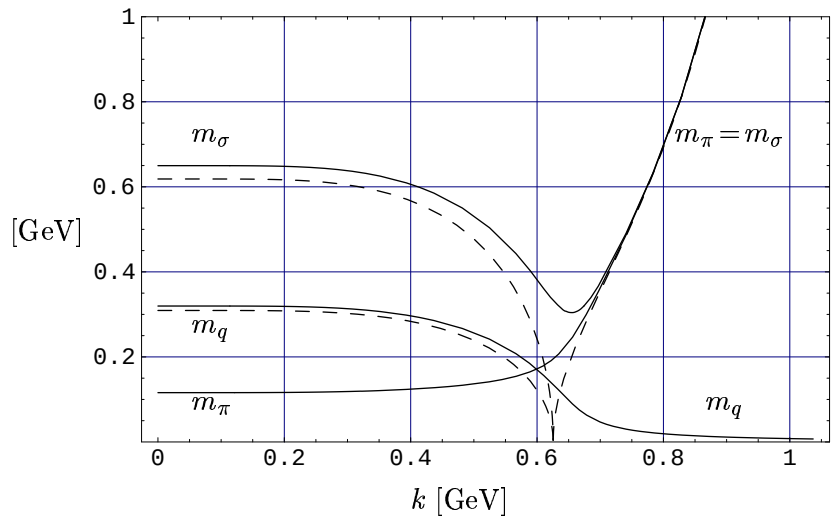

Figure 3.3: The renormalized masses of the exact solution as functions of the scale k in the chiral limit (dashed) and with an explicit symmetry breaking due to a current quark mass of 7 MeV (solid). The quark mass in the symmetric regime and the pion mass in the broken regime vanish in the chiral limit, whereas the pion acquires a mass of $m_\pi = 116$ MeV in the case of a finite current quark mass.

computations [7]. However, this changes considerably at order $1/N_c$ as will be discussed in Section 3.5.

Truncated potential

The analytic solution of Eqs. (3.65, 3.66) can test the usual parametrizations of the model. One relies on such parametrizations, if higher corrections are regarded, e.g. mesons are taken into account [23, 37]. As described in Appendix D, a standard approach is to expand the model in powers of Φ^2 up to a given order $p_{\max}$.
The potential U evolves under the renormalization flow from a trivial to a nontrivial form. Therefore we consider two parametrizations. In the simplest quartic truncation with $p_{\max} = 2$, they read in the chiral symmetric regime $U(\Phi^2, k) = \frac{m^2(k)}{2}\Phi^2 + \frac{\lambda(k)}{4}(\Phi^2)^2$ and in the broken regime $U(\Phi^2, k) = \frac{\lambda(k)}{4}(\Phi^2 - \Phi_0^2(k))^2$. Since the wave function renormalization factor Z_ϕ arises together with the dynamical term of mass dimension four, it is correspondingly expanded up to order $p_{\max} - 2$ and is therefore Φ-independent in the simplest approximation.

The evolution equations for the couplings m^2 and λ can either be derived from Eq. (3.65) or can simply be obtained by neglecting the bosonic contributions in Eqs. (3.61-3.64). We find for large N_c in the symmetric case ($g = Z_q = 1$):

$$k\frac{\partial m^2}{\partial k} = +\frac{N_c N_f}{4\pi^2}\, k^2 \,, \tag{3.77}$$

$$k\frac{\partial \lambda}{\partial k} = -\frac{N_c N_f}{2\pi^2} \,, \tag{3.78}$$

$$k\frac{\partial Z_\phi}{\partial k} = -\frac{N_c N_f}{4\pi^2} \,, \tag{3.79}$$

and for the broken regime:

$$k\frac{\partial \Phi_0^2}{\partial k} = -\frac{N_c N_f}{4\pi^2}\,\frac{1}{\lambda}\,\frac{k^2}{\left(1+\Phi_0^2/k^2\right)^2}\,, \tag{3.80}$$

$$k\frac{\partial \lambda}{\partial k} = -\frac{N_c N_f}{2\pi^2}\,\frac{1}{\left(1+\Phi_0^2/k^2\right)^3}\,, \tag{3.81}$$

$$k\frac{\partial Z_\phi}{\partial k} = -\frac{N_c N_f}{4\pi^2}\,\frac{1}{\left(1+\Phi_0^2/k^2\right)^3}\,. \tag{3.82}$$

To solve these equations numerically, we use again the initial values Eq. (3.76). In addition we choose $\lambda_{\rm uv}=0$ to have the same UV potential as before (cf. Eq. 3.60). In the symmetric regime the exact and approximate solutions are identical. In the broken regime we switch to the second parametrization and follow the flow given by Eqs. (3.80-3.82) to $k=0$. Now we have a set of *coupled* equations. This comes from the fact that we are tracking the evolution of the minimum Φ_0 of the potential U, which has no analytical solution from Eq. (3.69). In the IR we find a pion decay constant $f_\pi = 105$ MeV compared to a value of 92 MeV for the exact solution. The IR masses and couplings from these truncated flow equations are given in the third column of Table 3.1. When the truncation is extended to higher orders $p_{\rm max}$, the IR value of f_π converges fast to the exact solution with a pion decay constant of 92 MeV, as indicated by the thick points in Fig. 3.4. On the other hand, if only the effective potential is expanded, the flow still converges, however to a strongly deviating result of 111 MeV, shown by the thin points in Fig. 3.4. This is in contrast to a naive dimensional analysis, which would suggest that the higher order momenta of Z_ϕ should be suppressed by their high mass dimension in the vicinity of an IR fixed point. Although this does not seem to be the case in large N_c it may be the case when meson corrections are included, where a partial fixed point behavior occurs as will be discussed in Section 3.5. Nevertheless, in order to obtain a credible solution it is necessary to choose the truncation order in such away, that convergence with respect to *all* model parameters is achieved. Indeed, at order $p_{\rm max}=7$ the results are to the given accuracy exactly the ones of the exact solution in the second column of Table 3.1.

3.5 RG-FLOW INCLUDING MESON FLUCTUATIONS

The equivalence of the standard self consistent approach to the NJL model via Schwinger Dyson equations and the RG approach in large N_c established in the last section is an important basis, since it makes contact with numerous results obtained so far within this model and allows to improve them in a well defined way in the framework of renormalization group flow equations. Thereby it serves as the starting point to include corrections in $1/N_c$ within the RG scheme in a straightforward manner. This extension to higher order in $1/N_c$ by the inclusion of meson dynamics will be discussed in this section.

The inclusion of corrections in $1/N_c$ has been performed within self consistent solution schemes [68, 69]. Mesons, that appear in the form of a quark chain in self consistent approaches, are introduced as so called meson cloud contributions, into the elementary graphs that are used to derive self consistency equations. However, if such fluctuations are taken into account one needs an additional cutoff [68, 69], which reduces the predictive power of the model. Moreover, the chiral symmetry constraints that ensure the correct Ward-Takahashi identities and low energy theorems are not automatically fulfilled in these approaches but

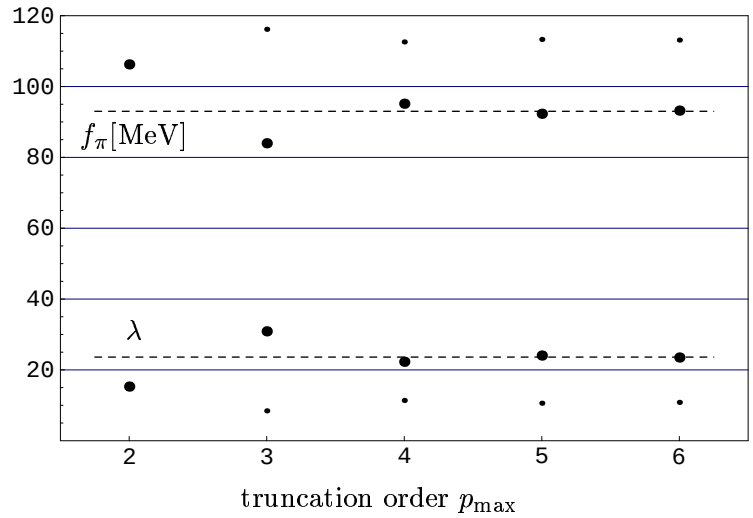

Figure 3.4: The dependence of the physical pion decay constant f_π and the 4-meson coupling λ on the truncation order $p_{\max}$ of a polynomial parametrization. Thin points give the behavior when only the potential U is expanded and the wave function renormalization factor Z_ϕ is considered Φ-independent. They do not converge to the exact results given by the dashed lines. Thick points show the dependence when U and Z_ϕ are expanded and exhibit a fast convergence to the exact results.

require a careful selection of included dynamics. This complicates a further extension of the approximation scheme considerably.

Such problems are absent in a RG treatment of the NJL-model in its bosonized form given by the linear σ-model. Due to the use of the effective action formalism all symmetries of the UV action are automatically fulfilled as long as the they are respected by the employed regularization. In addition the RG flow allows to start in the ultraviolet with the NJL model and then evolve it to the infrared without new parameters. Thereby, mesons arise in a very natural way during the evolution and in this process the chiral symmetry constraints are automatically fulfilled.

Compared to the large N_c case the full set of equations Eqs. (3.43-3.46) contains considerably more dynamics as visualized by the Feynman graphs in Section 3.3. Moreover, the large N_c approximation includes even less dynamics than it suggests. On one hand the large N_c approximation includes a running bosonic wavefunction renormalization factor and therefore satisfies the NJL enforced initial condition $Z_\phi = 0$. On the other hand Z_ϕ is not an independent quantity in this case, but connected to the effective potential U by

$$Z_\phi^{\text{large } N_c} = \frac{\delta^2 U^{\text{large } N_c}}{(\delta\Phi^2)^2} \,, \tag{3.83}$$

whereby U describes the complete physical content of the theory. In contrast, in the full approximation the physical content is stored in four partial differential equations which are profoundly coupled on account of the renormalization group improvement.

For a numerical solution of the full flow Eqs. (3.43-3.46), we need initial conditions at the UV scale k_{uv} of the evolution. The NJL initial conditions fix all parameters other than g_{uv} and m_{uv} to the values given in Eqs. (3.59, 3.60). Since neither the four fermion coupling

$g_{\rm NJL}$ nor the derived bosonic mass parameter $m_{\rm uv}$ is known at the UV scale, we adjust $m_{\rm uv}$ in order to obtain for the renormalized pion decay constant $f_\pi \equiv \sqrt{Z_\phi}\,\Phi_0$ the physical value of $f_\pi = 93$ MeV in the IR. Compared to the large N_c case the mesonic dynamics weakens the chiral condensation, as can be seen from the different sign of the mesonic contributions compared to the quark term in Eq. (3.43). Therefore, the 4-fermion coupling $g_{\rm NJL}$ has to be enhanced at the UV scale compared to its large N_c value in order to obtain the correct value for the pion decay constant [70]. Alternatively, it is equally possible to start the evolution at a larger scale $k_{\rm uv}$. By choosing an UV scale of $k_{\rm uv} \approx 1.15$ GeV, we obtain the physical value for f_π using the same NJL coupling as in the large N_c case. According to the above argument in this case the system enters the chiral broken regime at $k_{\chi\rm SB} = 701$ MeV compared to a value of $k_{\chi\rm SB} = 799$ given by Eq. (3.75). The large cutoff scale in the range of 1-1.3 GeV is characteristic for Schwinger proper time flow equations compared to the exact RG scheme, where the UV scale is in the range of 0.6-0.8 GeV. This difference has been ascribed to the different regulating behavior in the momentum integral in the SPT and the exact RG scheme in [70]. In particular this points out that due to the soft cutoff behavior these scales are not directly related to a physical momentum scale.

As already discussed the theory should only depend on the ratio of $g_{\rm uv}$ and $m_{\rm uv}$ in the form of the initial 4-fermion coupling $g_{\rm NJL}$. The residual dependence on $g_{\rm uv}$ for fixed $g_{\rm NJL}$ is shown in Fig. 3.5, where as characteristic parameters f_π and λ are shown[35]. It proves to be negligible over a large range. This serves as an important test for the considered approximation, since, in contrast to the large N_c approximation, the flow equations depend manifestly on both parameters in the full case[36], cf. Eqs. (3.43-3.46).

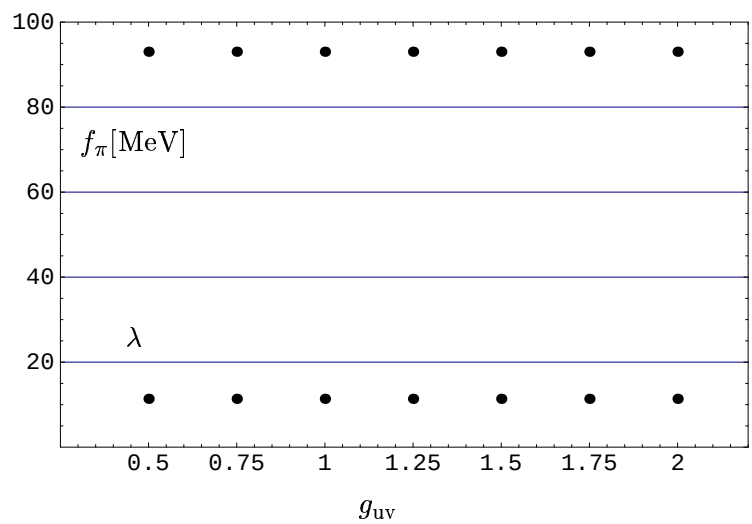

Figure 3.5: The pion decay constant f_π and the 4-boson coupling λ are shown for different values of $g_{\rm uv}$, where $m_{\rm uv}$ is respectively adjusted to keep the relevant four fermion coupling $g_{\rm NJL} = \frac{g_{\rm uv}^2}{2\,m_{\rm uv}^2}$ fixed. The residual dependence on $g_{\rm uv}$ is negligible over a large range of values.

Therefore we can set $g_{\rm uv} = 1$ leaving $m_{\rm uv}$ in the chiral limit as only free parameter which is directly given by $g_{\rm NJL}$ through Eq. (2.30).

[35] This independence holds also for the other renormalized quantities.

[36] In particular they enter as starting values in different coupled flow equations.

The set of partial differential equations for full field dependent flow variables makes it possible to explore the importance of the non-renormalizable couplings and the convergence of the series Eqs. (3.52-3.54). As in the large N_c case, we show as characteristic parameters, the pion decay constant f_π and the four boson coupling λ. Unfortunately due to the rising complexity of the equations for the higher order couplings our numerics did only allow to perform this expansion up to $p_{\max} = 5$ when all flow variables are expanded. Nevertheless a convergence pattern is already transparent, which is shown in Fig. 3.6. As in the large N_c case the parameter m_{uv} is fixed for the whole series to obtain $f_\pi = 93$ MeV in the highest order.

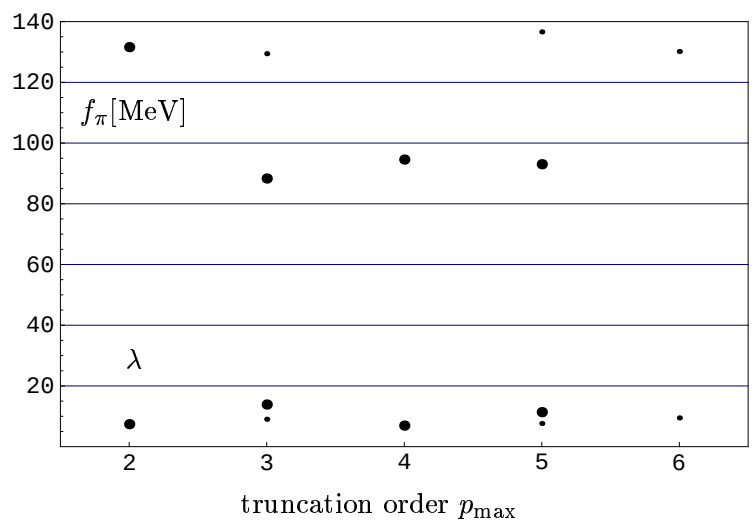

Figure 3.6: The dependence of the physical pion decay constant f_π and the 4-meson coupling λ on the truncation order $p_{\max}$ of a polynomial parametrization. Compared to the corresponding Fig. 3.4 in large N_c approximation all four Φ-dependent couplings have been expanded. Again, the thin points give the behavior when only the potential U is expanded and the other variables are considered Φ-independent, whereas thick points show the dependence when all four couplings are expanded to the given order and exhibit a fast convergence for f_π, whereas λ - as the second derivative of the potential - is more sensitive to the truncation. The initial conditions are fixed to obtain the physical value for the pion decay constant in highest order.

However, if only the effective potential is expanded we find again a very deviating result. Also the convergence is weaker than in the full expansion.

The solution of the evolution of the flow equations Eqs. (3.43-3.46) is given by four Φ-dependent functions shown in Fig. 3.7. As will be discussed in Chapter 4 the potential becomes convex in the IR. Thereby, the convergence radius of the series expansion goes to zero in the $k \to 0$ limit and correspondingly we show these functions only in the physically relevant region in the vicinity of the vacuum state[37]. As can be seen, all parameters have a non negligible field dependence. In particular, the linear dependence is quite strong around the vacuum state.

[37] First results of the full flow equations solved on a grid show that this Φ-dependence is considerable over the full relevant Φ axis. However, due to numerical problems it has not been possible so far to evolve the system all the way down to the IR, but only up to a scale $k \approx 300$ MeV.

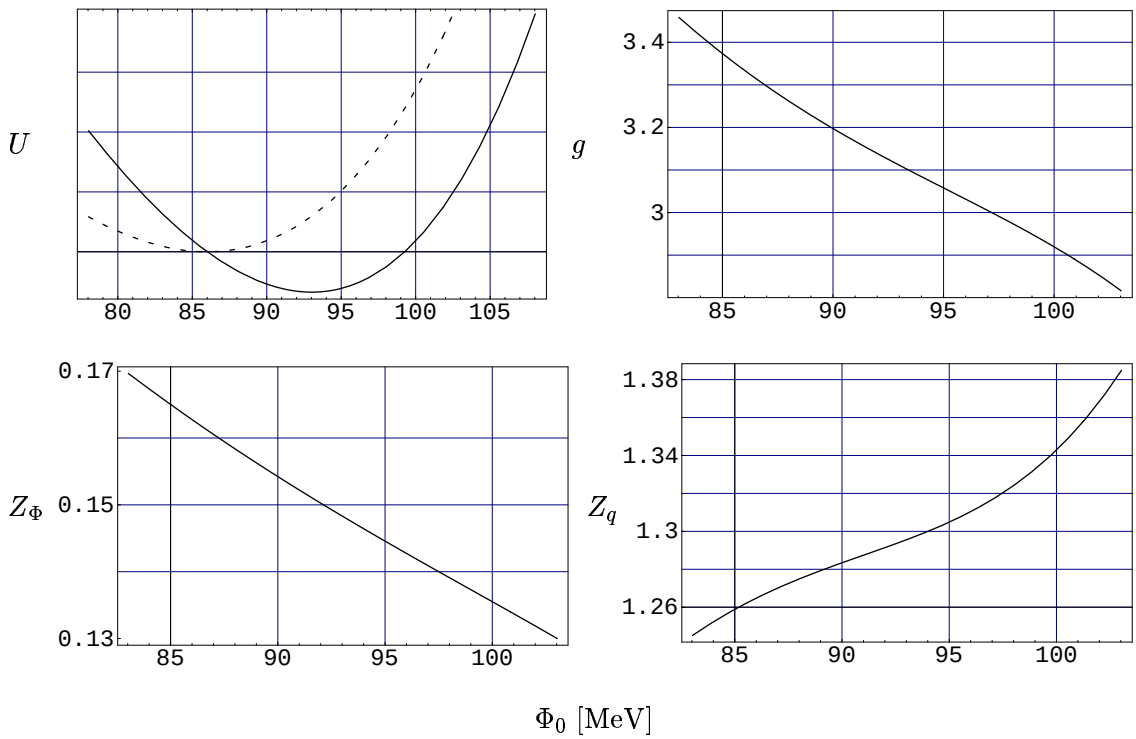

Figure 3.7: The Φ-dependent renormalized flow variables of the model are given at an infrared scale of 138 MeV. In the case of the effective potential U both in the $m_q = 0$ limit (dashed) and for $m_q = 7$ MeV (solid), where the vertical shift is arbitrary. The other functions are identical for $m_q = 0$ and $m_q \neq 0$.

As in the large N_c case, we show the evolution of the pion decay constant f_π and of the quark condensate in Fig. 3.8. We find a somewhat high value for the quark condensate in the IR. The evolution of the masses entering the theory is plotted in Fig. 3.9. This plot should be compared with the respective one in the large N_c approximation given in Fig. 3.3. As in the large N_c case, one obtains a reasonable splitting of the mass scales. The same mass plot is also shown in Fig. 3.10, neglecting the Φ-dependence of all couplings except of the effective potential. As also found in [70] in this case we obtain too small values as for instance a quark mass just above 200 MeV in the IR. This behavior is only slightly enhanced by the use of a lower cutoff scale[38] $k_{\rm uv}$. In particular it was not possible to obtain a quark mass of the order of $m_q \approx 300$ MeV in this case, whereas in the full expansion values up to $m_q \approx 330$ MeV could be obtained. This shows the great importance of the higher order couplings, which have been neglected so far in previous approaches. Finally we give the evolution of the couplings in Fig. 3.11. In particular the Yukawa couplings for the different chiral modes split at $k_{\chi\rm SB}$ and induce different dynamics for the different particles[39].

[38] A lower cutoff scale did also not raise the scale $k_{\chi\rm SB}$, where the flow enters the broken regime, significantly.

[39] The wavy "flow" of the Yukawa coupling in the case of an explicit symmetry breaking is due to its subsequent computation from the actually evolved coupling in the chiral limit as discussed below. According to Eq. (3.31) it involves derivatives of G and Z_q and is thereby sensitive to the computation method which seems overemployed in this case. We will therefore only give the IR value in the chiral limit in Table 3.2.

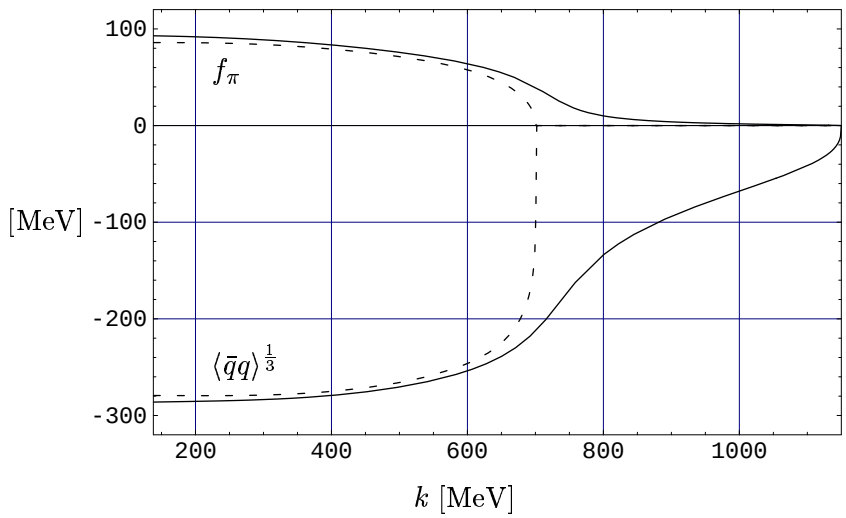

Figure 3.8: The corresponding plot to Fig. 3.2. Shown is the evolution of the pion decay constant and the chiral quark condensate, as a function of the renormalization scale k. The dashed curves show the case of the chiral limit, whereas the solid curves represent the physical case with an explicit symmetry breaking due to a current quark mass of $m_q = 7$ MeV.

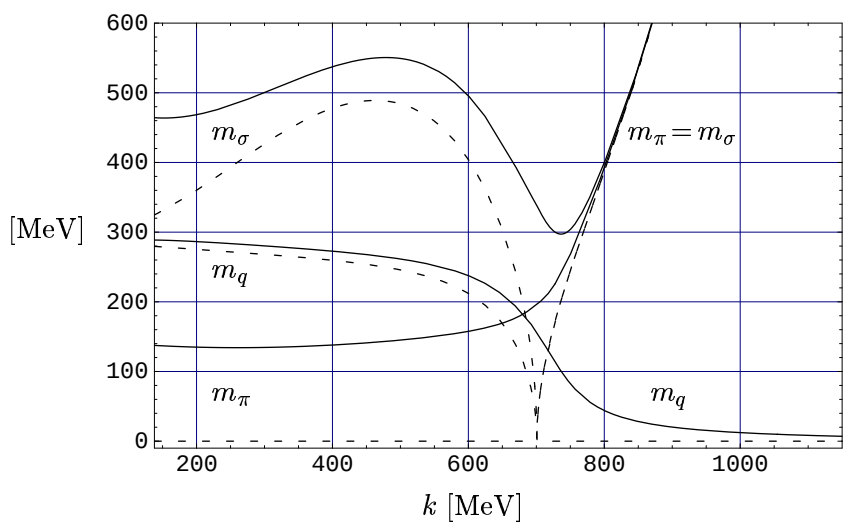

Figure 3.9: The renormalized masses as functions of the scale k in the chiral limit (dashed) and with an explicit symmetry breaking due to a current quark mass of 7 MeV (solid). The quark mass in the symmetric regime and the pion mass in the broken regime vanish in the chiral limit, whereas the pion acquires a mass of $m_\pi = 137$ MeV in the case of a finite current quark mass.

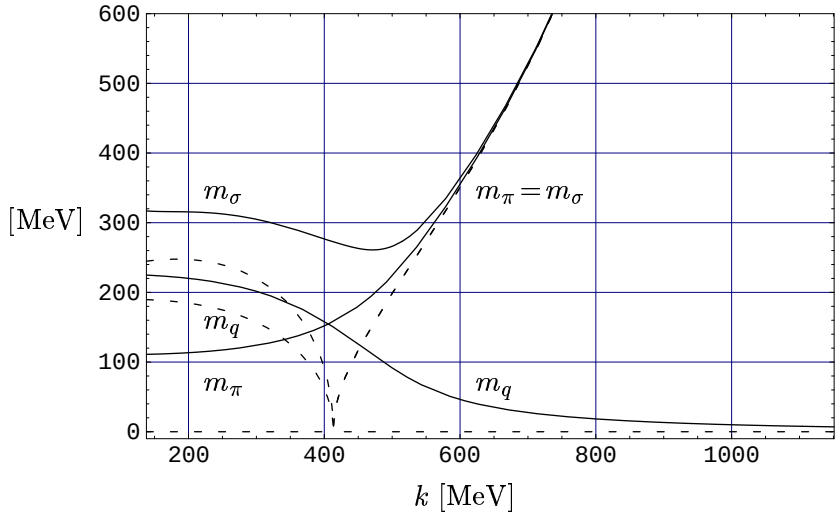

Figure 3.10: The renormalized masses as functions of the scale k, when the Φ dependence of the other couplings is neglected. Again shown in the chiral limit (dashed) and with an explicit symmetry breaking due to a current quark mass of 7 MeV (solid). The values for the respective masses are too low compared with phenomenology. This shows the great importance of the higher order non-renormalizable couplings.

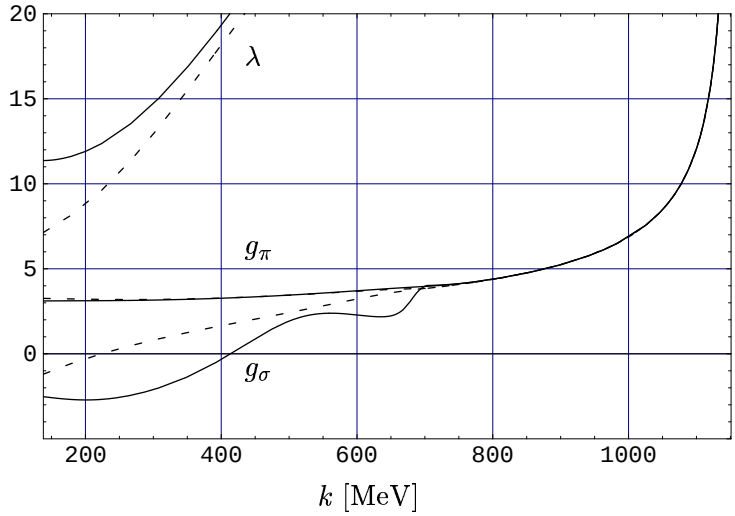

Figure 3.11: The renormalized Yukawa couplings g_π and g_σ and the renormalized four pion coupling λ as functions of the scale k in the chiral limit (dashed) and with an explicit symmetry breaking due to a current quark mass of 7 MeV (solid).

		large N_c	with $1/N_c$ corrections
$k_{\rm uv}$	[MeV]	1037	1151
G	[GeV^{-2}]	9.6	9.6
$m_{\rm uv}$	[MeV]	228	228
$k_{\chi\rm SB}$	[MeV]	626	701
f_π	[MeV]	93.0 (92.0)	93.0 (86.0)
$\langle\bar{q}q\rangle^{\frac{1}{3}}$	[MeV]	-254 (-254)	-286 (-280)
m_q	[MeV]	320 (309)	289 (280)
m_σ	[MeV]	650 (618)	464 (325)
m_π	[MeV]	116 (0)	137 (0)
g_π		3.44 (3.36)	3.11 (3.26)
g_σ		3.44 (3.36)	(-1.20)
λ		23.6 (22.6)	11.4 (7.1)
Z_π		0.085 (0.089)	0.148 (0.163)
Z_q		1 (1)	1.30 (1.26)
m_σ/m_q		2.03 (2)	1.61 (1.5)
λ/g_π^2		1.99 (2)	1.18 (1.13)
$f_\pi - f_\pi^{(0)}$	[MeV]	1.0	7.0

Table 3.2: The IR values for the different approximations are shown. The computations are done at the given UV scale $k_{\rm uv}$ with the given UV initial condition for $m_{\rm uv}$ and all other parameters take trivial initial values fixed by the UV NJL action. In each case, the first value correspond to an explicit symmetry breaking due to a current quark mass of $m_c = 7$ MeV and the second one in brackets to the chiral limit. The first column shows the analytic large N_c result. In the second column the result in next to leading order derivative expansion and uniform wavefunction approximation is given which contains corrections in $1/N_c$.

Coming finally to the physical observables, given by the IR values of the flow. Since the explicit symmetry breaking term in the bosonic potential does not change under the renormalization group flow the actual flow is computed in the chiral limit. The effective potential including the explicit symmetry breaking is computed subsequently by a tilt of original potential due to the linear symmetry breaking term. However, since we do a local series expansion and the convergence radius shrinks to zero in the IR this procedure shifts the physical relevant minimum of the potential out of the convergence region of the expansion at small k-values. Therefore, we have to stop the evolution at a finite k scale in order to ensure that we obtain the valid results for the physical observable. We choose as such an IR scale the physical pion mass of 138 MeV. Thereby, we have checked that the flow of the physical observables has nearly settled at that scale.

The results are given in the second column of Table 3.2 compared to the respective values in the large N_c approximation given in the first column. We find a reasonable value for the quark mass and the chosen current quark mass of 7 MeV yields the correct value for the pion mass. The chiral condensate takes a too large value compared to lattice simulations which find a value of $(-245 \pm 15\,\text{MeV})^3$ [71]. Furthermore, the well known property in large N_c, that the ratio of the σ and the quark-mass takes exactly the value 2, does not hold anymore

including meson dynamics, as well as the respective relation for the couplings.

Instead m_σ takes a lower value around 450 MeV which is at the lower end of the uncertainty interval for its mass [58]. However, taking into account the width of this faint resonance it is not surprising that it cannot fully be described within our approximation. In addition our approximation includes different Yukawa couplings for the σ-meson and the pion. We find for g_σ a smaller value than for the pion coupling g_π and in particular a different sign. Whereas the non relativistic Yukawa potential for this exchange in the limit of very heavy fixed quarks used in nuclear physics is depends only on g_σ^2 [72], the sign could have an influence in relativistic scattering amplitudes.

Altogether, the inclusion of mesonic dynamics yields moderate changes compared to the large N_c approximation. This was also observed in the self-consistent approximation scheme [68]. Nevertheless, there is one property which changes quite substantially between the large N_c and the improved approximation, namely the influence of the explicit symmetry breaking on physical quantities. For instance the difference of the pion decay constant with explicit symmetry breaking and in the chiral limit amounts to 7 MeV, whereas it was only 1 MeV in large N_c approximation. This larger value compares better to the one of chiral perturbation theory [7] which gives a value of 5 MeV.

3.6 THE SPECTRUM OF THE DIRAC OPERATOR

The QCD Dirac operator contains all information about the quark dynamics in QCD. This explains the interest in it and the many publication that have been devoted to its spectrum. In the literature one considers the Euclidean Dirac operator which reads $D = \partial\!\!\!/ + i\, g A\!\!\!/$. Since the Dirac operator is antihermitean, its eigenvalues are purely imaginary. With the eigenvalue equation

$$D\,|\psi_k\rangle = i\lambda_k|\,\psi_k\rangle \tag{3.84}$$

one defines the spectral density

$$\rho(\lambda) = \left\langle \sum_k \delta\left(\lambda - \lambda_k\right)\right\rangle , \tag{3.85}$$

where the averaging is over the gluon background. The first discovery about the spectral density has been made by Banks and Casher [73] who connect the order parameter of spontaneous chiral symmetry breaking, i.e. the chiral condensate, to the QCD spectrum at zero eigenvalues. Since then, different approaches have led to a steady progress in this field. As the dynamics at low energies is mainly driven by chiral symmetry the behavior of the spectral density in the vicinity of $\lambda = 0$ can be analyzed using chiral perturbation theory. The first correction to the Banks–Casher relation was found by Smilga and Stern [74]

$$\rho(\lambda) = \frac{V_4\langle\bar{q}q\rangle}{\pi} + V_4\frac{\langle\bar{q}q\rangle^2\left(N_f^2-4\right)}{32\pi^2 N_f f_\pi^4}\,|\lambda| + O(\lambda^2)\ , \tag{3.86}$$

where V_4 denotes the Euclidean 4–volume. The constant term is the Banks–Casher result, whereas the linear term vanishes in the case $N_f = 2$.

Chiral random matrix theory considers the so called microscopic spectral density, in which all eigenvalues are rescaled according to the average spacing of small eigenvalues. It successfully describes the Dirac spectrum in the extreme infrared regime, where the spectral density

is completely determined by the global symmetries of the Dirac operator (see e.g. [75]). Universal properties of the microscopic spectral density have been derived and identified in lattice calculations [76, 77]. Furthermore partially quenched chiral perturbation theory combines the results of chiral perturbation theory and chiral random matrix theory [78].

The Dirac spectrum for small eigenvalues is driven by chiral symmetry which determines hadron dynamics for small momenta. Thus chiral perturbation theory and chiral random matrix theory can be successful in describing the Dirac spectrum. The same holds for the Nambu–Jona-Lasinio (NJL) model as an effective model for chiral symmetry. The QCD Dirac spectrum and the spectrum for the NJL model which we analyze in this paper should coincide in the regime, where the NJL model is a good effective description for QCD, that is for

$$\lambda < k_{\rm uv} \ . \tag{3.87}$$

Here $k_{\rm uv} \approx 1$ GeV defines the momentum scale below which a hadronic description of QCD may be useful.

Extracting the Dirac operator spectrum from the flow equations

As an application of the solution to the NJL model presented in the preceding sections, we will in the following analyze the spectrum of the Dirac operator within the NJL model. We restrict our analysis of the Dirac spectrum to the large N_c approximation discussed in Section 3.4 which lends itself favorably to this purpose due to the analytic form of the solution. However, a calculation of the Dirac spectrum in the context of the complete set of flow equations Eqs. (3.43-3.46) is equally possible[40].

For later purposes we explicitly stress the dependence of the meson potential on the current quark mass m_q, given in Eq. (2.29). The parameter δ is scale independent, since a linear symmetry breaking term does not evolve under RG flow [15]. To make this explicit, we denote the full meson potential in the presence of an explicit symmetry breaking due to a finite current quark mass by $V_k(\sigma, \vec{\pi}, m_q)$ given by[41]

$$V_k(\sigma, \vec{\pi}, m_q) = U_k(\Phi^2) - \delta\sigma \ , \tag{3.88}$$

where only the chiral symmetric part $U_k(\Phi^2)$ evolves under flow of the IR cutoff scale k and δ is given by (2.30).

While the QCD–Dirac operator D is antihermitean, the Dirac operator in the linear σ-model

$$\tilde{D} = \partial\!\!\!/ + g(\sigma + i\vec{\tau}\vec{\pi}\gamma_5) \tag{3.89}$$

can have complex eigenvalues. As mentioned earlier, in the flow equations we have neglected the imaginary part of the fermion determinant, which is related to anomalous processes [54]. In this approximation the eigenvalues of the Dirac operator in the linear σ-model are purely imaginary in coincidence with the QCD spectrum. For general complex eigenvalues $z = x + iy$ it is useful to consider the two dimensional spectral density [79, 80]

$$P(x, y) = \left\langle \sum_k \delta(x - x_k)\, \delta(y - y_k) \right\rangle_\Phi \ , \tag{3.90}$$

[40] This requires the application of replica methods but otherwise allows to adopt the formalism employed in the large N_c case.

[41] For conciseness of the notation, we write the scale parameter k as a subscript.

which can be obtained from the complex resolvent [79]

$$G(z) \equiv \left\langle Tr \frac{1}{z-\tilde{D}} \right\rangle_\Phi = \left\langle Tr \frac{\partial}{\partial_z} \log\left(z-\tilde{D}\right) \right\rangle_\Phi = \left\langle \frac{\partial}{\partial_z} \log \text{ Det}\left(z-\tilde{D}\right) \right\rangle_\Phi$$
$$= \left\langle \frac{\partial}{\partial_z} \log \int Dq\, D\bar{q} \exp\left[-\int d^4x \left(\bar{q}\left(z-\tilde{D}\right) q\right)\right] \right\rangle_\Phi . \tag{3.91}$$

The complex eigenvalue z is the generator in this resolvent, which in our low energy effective theory involves an average over the meson fields denoted by $\langle ... \rangle_\Phi$. In large N_c approximation there are no meson fluctuations. Therefore the averaging over the meson fields can be interchanged with the logarithm in the last line and one finds

$$G(z) = -V_4 \langle \bar{q}q \rangle (z) . \tag{3.92}$$

The connection between $G(z)$ and $P(x,y)$ can be derived with Eq. (3.90)

$$G(z) = \left\langle Tr \frac{1}{z-\tilde{D}} \right\rangle_\Phi$$
$$= \left\langle \int dx'\, dy' \frac{\sum_k \delta(x'-x_k)\delta(y'-y_k)}{x-x'+i(y-y')} \right\rangle_\Phi$$
$$= \int dx'\, dy' \frac{P(x',y')}{x-x'+i(y-y')} . \tag{3.93}$$

Combining eqs. (3.92) and (3.93) yields

$$G(x,y) = -V_4 \langle \bar{q}q \rangle = \int dx' \int dy' \frac{P(x',y')}{x-x'+i(y-y')} . \tag{3.94}$$

This relation can be inverted [79] and gives

$$P(x,y) = -\frac{V_4}{\pi} \frac{\partial}{\partial z^\star} \langle \bar{q}q \rangle (z) , \tag{3.95}$$

where

$$\frac{\partial}{\partial z^\star} = \frac{1}{2}\left(\frac{\partial}{\partial x} + i \frac{\partial}{\partial y}\right) . \tag{3.96}$$

The complex eigenvalue z enters in the resolvent Eq. (3.91) just as an explicit quark mass. Therefore no new flow equations have to be evaluated. After bosonization z appears in a linear symmetry breaking term in the meson potential via Eq. (2.30) with $m_q = z$.

As the resulting meson potential $V_k(\sigma, \vec{\pi}, z)$ becomes complex, we must comment on the meaning of $\Phi_{0,k}(z)$. Instead of restricting ourselves to positive real values $\Phi_{0,k}$, we now have to allow also complex fields $\Phi_{0,k}(z)$. Instead of finding a real minimum of the potential $V_k(\sigma, \vec{\pi}, m_q)$ we have to determine a complex saddle point, which minimizes the real part of the complex meson potential $V_k(\sigma, \vec{\pi}, z)$.

From Eq. (3.95) it is obvious, that the two dimensional spectral density is zero if $\langle \bar{q}q \rangle (z)$ is analytic in z. In presence of the complex quark mass z the chiral condensate at $k = 0$ becomes in the large N_c limit with Eq. (3.51)

$$\langle \bar{q}q \rangle (z) = \frac{N_c}{4\pi^2} \left[\frac{-\Phi_0(z) k_{\text{uv}}^2 \left(k_{\text{uv}}^2 + 2\Phi_0(z)^2\right)}{k_{\text{uv}}^2 + \Phi_0(z)^2} + 2\Phi_0(z)^3 \log\left(1 + \frac{k_{\text{uv}}^2}{\Phi_0(z)^2}\right) \right] . \tag{3.97}$$

This expression is analytic if $\Phi_0(z)$ is analytic and $\mathrm{Re}\,(\Phi_0(z)) \neq 0$. As $\Phi_0(z)$ is the bare pion decay constant in presence of z and therefore minimizes $\mathrm{Re}\,(V(\sigma, \vec{\pi}, z))$, the second condition $\mathrm{Re}\,(\Phi_0(z)) \neq 0$ is always true. But the global minimum of $\mathrm{Re}\,(V(\sigma, \vec{\pi}, z))$ can switch if z changes infinitesimally. This is exactly what happens and leads to a discontinuity in $\Phi_0(z)$. Fig 3.12 demonstrates this behavior.

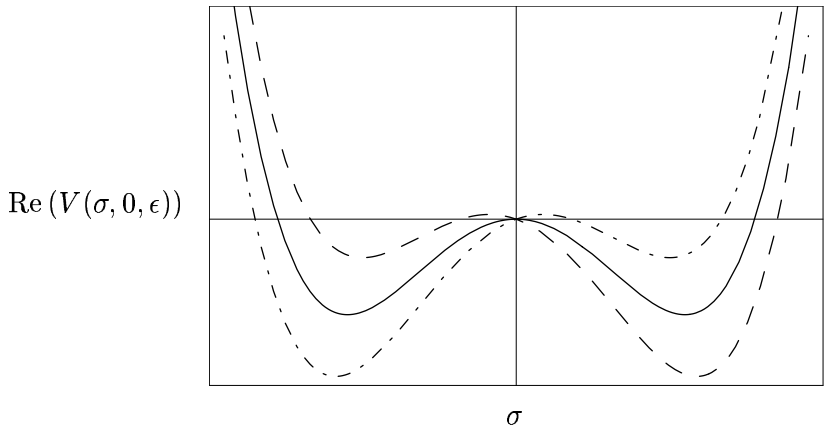

Figure 3.12: Projection of the real part of the meson potential depending on σ. The sign of the explicit symmetry breaking term induces the choice of the global minimum and hence the vacuum expectation value. The solid curve is the potential without explicit symmetry breaking. The dashed and dashed dotted curves result from $x = +\epsilon$ and $x = -\epsilon$ respectively.

For $z = 0$ it follows from Eqs. (3.88, 3.69) in the chiral limit that with Φ_0 as a global minimum of $\mathrm{Re}\,(V(\sigma, \vec{\pi}, z))$ also $-\Phi_0$, $\Phi_0^\star$ and $-\Phi_0^\star$ are global minima of $\mathrm{Re}\,(V(\sigma, \vec{\pi}, z))$. Additionally they are saddle points of $V(\sigma, \vec{\pi}, z)$. For either $z = x$ or $z = iy$ the global minimum is still twice degenerate. In case of an infinitesimal x the sign of x chooses the minimum, i.e. $\mathrm{Re}\,(\Phi_0)$ changes its sign under the transformation from $x = +\epsilon$ to $x = -\epsilon$. The same holds for infinitesimal y and for $\mathrm{Im}\,(\Phi_0)$, but in this case an infinitesimal y only gives rise to an infinitesimal $\mathrm{Im}\,(\Phi)$, consequently no discontinuity arises in $\Phi(z)$. We are thus left with the result, that $P(x, y)$ can only be nonzero for $x = 0$. The position of our Dirac spectrum thus coincides with the QCD spectrum. Using the ansatz $P(x, y) = \delta(x)\rho(y)$ we find from eqs. (3.94), (3.95) and (3.96)

$$\rho(y) = \frac{V_4}{2\pi} \lim_{\epsilon \to 0} \left[\langle \bar{q}q \rangle (iy - \epsilon) - \langle \bar{q}q \rangle (iy + \epsilon) \right] . \tag{3.98}$$

Now let us consider the flow equations for the potential and the chiral condensate. In the large N_c limit they reveal a simple connection, namely[42]

$$\partial_k \langle \bar{q}q \rangle_k (\Phi(z)) = \partial_k \partial_\Phi U_k (\Phi(z)) . \tag{3.99}$$

With the initial conditions $\langle \bar{q}q \rangle_{\mathrm{uv}} = 0$ and $U_{\mathrm{uv}} = \frac{m_{\mathrm{uv}}^2}{2} \Phi^2$ at $k = k_{\mathrm{uv}}$ this equation can be integrated out and yields

$$\langle \bar{q}q \rangle (\Phi(z)) = \partial_\Phi U (\Phi(z)) - m_{\mathrm{uv}}^2 \Phi(z) . \tag{3.100}$$

[42] To be correct we should have written $\partial_k \langle \bar{q}q \rangle_k (\sigma(z), \vec{\pi})|_{\vec{\pi}=0} = \partial_k \partial_\sigma U_k (\sigma(z), \vec{\pi})|_{\vec{\pi}=0}$. As the expectation value of the pion field vanishes the notation above is unambiguous.

Eq. (3.98) gives the spectral density in terms of the discontinuity of the generalized chiral condensate $\langle\bar{q}q\rangle(z)$ across the real axis, which can be calculated from the saddle point $\Phi_0(z)$ of $V(\Phi,z)$ fulfilling $\partial_\Phi V(\Phi,z)|_{\Phi=\Phi_0}=0$. With Eq. (3.100) we find in the chiral limit

$$\begin{aligned}\rho(y) &= \frac{V_4}{2\pi}\lim_{\epsilon\to 0} m_{\rm uv}^2\left[\Phi(i\,y+\epsilon)-\Phi(i\,y-\epsilon)\right]\\ &= \frac{m_{\rm uv}^2 V_4}{\pi}{\rm Re}\left(\Phi(iy+\epsilon)\right)\ .\end{aligned} \tag{3.101}$$

The result is plotted in Fig. 3.13.

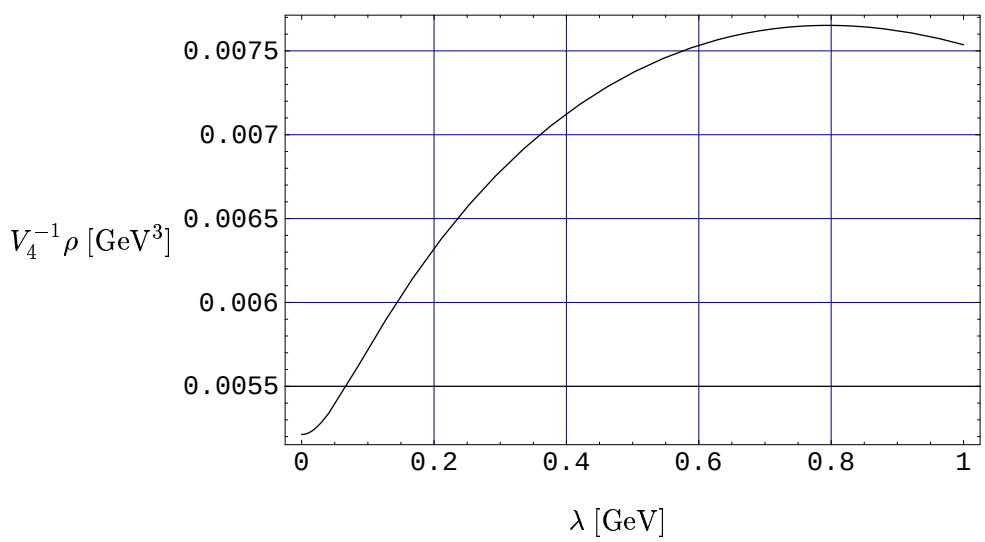

Figure 3.13: The spectral density $\rho(\lambda)$ of the Dirac operator $\tilde{D}$ computed in the linear σ-model with quarks. Note the suppressed zero on the scale for $V_4^{-1}\rho$.

Next we derive the behavior of the spectral density at small eigenvalues. Therefore we have to evaluate $\Phi_0(iy)$ for small y. The value $\Phi_0(iy) := \Phi_0(0)+\alpha(y)+i\beta(y)$ is determined by the saddle point equation

$$\partial_\Phi V(\Phi,y)|_{\Phi=\Phi_0} = \partial_\Phi U(\Phi)|_{\Phi=\Phi_0(0)+\alpha(y)+i\beta(y)} - i m_{\rm uv}^2\, y = 0\ . \tag{3.102}$$

$\alpha(y)$ and $\beta(y)$ can be expanded in a Taylor series. The coefficients are obtained from

$$\frac{d^{(n)}}{dy^{(n)}}\left[\partial_\Phi U(\Phi)|_{\Phi=\Phi(0)+\alpha(y)+i\beta(y)} - i m_{\rm uv}^2\, y\right]_{y=0} = 0 \quad , \quad n=0,1,2\ . \tag{3.103}$$

We find

$$\Phi_0(y) = \Phi_0(0) + i\frac{m_{\rm uv}^2}{\partial_\Phi^2 U(\Phi)\big|_{\Phi=\Phi_0(0)}}y + \frac{1}{2}\frac{m_{\rm uv}^4\ \partial_\Phi^3 U(\Phi)\big|_{\Phi=\Phi_0(0)}}{\left[\partial_\Phi^2 U(\Phi)\big|_{\Phi=\Phi(0)}\right]^3}y^2 + ... \tag{3.104}$$

With Eq. (3.101) the spectral density

$$\rho(y) = \frac{m_{\rm uv}^2 V_4}{\pi}\left[{\rm Re}\left[\Phi_0(0)\right] + \frac{1}{2}\frac{m_{\rm uv}^4\ \partial_\Phi^3 U(\Phi)\big|_{\Phi=\Phi_0(0)}}{\left[\partial_\Phi^2 U(\Phi)\big|_{\Phi=\Phi_0(0)}\right]^3}y^2 + O(y^3)\right] \tag{3.105}$$

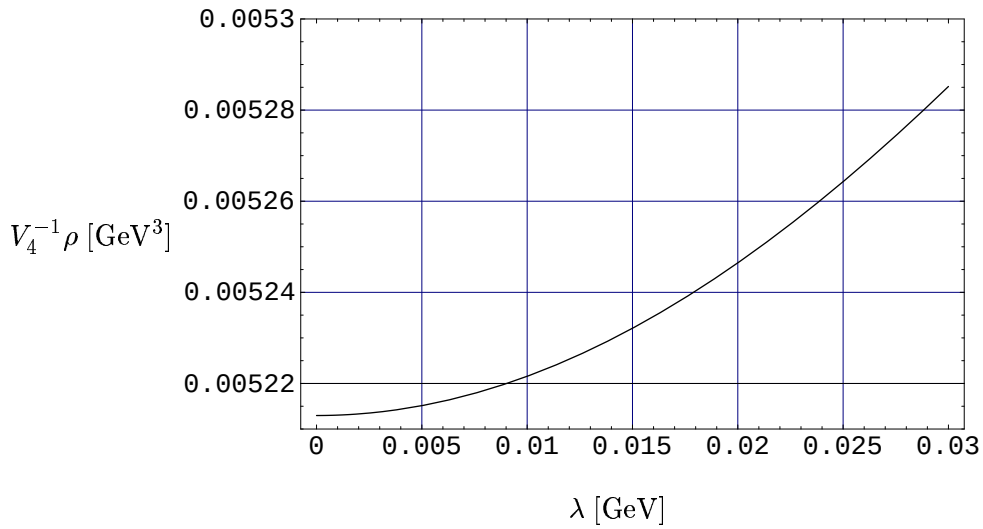

Figure 3.14: Behavior of the spectral density at small eigenvalues, which exhibits a quadratic rise due to the absence of a linear contribution in the case $N_f = 2$.

can be calculated explicitly for small eigenvalues, see Eq. (3.69) and (3.100)

$$V_4^{-1}\rho(y) = \frac{\langle\bar{q}q\rangle}{\pi} + \frac{2\pi^3 m_{\rm uv}^6}{\Phi_0(0)} \tag{3.106}$$
$$\cdot \frac{12\pi^2 m_{\rm uv}^2 \left(k_{\rm uv}^2 + \Phi_0(0)^2\right)^6 - N_c k_{\rm uv}^6 \left(3k_{\rm uv}^2 - \Phi_0(0)^2\right)\left(k_{\rm uv}^2 + \Phi_0(0)^2\right)^3}{\left[4\pi^2 m_{\rm uv}^2 \left(k_{\rm uv}^2 + \Phi_0(0)^2\right)^2 - N_c k_{\rm uv}^6\right]^3} y^2 + O(y^3)\ .$$

The constant coefficient is the Banks–Casher result [73]. Since our computation is done for $N_f = 2$ there is no linear term in agreement with the findings of Smilga and Stern for $N_f = 2$ [74]. Numerically, the quadratic coefficient is 87 MeV for the choice of parameters used in Section 3.4. The quadratic term in y can be related to the correlation function of three scalar σ–quanta. In the numerator of Eq. (3.105) one sees the effective σ^3 coupling constant contained in our potential $U(\Phi)$ multiplied by the cube of the σ–propagator $\frac{1}{m_\sigma^2}$ at zero momenta. This result can also be found in the paper of Smilga and Stern [74].

The Dirac operator in the strong coupling regime of QCD

We have presented a method to obtain the spectral density of the Dirac operator for the linear σ-model in the large N_c limit. Because of asymptotic freedom in QCD, we expect $\rho(\lambda) \propto \lambda^3$ for asymptotically large eigenvalues, since for a free theory the spectral density is only determined by the phase space. This situation of a non interacting theory can be tested within our approach in the limit $m_{\rm uv} \to \infty$. In this case the NJL four fermion interaction $G \propto 1/m_{\rm uv}^2$ [128] vanishes. As shown in Fig. 3.15 the resulting spectral density becomes the density of a free theory. For $\lambda \geq k_{\rm uv}$ the phase space is cut off sharply.
If the interaction strength G is turned on by a finite $m_{\rm uv}$ one sees that quark-quark interactions lead to a level repulsion increasing the density for small λ and pushing some strength above

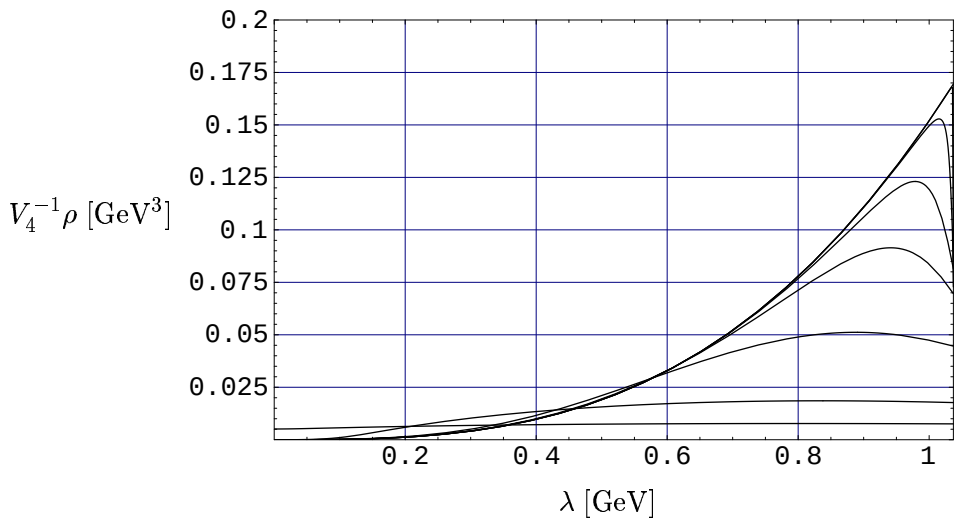

Figure 3.15: The spectrum for different values of $m_{\rm uv}$. As $m_{\rm uv}$ approaches infinity the curve resembles more and more the free spectrum with a sharp cutoff at $k_{\rm uv}$. The spectra are plotted for $m_{\rm uv} = 0.228,\ 0.5,\ 1.5,\ 4,\ 10,\ 50,\ 2000$ GeV. The free spectrum differs from the spectrum with $m_{\rm uv} = 2000$ only for values of λ very close to $k_{\rm uv}$.

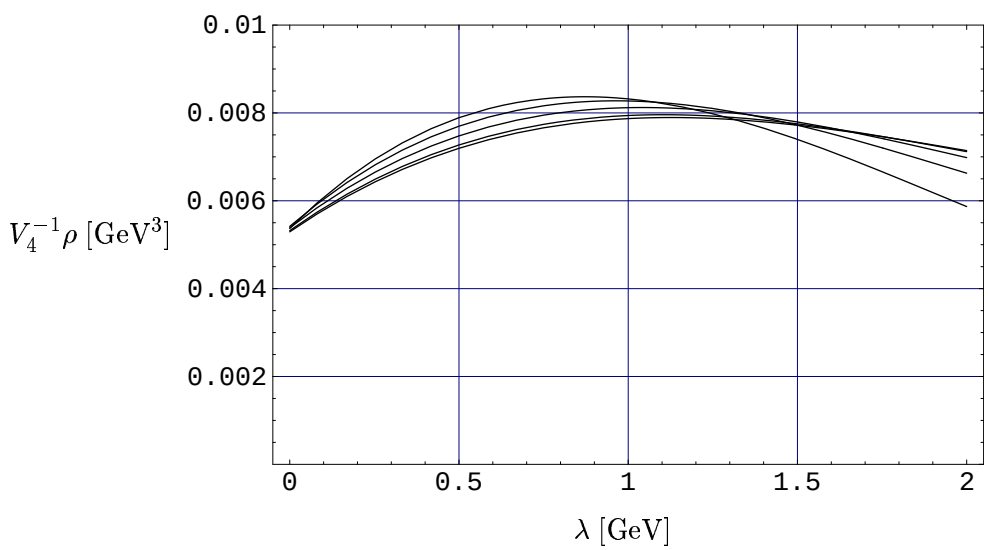

Figure 3.16: The spectral density for different regulator functions $f_k^{(n)}$. The uppermost curve corresponds to n=2. The others are respectively $n = 3,\ 5,\ 10,\ 15$, where the last two are already nearly equal.

1 GeV. Varying n and thereby the shape of the cutoff functions $f^{(n)}$ in Eq. (3.39) we adjust the cutoff parameters $m_{\rm uv}$ and $k_{\rm uv}$ in such a way that f_π and M_q are kept constant. This way we can test the sensitivity of the spectral density to the cutoff function. We see that below 1 GeV the choice of the cutoff function leads to stable results within 10%.

In the realistic case of QCD we expect that gluonic interactions above $k_{\rm uv}$ influence the spectrum nearby and below. Therefore, the decrease of the spectral density $\rho(\lambda)$ above $\lambda \approx 0.8$ GeV is probably an artifact of the model space, which is restricted by the soft cutoff.

The interactions in the strong coupling regime of QCD induce level repulsion. Higher modes are strongly suppressed, while the increase of the average eigenvalue density for smaller eigenvalues drives the chiral condensate which appears on the low energy end of the spectrum. It seems that level repulsion and condensation are the dominating effects for the Dirac operator spectral density in the strong coupling regime of QCD.

3.7 CONCLUSION

On the basis of previous works [23, 24, 36, 70] we have explored an improved solution scheme for the NJL model in the context of RG flow equations for its bosonized form given by a generalized linear σ-model. These flow equations are derived in the Schwinger proper time scheme and contain the momentum dependence in next to leading order and the entire bosonic field dependence. Thereby they provide a framework to include meson loops in the NJL-model without an additional cutoff. Although the flow equations include arbitrary many couplings, they can directly be related to one loop dynamics by means of respective Feynman graphs.

We have established an equivalence between the self-consistent approach to the NJL model via gap equations and the SPT flow equations in the large N_c approximation. In this approximation, we have explored the analytic solution for the effective action and find the same vacuum phenomenology as computations with a sharp 3-momentum cutoff.

The inclusion of the mesonic dynamics within the full set of flow equations which corresponds to corrections in $1/N_c$ equally yields reasonable values for the masses, condensates and couplings of the chiral broken groundstate. We find a complete independence on the additional parameter introduced in the bosonization procedure. As expected for a next to leading order approximation, the corrections are moderate compared to the large N_c limit. However, we find a much more pronounced dependence of the system on an explicit chiral symmetry breaking which is in the same order as found by chiral perturbation theory [7].

As a first application of the derived flow equations we have computed the spectrum of the Dirac operator in large N_c. Since our approach should be valid for eigenvalues up to several hundred MeV, it allows to enter a new regime which may complement other results from chiral perturbation theory and chiral random matrix theory.

Since the obtained general effective action contains within the considered approximation the whole information about the NJL model at low energies, its derivation is only the starting point in order to apply it to explore physical problems. The most challenging application in this respect is the thermal behavior and the chiral phase transition explored in the next chapter.

Chapter 4

Hot and dense systems

Since neither the chiral asymmetric form of nature, discussed in Sec. 2.1, nor the confinement of color is a fundamental property of the underlying theory but only of its groundstate, there can be the possibility to reach other states of matter. Therefore, the exploration of its phase structure is one of the challenging subjects in strong interaction physics. This challenge is currently met at the Relativistic Heavy Ion Collider (RHIC) in Brookhaven which reaches energies up to 200 GeV per nucleon in Au-Au-collisions. The forthcoming Large Hadron Collider (LHC) in Geneva will even exceed this by far with energies of several TeV per nucleon in Pb-Pb collisions. From all that is known so far about the phase structure of strong interaction this would be sufficient to produce an energy density that is large enough to form a new state of matter which should resemble closely a plasma of nearly free quarks and gluons.

In particular these high energy densities reached at LHC should permit to observe directly the thermal radiation of the plasma which would be a clear signature for its existence. At RHIC such an analysis is also planned, although it should be much harder due to the enormous background of radiation from non-thermal sources. Therefore, so far one has to rely on more indirect signatures which often involve models and are much less conclusive. Prominent examples for such signatures are dilepton yields and J/ψ suppression [82]. Furthermore, the successful description of the collision process at RHIC by hydrodynamical models [83] and the account of particle ratios by thermal resonance gas models [84] suggests that the system should be partially thermalized in a local co-moving frame. Although the picture gets clearer, all that can safely be said so far is that at RHIC there is probably a new state of matter produced that exhibits strong collective behavior and can better be described in terms of quark-gluon degrees of freedom than in terms of hadrons.

On the theoretical side the situation is clearer as far as the high temperature behavior of strong interaction is concerned. There are several methods, which yield comparable results. Nevertheless, the situation depends on the actual system that is regarded. The most direct results are available for pure $SU(3)$ gauge theory, where quite general arguments suggest a first

order phase transition separating a confined low temperature phase from a deconfined high temperature phase [85] which has been confirmed in lattice simulations [86, 12]. The inclusion of quarks complicates the situation considerably, since the exact behavior at finite temperature depends strongly on the number and masses of the quarks considered. Furthermore, the inclusion of fermions makes much greater demands on lattice computations. However it has been shown that the two flavor QCD lies in the universality class of the O(4)-model [87]. This opened the possibility to compute the critical behavior with RG methods and showed that for two massless flavors there is a second order phase transition at a critical temperature in the range of $100 \lesssim T \lesssim 200$ MeV [27, 37], whereas the transition becomes first order for a larger number of massless flavors [87]. Furthermore, new methods and the increasing computational resources enabled to cover dynamic quarks on the lattice. Although the lattice method is still restricted to rather large quark masses, it gave a rich picture of the quark mass dependence [14] of the finite temperature behavior and showed that for realistic quark masses there is a smooth crossover between a confined and chiral broken to a deconfined and chiral symmetric phase. Moreover, these analyses exhibited a remarkable connection between the chiral phase transition and the deconfinement transition, which seem to occur at nearly the same temperature.

At finite densities the situation is less conclusive. QCD can only rigorously be solved for asymptotically large temperature and densities. However, at accessible densities the appearance of a complex functional determinant in the presence of a chemical potential prevents so far first principle computations. Namely, such computations within a lattice treatment are based on an averaging over different configurations and rely on the method of importance sampling to weight certain individual configurations. However there are methods to partially circumvent this difficulty. One method is the analysis of higher order momenta as susceptibilities with respect to chemical potential but evaluated at $\mu = 0$ in order to extrapolate into the finite density regime via Taylor expansion [88]. The multi parameter re-weighting technique [89] developed recently introduces a re-weighting of certain vacuum configurations in order to extract information about the properties at finite density. Finally, for simple systems it has even been possible to solve the above problem in a rigorous manner [90]. Furthermore, there are semi-perturbative techniques like e.g. the hard thermal and dense loop method [91], that are also applicable at finite densities. However, in order to reach the interesting regime of physical systems all these methods have to rely on extrapolations. An alternative is given by effective low energy models of strong interaction. Although they mostly neglect confinement, they include the relevant symmetries and have proven to give a reasonable description of the physics involved. In particular, these effective theories are so far the only method that covers the full phase diagram [92, 98].

Due to the complex non-perturbative interactions there are a whole range of possible phases at high density. The current picture [1, 92] is that a first order transition at high densities separates the confined and chiral broken regime of normal matter from a two flavor color superconducting phase [93, 94, 95] (2SC) in which chiral symmetry is restored. At at even higher densities when the strange quark mass becomes small compared to the chemical potential the system goes over to a color flavor locked phase [96], where chiral symmetry is broken again and the respective excitations have integer quantum numbers as in vacuum. However, as previous analyses show the inclusion of the color superconducting phase in the computation of the chiral restoring first order phase transition has only minor impact on its properties.

Unfortunately, the exact phase structure at high densities depends on the particular model,

the approximation scheme and the exact parameter values used to fix the model. This makes the current picture of the phase structure so far rather qualitative and vague. Further, most of the current analyses of the high density region are done in simple approximation schemes which involve only basic dynamics. Therefore, it is desirable to consider the high density region in an improved approximation scheme, which is provided by the renormalization group approach within an effective field theory framework.

As can be inferred from the chiral phase transition at the T- and μ-axis of the phase diagram, in the regime of finite temperature and density the two flavor chiral phase diagram exhibits a tricritical point [92, 97, 98]. Since this point is connected to long range fluctuations [99], it is of special importance for a possible experimental observation of new phase of matter in relativistic heavy ion collisions. In particular it has been pointed out that a possible thermalized system in the course of a heavy ion collision could come close to this point for a broad range of initial conditions [99]. This critical point has been analyzed in effective models [92, 97, 98] and recently also in the context of lattice gauge theory [101, 100]. So far there is a discrepancy between this two methods, since effective models yield a lower temperature for the critical point compared to lattice simulations. This could be connected to the rather low values for the critical density of the first order phase transition at vanishing temperature in effective models

This work is based on previous renormalization group (RG) treatments [27, 28, 37, 38] that explored the chiral phase transition at either the T or the μ-axis of the phase diagram and tries to extend these results to the full T-μ-plane. This opens the chance to resolve the critical point in the phase diagram. In this respect, a challenging motivation for the inclusion of the full field dependence in the RG analysis as introduced in Chapter 3 stems from the chiral phase transition at high densities and moderate temperatures which involves a first order region with two competing groundstates. In order to include both of these minima it is necessary to consider the evolution of the full grand canonical potential $\Omega(\Phi^2)$. However, for a consistent improvement of the approximation by the inclusion of the Yukawa coupling and of the wavefunction renormalization factors into the flow, it is necessary that these quantities are equally field dependent in order to provide the correct evolution for both of these groundstates. As has been shown in Section 3.5 these other variables have a remarkable field dependence already in vacuum. Therefore, the correct description of the two competing groundstates at finite density could be altered considerably if each groundstate is renormalized by its own wavefunction renormalization factors instead of common ones. This could solve the long standing puzzle, that the NJL model describes the bulk properties of strongly interacting systems successfully including their thermal behavior, but gives transition densities for the first order chiral phase transition that are below or only slightly above nuclear matter density.

4.1 THERMAL FLOW EQUATION IN LPA

In this section we will derive, the flow equation for the thermal system in the local potential approximation[1] (LPA), which represents the lowest order in the derivative expansion of the linear σ-model and incorporates fermionic as well as bosonic contributions to the thermodynamic bosonic potential[2] Ω.

First of all however, the introduction of a chemical potential with respect to the conserved baryon number density ρ_B needs some care. According to Eq. (2.8) it gives rise to the additional term

$$\mathcal{L}_\mu = -\mu\rho_B = -\mu\psi^\dagger\psi = -\mu\bar{\psi}\gamma_0\psi\,. \tag{4.1}$$

The fermionic determinant thereby takes the form

$$\Delta\Gamma_F = -\mathrm{Tr}\log D(\mu) \equiv -\mathrm{Tr}\log\left(\partial\!\!\!/ + g\Sigma - \mu\gamma_0\right)\,. \tag{4.2}$$

where $D(\mu)$ denotes the Dirac operator at finite chemical potential. As discussed in Section 3.6, the Dirac operator of QCD has a purely imaginary spectrum. Therefore the additional real term due to the chemical potential makes the Dirac determinant complex. This prevents so far direct lattice simulations since a lattice treatment is based on an average over different configurations within a Monte Carlo analysis that relies on real probabilities to weight the individual configurations.

However, in the local potential approximation which we will employ, the effective action is actually *real*. To see this and analyze the fermionic part in the proper time scheme it is again necessary to square it. However this time we do not restrict ourselves to the real part Eq. (3.15), but consider the full Dirac determinant in the form

$$\Delta\Gamma_F = -\tfrac{1}{2}\mathrm{Tr}\log\left(D(\mu)^2\right)\,. \tag{4.3}$$

By an analysis of the fermionic logarithm in its explicit series form and the use of the Dirac algebra we find, that it is diagonal in Dirac space and the 1-loop correction to the effective action in LPA takes the simple form

$$\Delta\Gamma = \tfrac{1}{2}\,\mathrm{Tr}\log\left(p^2 + M_\Phi^2\right) - \tfrac{1}{2}\,\mathrm{Tr}\log\left(\left(p^0 + i\mu\right)^2 + \vec{p}^2 + M_q^2\right) \tag{4.4}$$

As discussed in Sections 2.3 and 2.4, compared to the vacuum case the respective computation is complicated by the fact that the momentum components are treated differently in a thermal system and only discrete Matsubara frequencies are allowed. A straightforward partial evaluation of the trace in momentum space and a transformation of the expression to proper time form[3] using Eq. (C.1) yields

$$\begin{aligned}\Omega =&\Omega^{\mathrm{uv}} + \tfrac{1}{2}\int\frac{d\tau}{\tau}T\sum_{n=-\infty}^{\infty}\int\frac{d^{d-1}p}{(2\pi)^{d-1}}\Big(4N_cN_f\mathrm{e}^{-\tau\left((\nu_n+i\mu)^2+\vec{p}^2+M_q^2\right)}\\ &-3\mathrm{e}^{-\tau\left(\omega_n^2+\vec{p}^2+M_\pi^2\right)} - \mathrm{e}^{-\tau\left(\omega_n^2+\vec{p}^2+M_\sigma^2\right)}\Big)\,f(\tau k^2)\,.\end{aligned} \tag{4.5}$$

[1]Note, that although the linear σ-model is just a bosonized version of the NJL model, it is not equivalent to the fermionic theory in the LPA approximation, since it does not fulfill the respective initial condition $Z_\phi = 0$ at the UV scale of the RG flow.

[2]In the following, we denote the bosonic potential Ω instead of U in order to emphasize its thermodynamic role.

[3]The transformation of the apparently complex expression to proper time form is possible, since all imaginary parts cancel each other in the Matsubara sum.

where corresponding to Eq. (2.17) the Matsubara frequencies take the values $\omega_n = 2n\pi T$ for the mesons and $\nu_n = (2n+1)\pi T$ for the quark fields. As in the vacuum case Eq. (3.41) the proper time integral is regularized by a smooth cutoff function $f^{(a)}(\tau k^2)$ from the general set of functions Eq. (C.7). After performing the momentum integration over the spatial components

$$\begin{aligned}\Omega =&\Omega^{\text{uv}} + \frac{T}{2^d \pi^{\frac{d-1}{2}}} \int \frac{d\tau}{\tau^{\frac{d+1}{2}}} \sum_{n=-\infty}^{\infty} \Big(4N_c N_f \mathrm{e}^{-\tau\left((\nu_n+i\mu)^2+\vec{p}^2+M_q^2\right)} \\ &-3\mathrm{e}^{-\tau\left(\omega_n^2+\vec{p}^2+M_\pi^2\right)} - \mathrm{e}^{-\tau\left(\omega_n^2+\vec{p}^2+M_\sigma^2\right)}\Big) f(\tau k^2)\,,\end{aligned} \tag{4.6}$$

half integer powers of the proper time variable τ emerge. If the respective integral is regularized with a cutoff function specified by an integer parameter n as has been used in the vacuum case and previous work [37, 38, 128], an analytic performance of both the proper time integral and the Matsubara sum is not possible. However, in the thermal case effectively only an $d-1$-dimensional integral has to be regularized. From the derivative of the cutoff function Eq. (C.8), which is employed to derive the renormalization group equation, it can be seen, that a cutoff function specified by a *half integer* index $a = \alpha + \frac{3}{2}$, $\alpha \in \mathbb{N}$ equally involves a half integer power of the proper time variable τ. Combined with the τ-contribution from the momentum integration the τ integration over an integer power of the proper time variable can be performed using Eq. (C.3). Such half integer cutoff functions have also been applied to odd-dimensional spaces in [39]. The resulting flow equation takes the form

$$\begin{aligned}k\frac{d\Omega}{dk} =&\frac{T\,k^{2\alpha+d}(-1)^\alpha}{(2\sqrt{\pi})^{d-1}\Gamma\left(\frac{2\alpha+d+1}{2}\right)} \sum_n \frac{d^\alpha}{(dk^2)^\alpha} \\ &\cdot\left(\frac{3}{\omega_n^2+k^2+M_\pi^2} + \frac{1}{\omega_n^2+k^2+M_\sigma^2} - \frac{4N_cN_f}{(\nu_n+i\mu)^2+k^2+M_q^2}\right)\end{aligned} \tag{4.7}$$

where the k^2-derivatives on the right hand side have been introduced to bring the expression to a form that allows a convenient summation over the Matsubara modes. Furthermore, in order to perform this last sum the fermionic part needs to be reordered[4] to separate the contributions from quarks and anti quarks which are distinguished by a finite chemical potential

$$\sum_n \frac{1}{(\nu_n+i\mu)^2+E^2} = \frac{1}{2E}\sum_n\left(\frac{E+\mu}{\nu_n^2+(E+\mu)^2} + \frac{E-\mu}{\nu_n^2+(E-\mu)^2}\right) \tag{4.8}$$

In the form Eqs. (4.7, 4.8) the Matsubara sums can finally be performed using the standard results [102]

$$\sum_{n=-\infty}^{\infty} \frac{1}{\nu_n^2+x^2} = \frac{1}{2Tx}\tanh\left(\frac{x}{2T}\right) \quad , \quad \sum_{n=-\infty}^{\infty} \frac{1}{\omega_n^2+x^2} = \frac{1}{2Tx}\coth\left(\frac{x}{2T}\right) \tag{4.9}$$

Inserting these expressions and rearranging them into a physically instructive form, leads to an *analytic* RG improved flow equation for the grand canonical potential Ω

$$\begin{aligned}k\frac{\partial\Omega(\Phi^2,k)}{\partial k} =&\frac{k^5}{6\pi^2}\left(\frac{3}{E_\pi}\left(\frac{1}{2}+n_B(E_\pi)\right) + \frac{1}{E_\sigma}\left(\frac{1}{2}+n_B(E_\sigma)\right)\right. \\ &\left.-\frac{2N_cN_f}{E_q}\left(1-n_F(E_q)-\bar{n}_F(E_q)\right)\right)\,.\end{aligned} \tag{4.10}$$

[4]This can be done by exploiting the symmetry $\nu_{-i} = -\nu_{i-1}$ in the sum.

The appearing effective energies are defined by

$$E_i = \sqrt{k^2 + M_i^2}\,, \quad i \in \{\pi, \sigma, q\}\,,$$

the effective masses analogously to Eq. (3.27) by

$$M_q^2 = g^2\Phi^2\,, \quad M_\pi^2 = 2\,\frac{\delta\Omega}{\delta\Phi^2}\,, \quad M_\sigma^2 = 2\,\frac{\delta\Omega}{\delta\Phi^2} + 4\,\Phi^2\,\frac{\delta^2\Omega}{(\delta\Phi^2)^2}$$

and the occupation numbers have the usual forms

$$n_B(E) = \frac{1}{e^{\beta E} - 1}\,, \quad n_F(E) = \frac{1}{e^{\beta(E-\mu)} + 1}\,, \quad \bar{n}_F(E) = \frac{1}{e^{\beta(E+\mu)} + 1}\,.$$

Note the exceptionally simple form of this evolution equation. One can immediately read off the contributions from the vacuum and thermal dynamics of the respective particles appearing with their proper degeneracy factors. Especially, compared to previous vacuum equations (cf. Section 3.2) energy denominators appear instead of the usual relativistic propagator terms, which is natural for a thermal equation because of the broken Poincaré invariance. Moreover the vacuum and thermal parts are strictly separated and contribute additively in each evolution step.

In the limiting case of vanishing temperature this equation simplifies even further since thermal contributions of the bosons and antiquarks vanish and the quark partition function reduces to a θ-function

$$k\frac{\partial\Omega(\Phi^2,k)}{\partial k} = \frac{k^5}{12\pi^2}\left(\frac{3}{E_\pi} + \frac{1}{E_\sigma} - \frac{4N_cN_f}{E_q}\,\theta\left(E_q - \mu\right)\right)\,. \tag{4.11}$$

In this case the fluctuations with $E_q < \mu$ are suppressed due to the presence of a Fermi sea. This effect is known as "Pauli blocking". Compared to the respective equation derived with an integer cutoff [38] the flow equation Eq. (4.11) includes no additional terms due to the specific form of the cutoff function and in particular involves no singularities at the Fermi surface.

4.2 NJL-THERMODYNAMICS IN LARGE N_c

Equivalently to the results for the groundstate discussed in Section 3.4 the large N_c approximation of the flow which proved to be equivalent to the standard self consistent solution is the simplest possible solution scheme at finite temperatures and densities. Since only the fermionic dynamics contributes, the flow equation for the grand canonical potential simplifies considerably

$$k\frac{\partial\Omega(\Phi^2,k)}{\partial k} = -\,\frac{N_cN_f\,k^5}{3\pi^2\,E_q}\left(1 - n_F(E_q) - \bar{n}_F(E_q)\right)\,. \tag{4.12}$$

As in the case of its vacuum counterpart Eq. (3.65), the right hand side of this flow equation is independent of Ω and the equation can be integrated directly. However, in the thermal case

this integration generally cannot be performed analytically[5]. An analytic integration is however possible at zero temperature and finite chemical potential, due to the great simplification of Eq. (4.11). The analytic finite density result reads

$$\Omega(\mu) = \frac{N_c N_f}{24\pi^2}\left(\frac{m_{\rm uv}^2}{2}\Phi^2 + k_{\rm uv}\sqrt{k_{\rm uv}^2+\Phi^2}(2k_{\rm uv}^2 - 3\Phi^2) + 3\Phi^4 \log\left(\frac{k_{\rm uv}+\sqrt{k_{\rm uv}^2+\Phi^2}}{\sqrt{\Phi^2}}\right)\right.$$
$$\left. -\theta(\mu^2-\Phi^2)\left(\mu^2\sqrt{\mu^2-\Phi^2}(2\mu^2-5\Phi^2)\right) + 3\Phi^4\log\left(\frac{\mu+\sqrt{\mu^2-\Phi^2}}{\sqrt{\Phi^2}}\right)\right). \quad (4.13)$$

The vacuum part in the first line takes a slightly different form as before in Eq. (3.69) due to the modified regularization, whereas the density dependent part in the second line is exactly the result that one obtains in a mean field treatment of the linear σ-model by a solution of the classical Euler-Lagrange equations in the presence of a bosonic condensate (cf. e.g. [103]).

In large N_c approximation one needs in addition the equation for the bosonic wavefunction renormalization factor Z_ϕ which can be obtained from the result of the derivative expansion discussed in Section 3.1 and Appendix B. The respective equation reads in direct generalization to Eq. (3.66)

$$k\frac{\partial Z_\phi}{\partial k} = -\frac{N_c N_f Z_\phi k^5}{3\pi^2}\frac{\partial^2}{(\partial k^2)^2}\left(\frac{1}{E_q}\left(1 - n_F(E_q) - \bar{n}_F(E_q)\right)\right) \quad (4.14)$$

and yields in the case $T = \mu = 0$

$$k\frac{dZ_\phi}{dk} = -\frac{N_c N_f Z_\phi}{4\pi^2}\frac{k^5}{E_q^5} \quad (4.15)$$

In the following we will give an overview of the thermodynamics of these equations, which are up to the different regularization equivalent to earlier self-consistent computations of the thermal behavior within the NJL model [104, 98, 50, 51]. We will work in the chiral limit in order to study the critical behavior and adjust our UV-parameters to obtain $f_\pi = 92$ MeV due to the observed small change of 1 MeV between f_π in the chiral limit and with explicit symmetry breaking (cf. Table 3.1) in large N_c approximation. In order to make the plots more accessible the constituent quark mass is fitted to $m_q = 300$ MeV. The UV parameters are therefore adjusted in this case to $k_{\rm uv} = 940$ MeV and $m_{\rm uv} = 246$ MeV. However, we note that the critical behavior as e.g. the exact transition temperature or the possibility to reconstruct a first order phase transition depends to some degree on the exact values of these parameters.

Using the Gibbs-Duhem relation the grand canonical potential density Ω is directly connected to the pressure of the system

$$\Omega(T,\mu) = -p(T,\mu)\,. \quad (4.16)$$

This provides the equation of state for the system, which is plotted as a function of T and μ in Fig. 4.1. Thereby, the vacuum pressure p_0 is subtracted which is meaningless in our context. It exhibits the characteristic rise $\mathcal{O}(T^4)$ with temperature known from a free gas

[5]This results from the quantum distribution functions, which are not integrable for massive relativistic gases.

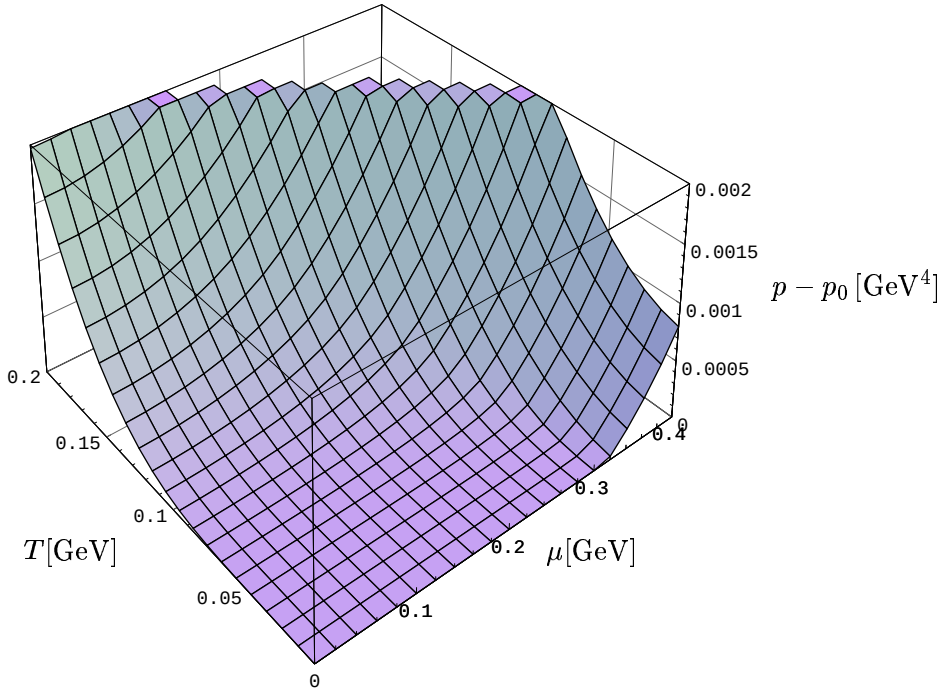

Figure 4.1: 3-dimensional illustration of the equation of state of quark matter within the NJL model in the large N_c approximation. Shown is the pressure where the vacuum pressure p_0 has been subtracted as a function of temperature T and quark chemical potential μ.

and vanishes at zero temperature until the chemical potential exceeds the constituent quark mass and there is a finite particle density.

To consider the temperature axis of Fig. 4.1 in more detail in order to analyze the asymptotic behavior of the equation of state, the strong rise at high temperature can be scaled out as shown in Fig. 4.2. As could be expected, the NJL model with a cutoff of roughly 1 GeV cannot describe the asymptotic behavior and the approach to the Boltzmann limit. Instead it is restricted to temperatures of roughly $T \lesssim \frac{k_{\rm uv}}{2\pi}$. Moreover, in the large N_c approximation it equally fails to describe the low temperature limit since the system contains only massive quark degrees of freedom which freeze out at low temperatures. Against it does not include thermal pions which dominate the low temperature behavior due to their Goldstone boson nature.

The baryon density of the system

$$\rho_B = -\frac{1}{3}\frac{\partial\Omega(T,\mu)}{\partial\mu} \tag{4.17}$$

is shown in Fig. 4.3 for various temperatures. It is more directly related to the experimental parameters in a heavy ion collision than the chemical potential μ. Furthermore, it is also the relevant parameter in the context of a first order phase transition. The baryon density exhibits the known discontinuous behavior in the first order region and becomes continuous at large temperatures.

The critical behavior is determined by the order parameter of chiral symmetry breaking which is given in the model by the expectation value of the (unrenormalized) bosonic field

Φ_0. In large N_c it is just the quark mass as discussed in Section 3.4. This order parameter is shown over the whole T-μ-plane in Fig. 4.4. At vanishing chemical potential it decreases with increasing temperature and goes continuously to zero signalizing a second order phase transition at a temperature of $T_c = 179$ MeV which compares well to both 3 and 2+1 flavor lattice simulations which congruently find a value in the range $T_c = 173 \pm 8$ MeV [14, 100]. At vanishing temperature we find a first order phase transition at a critical quark chemical potential $\mu_c = 318$ MeV. Correspondingly there is a tricritical point in the phase diagram. Compared to recent lattice results [100] which find the critical point at $T_3 = 160 \pm 3.5$ MeV and $\mu_3 = 242 \pm 12$ in our case it is at a very low temperature of $T_3 = 60$ MeV and at a higher chemical potential $\mu_3 = 290$ MeV. The full phase diagram which is just the projection of given Fig. 4.4 is shown in Fig. 4.5.

In the first order region of the phase diagram there are two competing groundstates. In this case the grand canonical potential, which describes a homogeneous system is not the appropriate thermodynamic potential to analyze this situation. Namely, the thermodynamically favored system in this case is one that is spatially nonuniform and exhibits separate regions - like droplets - where one of these two phases is realized. Generally such a nonuniform situation cannot easily be described within a simple thermodynamic analysis. However, under the assumption that the system is uniform and the separate phases coexist one can examine the free enthalpy density g which should have a minimum at the equilibrium configuration. This implies that the chemical potentials of the coexisting phases should be equal and from the analogue of the Gibbs-Duhem relation in this case $g = \mu\,\rho$ one obtains an equation for the free energy density $f = g - p$ in the coexistence region.

$$\frac{f}{\rho} = -p\,\rho^{-1} + \mu\,. \tag{4.18}$$

Therefore, by plotting the free energy over the density as a function of the inverse density one can find the equilibrium configuration within the restriction to spatial homogeneous configurations characterized by a uniform pressure and a common chemical potential. This is done via Maxwell's tangent construction shown for the considered system at $T = 0$ in Fig. 4.6. We find a coexistence region for baryon densities between 0.16 and 1.64 times nuclear matter density $\rho_0 = 0.17$ fm^{-3}. This is only an extreme case of the transition densities that have been obtained within the NJL model in the large N_c approximation, since they are all rather low [92, 28, 98].

Another interesting property is the modification of the equation of state in the presence of a chemical potential. The considered quantity in this respect which has also been studied in recent lattice simulations [105, 106, 107] is $\Delta p \approx p(T,\mu) - p(T,0)$. This quantity is given in a scaled form in Fig. 4.7 for the same values of the chemical potential as computed in [105]. We also give the temperature in units of our critical temperature $T_c = 179$ MeV, which nearly agrees with the one of [105]. Whereas the lattice simulation mainly covers the high temperature region above T_c where our computation breaks down, our computation covers the low temperature regime. In particular in the region around T_c, where both computations are applicable, they roughly agree. However, compared to [105] we find a much more pronounced peak below T_c. Although this plot might be quite sensitive to confinement effects that are neglected in our approach and which could invalidate it at low temperatures, at higher temperatures of the order $T \approx 100$ MeV, where the peak is located they should be moderate in our approach.

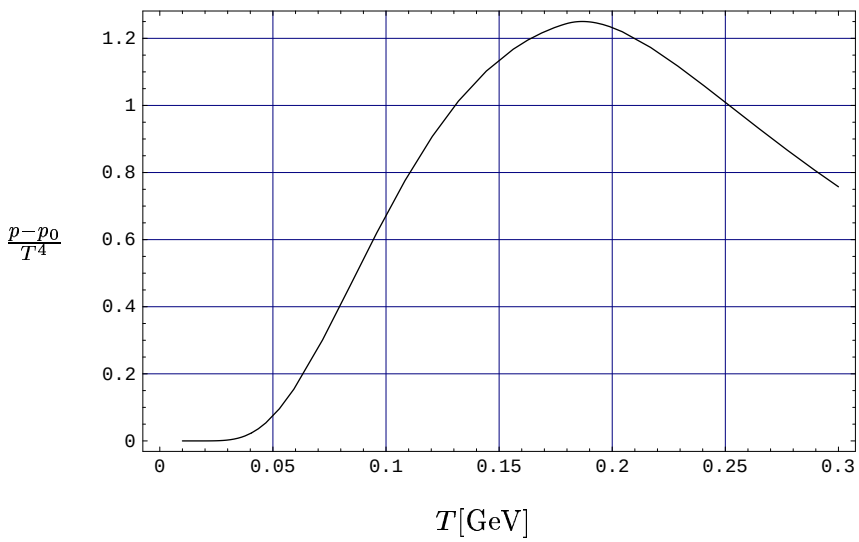

Figure 4.2: The scaled pressure as a function of temperature. Due to the UV cutoff the system does not reach its Boltzmann limit for $T \to \infty$. Thereby this plot shows the range of applicability of our low-energy model which reaches at most up to $T \approx 180$ MeV.

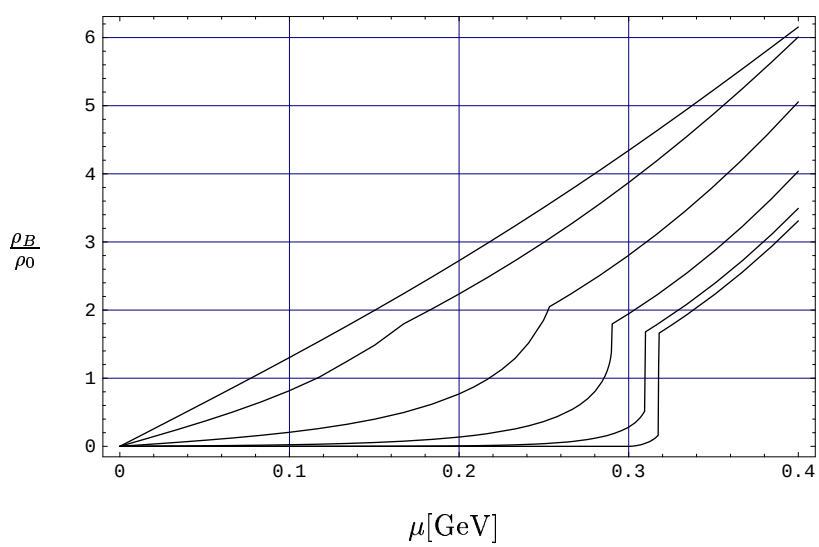

Figure 4.3: The baryon number density ρ_B in units of normal nuclear density $\rho_0 = 0.17$ fm^{-3} as a function of the quark chemical potential μ. Shown are the curves for the temperatures $T = 0$, 30 , 60, 100, 150 and 200 MeV in large N_c approximation. For $T \lesssim 60$ MeV the density is discontinuous within the first order phase transition, whereas it becomes a smooth function at high temperatures. At zero temperature the density vanishes identically below the constituent quark mass of $m_q = 300$ MeV.

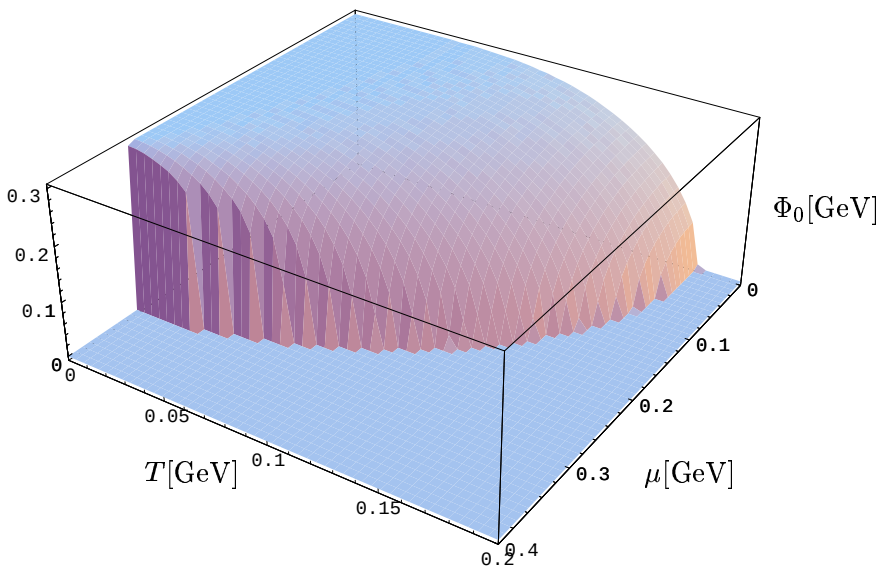

Figure 4.4: The order parameter Φ_0 of chiral symmetry as a function of T and μ which just corresponds to the quark mass in large N_c approximation. The "cut" to the left of the plot shows the discontinuous first order phase transition, whereas the continuous drop to zero reflects the second order phase transition where only the derivative of the order parameter is discontinuous. The grating comes from the finite resolution of the plot and unfortunately hides the tricritical point.

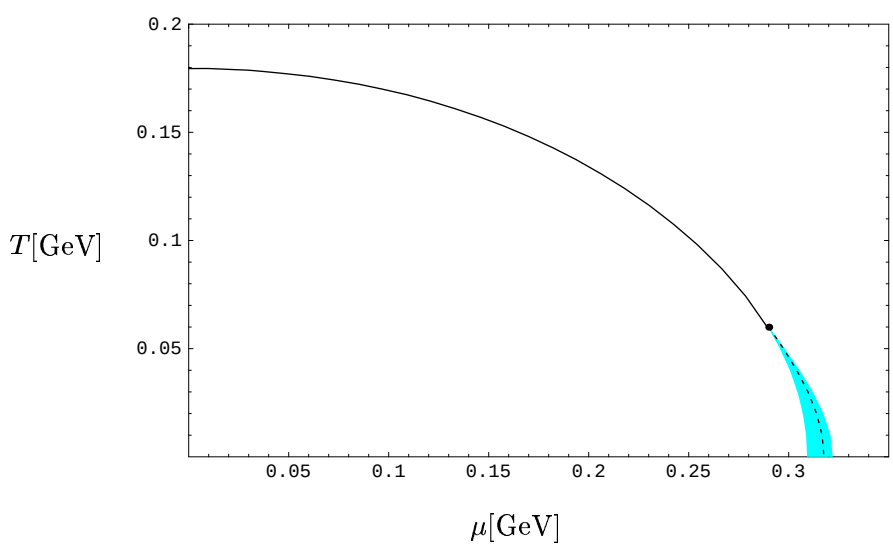

Figure 4.5: The phase diagram as a function of T and μ. The solid line denotes the second order transition and the dashed line the first order transition line which separate the chiral broken phase at low T and μ from the chiral symmetric phase at high T and μ. The shaded area shows the metastable region and the point denotes the critical point which we find at a rather low temperature.

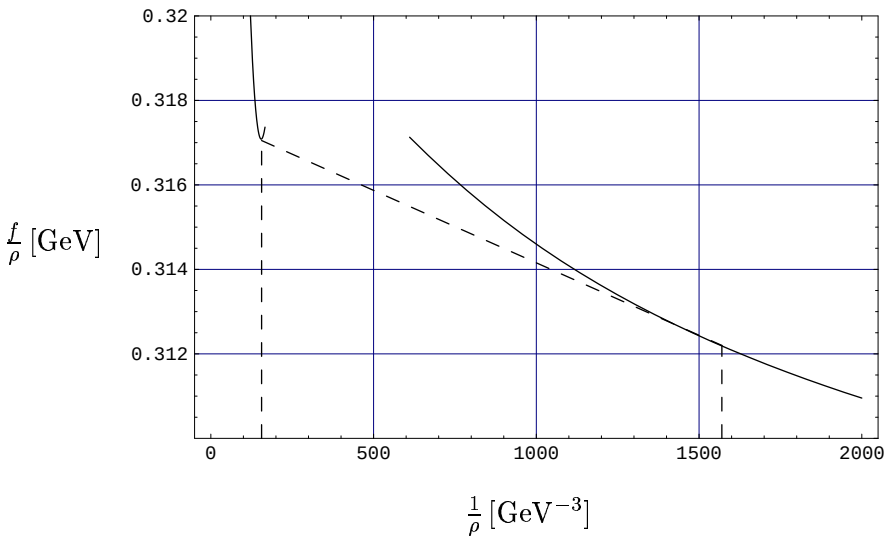

Figure 4.6: The Maxwell construction for the first order phase transition at vanishing temperature. It yields a first order coexistence region between 0.16 and 1.64 times nuclear matter density $\rho_0 = 0.17$ fm^{-3}.

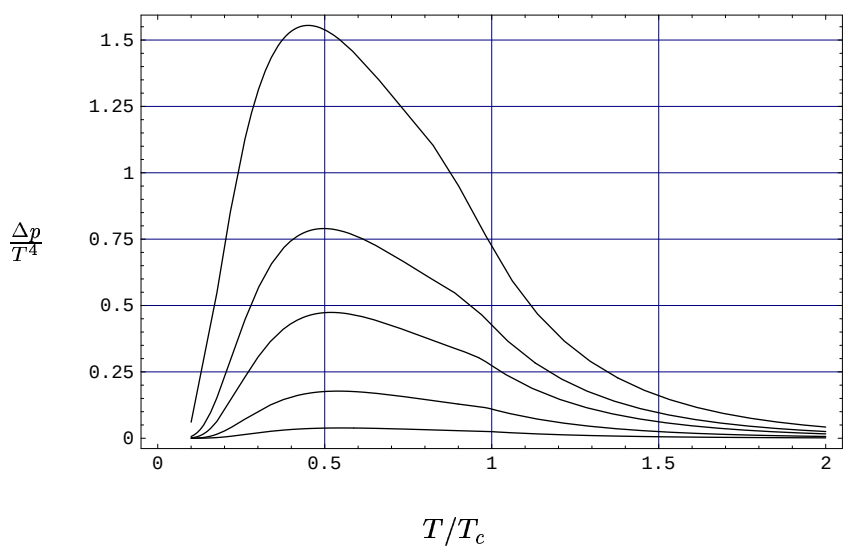

Figure 4.7: The dependence of the equation of state on the chemical potential. Shown is the quantity $\frac{\Delta p}{T^4}$, where $\Delta p \equiv p(T,\mu) - p(T,0)$ and the temperature dependence of a free relativistic gas is scaled out. This quantity is shown for baryon chemical potential $\mu_B = 100$, 200, 330, 410 and 530 MeV as used in [105].

4.3 Bosonic thermal fluctuations

Although the large N_c limit gives a reasonable description for many considered thermodynamic quantities, it has its limits where the thermal mesonic dynamics becomes relevant. This is especially the case where the quark dynamics is suppressed. Such a suppression occurs at small temperatures where the thermal quark dynamics freezes out due to the comparatively large quark mass. As discussed in the preceding section the quark dynamics is also suppressed at high chemical potential where the fermionic quantum fluctuations are blocked by the surrounding matter (cf. Eq. 4.11). This can be even more pronounced at small temperatures, since on the one hand the blocking is reduced but on the other hand the thermal pionic dynamics contributes in addition. Thereby, bosonic dynamics can have an impact on the first order chiral phase transition and the critical point. Hence we will in the following discuss the solution of the thermal flow equation for the grand canonical potential Ω derived in Section 4.1 which includes the mesonic fluctuations.

Despite its physically intuitive form Eq. (4.10) is still a very complicated nonlinear partial differential equation. In order to apply this equation in the context of a first order phase transition the series expansion technique used in Section 3.5 is no appropriate solution method. Instead the partial differential equation has to be computed by a discretization on a grid in Φ^2 (cf. Appendix D) to cover the whole potential which exhibits two competing minima[6] in this case. However, in the other regions of the phase diagram the series expansion method is still a valid alternative. The availability of two different calculation methods allows to cover the different regions of the phase diagram in an optimal manner. This also serves as a check in regions where both of them apply.

A direct solution of Eq. (4.10) however is plagued by instabilities. This can be seen directly from the flow equation, which involves derivatives of Ω in the denominators. If these derivatives are simply replaced by finite differences, these differences naturally involve errors due to a finite accuracy of the numerical evolution. Since these are negative in the inner parts of the symmetry breaking potential and k becomes small in the end of the evolution the energies in the denominators can become very small and thereby small errors can propagate very nonlinearly and invalidate the numerical computation. Similar to the method proposed in [129] this can be avoided by evolving not only the potential Ω but also its first two derivatives explicitly. Thereby, the finite differences appear only in the numerator and errors propagate linearly. This method provides a stable solution in vacuum and at finite temperatures and moderate densities.

The number of starting parameters that are required at the UV scale k_{uv} are heightened in the LPA approximation, since a nonzero value for the 4-boson coupling λ_{uv} is required to achieve a chiral condensation in the IR. Again, the model parameters are fixed in order to obtain vacuum quantities of $f_\pi = 92$ and $m_q \approx 300$ MeV. We use the set of parameters $g = 3.2$, $m = 320$ MeV and $\lambda = 30$ for the parametrization $\Omega_{\mathrm{uv}} = \frac{m_{\mathrm{uv}}^2}{2}\Phi^2 + \frac{\lambda_{\mathrm{uv}}}{4}\Phi^4$ of the potential at the UV scale $k_{\mathrm{uv}} = 1$ GeV. In vacuum this yields an evolution similar to the one discussed in the previous chapter. As already mentioned, compared to the large N_c approximation Fig. 3.1 the potential becomes convex in the IR when bosonic fluctuations are considered. The evolution to convexity is shown in Fig. 4.8 where the effective potential in vacuum is shown at different k-scales. It shows a perfect convexity in the IR which emphasizes the quality of

[6]The expansion around both minima is inappropriate, since the series expansion around the symmetric vacuum turns out to be unstable.

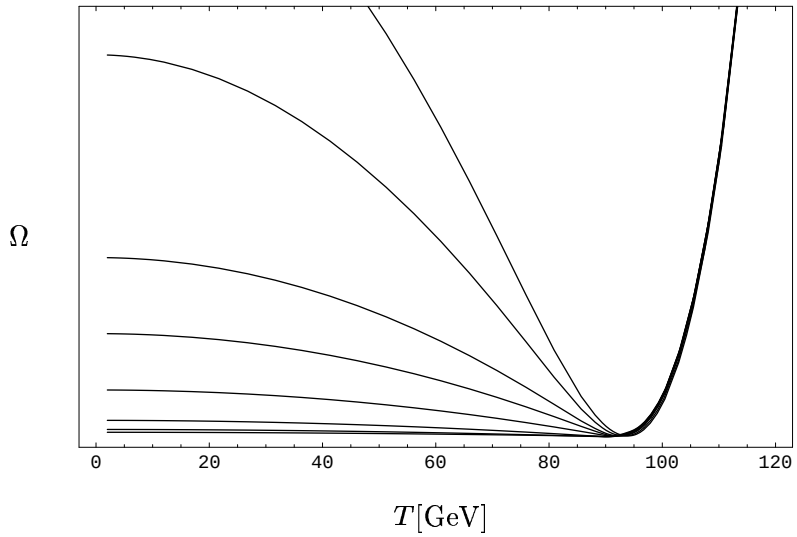

Figure 4.8: The evolution of the grand canonical potential to convexity. Shown is the effective potential at $k = 200$, 150 ,100, 75, 50, 30, 20 and 10 MeV respectively. The plot is obtained on a grid with 100 grid points.

the used numerics. [22]. In order to compute the second order chiral phase transition at finite temperature, however, the grid method is not ideal, since it involves a finite grid spacing which limits the accuracy on the exact transition temperature. A more exact determination is possible in the case of the series expansion. Nevertheless, within the uncertainty of 1.5 MeV the two methods agree. The result of the computation is shown in Fig. 4.9. We find a second order phase transition with temperature at a value of $T_c = 157$ MeV. This value is a bit lower than that obtained in large N_c, but compares well to the value of 164 MeV obtained in [37] within the SPT approximation in LPA but using a different cutoff function. A smaller value for the transition temperature has been obtained in an purely bosonic $O(4)$ description in the exact RG scheme [27]. For vanishing temperature and finite chemical potential we compute the evolution with Eq. (4.11), since the $T \to 0$ limit is not possible numerically in the general form Eq. (4.10). However, we experience the known problem, that the bosonic propagator terms in the evolution equation Eq. (4.10) turn negative during the flow in a certain region between the two minima. This problem has been discussed in [108] and has been traced back to the fact that the saddle point around which the fluctuations are considered becomes nontrivial. So far, this permits only a crude determination of the first order transition point. from the potential at a k value of roughly 200 MeV, where these instabilities occur. This suggests a transition point of about 315 MeV which is afflicted with a large error. Since the above problems occur only during the evolution due to the fact that in the end the potential has to become convex, they depend on the specific regularization used. Thereby, it could probably be cured by a different cutoff function which unfortunately itself complicates the numerics.

In principle, there is another solution to this problem, namely the introduction of a finite temperature. At finite temperature this problem should gradually vanish since the bosonic thermal fluctuations reduce the height of the barrier. A solution at finite temperature should then allow for an extrapolation to vanishing temperature. Because the exponentials in the

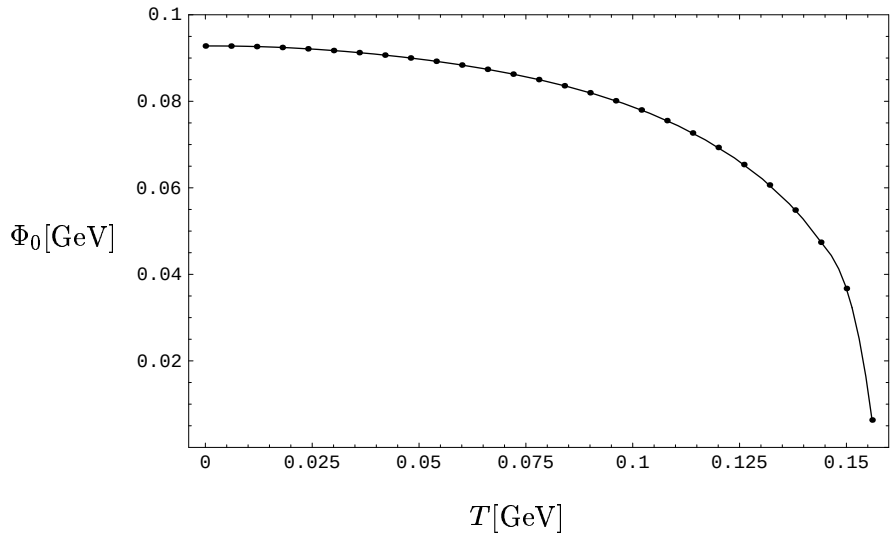

Figure 4.9: The order parameter Φ_0 at the second order phase transition. It vanishes at the transition point $T_c = 157$ MeV.

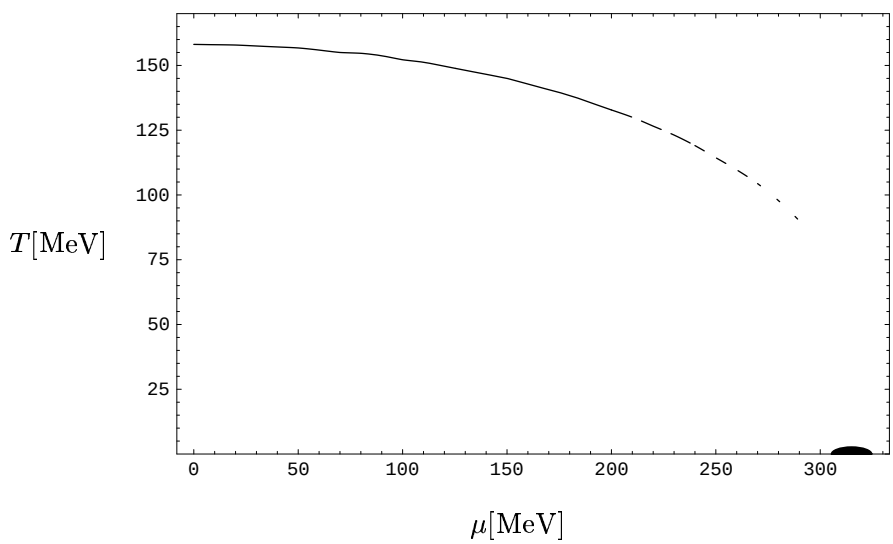

Figure 4.10: Preliminary phase diagram with respect to the chiral transition in the LPA approximation. The solid curve starting at $T_c = 157$ MeV represents the second order transition line, whereas the shaded area denotes the uncertainty on the position of the first order transition point at vanishing temperature and $\mu_c \approx 315$ MeV. Due to numerical instabilities we have not been able yet to determine the tricritical point in the phase diagram. In the figure, this is denoted by fading out the second order line, which is valid up to the tricritical point.

distribution functions Eq. (4.11) grow large at small T the numerics is only stable at $T > 15$ MeV. At this temperature the above problem has already disappeared - but unfortunately also the first order configuration. The reason is that in this region of finite temperature and chemical potential the bosonic terms dominate the flow equation at sufficiently small k. These large contributions introduce due to the finite difference scheme also large errors whereby the density effects at the Fermi surface are easily lost in the numerical evolution.

We have applied an additional method to improve the numerics in order to cover the first order region. The flow equation contains a bosonic and a fermionic part

$$k\frac{\partial U}{\partial k} = B(U(\Phi^2, k), k) + F(\Phi^2, k)\,. \tag{4.19}$$

We exploit that the fermionic part can be integrated directly as used in the large N_c case

$$U_F = \int_\kappa^\Lambda dk \frac{F(\Phi^2, k)}{k}\,. \tag{4.20}$$

Thereby, dividing the potential into a bosonic and a fermionic part $U = U_B + U_F$ we obtain a reduced equation for the bosonic part

$$k\frac{\partial U_B(\Phi^2, k)}{\partial k} = B(U_B(\Phi^2, k) + U_F(\Phi^2, k), k)\,, \tag{4.21}$$

where the fermionic part is computed with high accuracy in advance and "drives" the bosonic equation. Although, the numerics runs very stable with this method compared to the solution of the entire flow equation, a first order configuration with two minima that forms during the evolution is still lost in the IR. Another problem is that the smeared Fermi edge which is still rather steep at low temperatures complicates the necessary evolution of the derivatives considerably, since the derivatives of the Fermi edge yield quite peaked functions that propagate over the grid during the k evolution and easily introduce instabilities. Therefore, these problems require even improved numerical methods and prevent so far a determination of the critical point.

In this sense our RG approach is so far in the same position as lattice computations which by now are also able to cover a huge part of the phase diagram but cannot access the first order region [100, 101]. However, these simulation can exploit the transition to the continuum limit and analyze the analytic properties of the partition function by the method of Lee-Yang zeros. By this means they can indirectly obtain the position of the tricritical point in the phase diagram [100, 101]. Unfortunately, within our approach we do not have this possibility.

The preliminary result for the phase diagram is shown in Fig. 4.10. As in previous computations, we find a second order phase transition with temperature at vanishing chemical potential, which continues away from $\mu = 0$. This second order line should be valid up to the tricritical point which we could not determine so far.

4.4 CONCLUSION

We have derived a new analytic flow equation for the grand canonical potential at finite temperature and density by the introduction of a different set of cutoff functions than has been used in previous works. It involves energy denominators compared to the accustomed propagator-like terms and provides a very efficient description of the involved dynamics.

In the large N_c limit it can be solved analytically at vanishing temperature but finite chemical potential and gives for the density dependent part the same result as mean field theory. Within the large N_c approximation we have explored the equation of state over the full T-μ-plane. Moreover, we have analyzed the phase diagram of quark matter within this scheme. We find a transition temperature of $T_c = 180$ MeV for the second order phase transition with temperature at vanishing density. The transition density for the first order phase transition with density amounts to 0.16 time nuclear matter density and is thereby far to low. We have also studied the quantity Δp as a measure for the influence of the chemical potential on the equation of state. This quantity is accessible to lattice computations and has been explored in recent lattice simulations [105]. In the region where both computations apply we find consistent results. However, in the region below T_c we find a much stronger rise than the lattice method.

The solution of the full flow equation in LPA provides a reasonable description of the thermal system at finite temperature and moderate chemical potential. We have analyzed the evolution of the grand canonical potential to a convex form during the evolution. For the second order chiral phase transition at finite temperature we find a critical temperature $T_c = 157$ MeV, which compares well to previous computations [37]. Although, the simple form of the flow equation suggests the possibility of a straightforward numerical solution, an analysis in the finite density region holds a particular challenge for the numerical accuracy. Despite various numerical enhancements a full solution in this region has not been possible so far. However, we are confident to achieve this goal by a further refinement of the numerics. Although the LPA approximation will probably not change the results of the large N_c approximation and in particular the position of first order phase transition qualitatively, this could be the case for the improved approximation dicussed in the previous Chapter.

Chapter 5

Scale dependence and RG flow

Inherently, the renormalization group approach includes a scale dependence and defines an action at a given scale k (cf. Section 2.5). However, in RG schemes that employ a smooth cutoff function this direct connection is lost. This holds in particular for the Schwinger proper time regularization method, where the regulator acts in the integral over the proper time variable and not in the momentum integral itself. This virtue of the proper time scheme that on one hand allows to preserve required symmetries in the regularization, on the other hand prohibits to extract a scale dependence of physical quantities from the flow.

The accurate way to extract a scale dependence from the RG flow is to examine the momentum structure of considered vertices explicitly. That means to perform a derivative expansion to a sufficient high order. As shown in Chapter 3 and the dedicated Appendices A and B, the derivative expansion is a rather nontrivial task, especially if it has to be performed to higher orders. But this is necessary if one wants to cover the momentum dependence at higher momenta. Moreover the derivative expansion could break down completely if external momenta are larger than the characteristic scale of the theory. There may be the possibility to resum part of the derivative expansion. However one has to find a justification for such a procedure to neglect the remaining momentum dependence.

The need for an inclusion of the momentum dependence arises for instance if one wants to describe correlation functions of local operators that are separated in spacetime. Such point to point correlation functions involving physical currents have been computed on the lattice [11]. They provide interesting information about the groundstate, which are not included in the expectation values of local operators considered so far in this work. For instance they incorporate information about the actual propagating collective excitations. This information includes their mass and width which can differ from the particles and collective excitations that are parametrized in an effective low energy theory[1].

[1] For instance the resonance in the 0^{++} channel should exhibit a quite large width in contrast to the σ-degree of freedom in the linear σ-model [56].

From the point of view discussed above, it looks extremely hard to explicitly compute the momentum dependence needed to describe a physical correlation functions involving a large momentum scale from a fully integrated effective action. However, quantum fluctuations on very small momentum scales usually have only a minor impact on physical processes at large momentum scales. A striking example for this is the applicability of perturbative techniques due to asymptotic freedom in QCD [109]. In this case it is apparently not necessary to compute processes from an effective action that includes all non-perturbative dynamics. Therefore it may be possible even in more general cases to compute correlation functions that involve a certain momentum scale Λ from an action including quantum fluctuations only down to a scale $k \lesssim \Lambda$. In this case a much less involved treatment of the external momentum dependence should be sufficient.

Therefore, we will in this chapter approach the problem from the other direction and examine to what extend the momentum dependence of realistic correlation functions can be parametrized within the simplest momentum dependent coupling, namely a momentum dependent quark mass. The constituent quarks of the "naive", non-relativistic quark model are universal, i.e. hadron-channel independent degrees of freedom with a flavor-dependent but otherwise constant mass. This simple concept has been refined in several relativistic quark models. Usually, then, the quarks become "dressed" quasi-particles and their constituent mass turns into a momentum-dependent mean field or self-energy.

Constituent-quark masses with a different kind of momentum dependence have recently been employed for the description of diffractive vector-meson production processes in Ref. [110]. Guided by analogy with a non-relativistic quark-model amplitude, the authors of [110] model the vector polarization function in terms of a resolution-dependent quark mass (RDQM) $m_{\text{eff}}\left(Q^2\right)$, similar to the cutoff-dependent quark masses generated during renormalization group evolution of chiral quark models. Since this approach has proven quite successful in reproducing experimental data for the vector polarization amplitude, it seems worthwhile to explore its uses in a broader setting, i.e. in correlation functions of other important meson channels.

The specific implementation of the resolution-dependent quark mass in Ref. [110], namely as a replacement of the constant quark mass in the otherwise noninteracting correlators, lets one suspect that not the whole variety of physics in other meson channels can be captured in such a minimal way. In this regard the spin-0 correlators hold a particular challenge since their behavior can be qualitatively altered by the underlying vacuum physics. The strength of the interaction in the pseudoscalar isovector correlator, for example, gets up to two orders of magnitude larger than in the vector channel, and it sets in at smaller distances [111, 112]. Of course, this behavior is naturally explained by the spontaneous breakdown of chiral symmetry in the QCD vacuum and reflects the exceptionally strong attraction needed to generate almost massless Goldstone pions.

The pronounced differences in the behavior of the various mesonic correlators raise the question to which extent they can be described by a *universal* resolution (and flavor) dependent mass with an at least approximately channel-independent momentum dependence. Such a channel independence appears natural from the perspective of the naive quark model. Indeed, the spectroscopic successes of the latter suggest that important bulk features of most hadrons can be understood on the basis of universal constituent-quark properties, and especially without assuming their internal structure, as revealed by their momentum dependence, to depend on the hadron state considered.

Our strategy for exploring the virtues and limitations of the RDQM method beyond the

vector channel will rely mainly on a comparison of the resulting meson correlators with those obtained from other, as far as possible model-independent sources. As such input sources we employ experimental data, phenomenological estimates, and lattice results on point-to-point correlators. The latter constitute our main input in the spin-0 channels, which are not directly accessible to experimental probes. After outlining our calculational setup, we discuss generic properties of the resulting RDQMs and then proceed to their quantitative analysis. Finally, we present our conclusions and offer a few speculations about improved implementations of resolution-dependent masses.

5.1 MESONIC CORRELATORS WITH RESOLUTION-DEPENDENT QUARK MASSES

QCD correlation functions of interpolating currents with hadronic quantum numbers link hadron properties rather directly to quark properties. Hence they provide a suitable framework for phenomenological studies of resolution-dependent quark masses. The first such investigation [110] dealt with the correlator of two vector currents at spacelike momentum transfer and modeled several diffractive high-energy processes on its basis. Despite some motivation for this approach by an harmonic oscillator quark-model analogy for the photon wave function [110], however, the physical foundations and the implementation of the method deserve further study.

As a step in this direction, we will generalize the RDQM approach below to the light meson correlators

$$\Pi^{(i)}(x) = \langle 0| T J^{(i)}(x) J^{(i)\dagger}(0) |0\rangle \tag{5.1}$$

in those Lorentz channels for which phenomenological and lattice data exist. Hence we consider the isovector currents $J^{(i)} = \bar{u}\Gamma^{(i)}d$ in the channels i specified by $\Gamma^{(i)} \in \{1, i\gamma_5, \gamma^\mu, \gamma^\mu\gamma_5\}$. The Fourier transform of $\Pi^{(i)}(x)$ yields the polarization tensors

$$\tilde{\Pi}^{(i)}(q) = \int d^4z\, e^{iq\cdot x}\Pi^{(i)}(x) \equiv \Pi^{(i)}(q^2)K^{(i)}(q) \tag{5.2}$$

which we have factorized into an invariant amplitude $\Pi^{(i)}(q^2)$ and a Lorentz tensor $K^{(i)}(q)$ with

$$K^{(s)}(q) = K^{(p)}(q) = 1\ , \tag{5.3}$$

$$K^{(v)}(q) = K^{(at)}(q) = q^\mu q^\nu - q^2 g^{\mu\nu}\ , \tag{5.4}$$

$$K^{(al)}(q) = q^\mu q^\nu\ . \tag{5.5}$$

Here the superscripts denote the scalar (s), pseudoscalar (p), vector (v), as well as the longitudinal (al) and transverse (at) components of the axial-vector channel. The invariant amplitudes have the usual spectral representation

$$\Pi^{(i)}(Q^2 = -q^2) = \frac{1}{\pi}\int_0^\infty ds \frac{\mathrm{Im}\Pi^{(i)}(s)}{s + Q^2}\ . \tag{5.6}$$

We do not write subtraction terms explicitly since they will not enter our determination of the resolution-dependent masses.

Resolution-dependent quark masses

In this section we establish the basic formalism for obtaining resolution-dependent constituent masses $m_{\text{eff}}\left(\nu^2\right)$ from data on the meson correlators. To this end, we generalize the procedure of Ref. [110] where a model for the second Q^2-derivative of the physical vector correlator $\Pi^{(v)}\left(Q^2\right)$ was obtained by supplying the free quarks in the noninteracting vector correlator $\Pi_0^{(v)}$ with a resolution-dependent mass and by identifying the resolution scale ν with the momentum transfer Q. The derivatives with respect to Q^2 were taken mainly in order to remove the UV singularity of $\Pi_0^{(v)}$. A straightforward generalization of this procedure yields our model for the mesonic correlator amplitudes and their n-th derivative in the channel i,

$$\Pi_{\text{mod},n}^{(i)}(Q^2, m_{\text{eff}}) = \frac{\partial^n}{\partial\left(-Q^2\right)^n}\Pi_0^{(i)}(Q^2, m_0)\Big|_{m_0\to m_{\text{eff}}(Q^2)}, \tag{5.7}$$

where $\Pi_0^{(i)}$ are the invariant amplitudes of the free correlators

$$\tilde{\Pi}_0^{(i)}(-q^2, m_0) = iN_c\int\frac{d^4k}{(2\pi)^4}\,\text{tr}[S(k)\Gamma^{(i)}S(k+q)\Gamma^{(i)}] \tag{5.8}$$

and $S(k) = (\not{k} - m_0 + i\epsilon)^{-1}$ denotes the noninteracting fermion propagator.

In dimensional regularization, the free correlator amplitudes at spacelike momenta $Q^2 \equiv -q^2 > 0$ read

$$\begin{aligned}\Pi_0^{(s)}(Q^2) =& \frac{N_c}{8\pi^2}Q^2\left((1+\rho)^{\frac{3}{2}}\log\left(\frac{\sqrt{1+\rho}+1}{\sqrt{1+\rho}-1}\right) - 2\rho - \frac{5}{3}\right.\\ &\left.-\left(1+\frac{3\rho}{2}\right)\left[\frac{2}{\epsilon} - \gamma + \log(4\pi) + \log\left(\frac{\mu^2}{m_0^2}\right)\right]\right)\end{aligned} \tag{5.9}$$

$$\begin{aligned}\Pi_0^{(p)}(Q^2) =& \frac{N_c}{8\pi^2}Q^2\left(\sqrt{1+\rho}\log\left(\frac{\sqrt{1+\rho}+1}{\sqrt{1+\rho}-1}\right) - \frac{5}{3}\right.\\ &\left.-\left(1+\frac{\rho}{2}\right)\left[\frac{2}{\epsilon} - \gamma + \log(4\pi) + \log\left(\frac{\mu^2}{m_0^2}\right)\right]\right)\end{aligned} \tag{5.10}$$

for the spin-0 channels and

$$\begin{aligned}\Pi_0^{(v)}(Q^2) =& -\frac{N_c}{12\pi^2}\left(\left(1-\frac{\rho}{2}\right)\sqrt{1+\rho}\log\left(\frac{\sqrt{1+\rho}+1}{\sqrt{1+\rho}-1}\right) + \rho - \frac{5}{3}\right.\\ &\left.-\left[\frac{2}{\epsilon} - \gamma + \log(4\pi) + \log\left(\frac{\mu^2}{m_0^2}\right)\right]\right)\end{aligned} \tag{5.11}$$

$$\begin{aligned}\Pi_0^{(at)}(Q^2) =& -\frac{N_c}{12\pi^2}\left((1+\rho)^{\frac{3}{2}}\log\left(\frac{\sqrt{1+\rho}+1}{\sqrt{1+\rho}-1}\right) - 2\rho - \frac{5}{3}\right.\\ &\left.-\left(1+\frac{3\rho}{2}\right)\left[\frac{2}{\epsilon} - \gamma + \log(4\pi) + \log\left(\frac{\mu^2}{m_0^2}\right)\right]\right)\end{aligned} \tag{5.12}$$

$$\Pi_0^{(al)}(Q^2) = \frac{N_c}{8\pi^2}\rho\left(\sqrt{1+\rho}\log\left(\frac{\sqrt{1+\rho}+1}{\sqrt{1+\rho}-1}\right) - 2 - \left[\frac{2}{\epsilon} - \gamma + \log(4\pi) + \log\left(\frac{\mu^2}{m_0^2}\right)\right]\right) \tag{5.13}$$

for the spin-1 channels. Above, we have introduced the abbreviation $\rho \equiv 4m_0^2/Q^2$, the regulator $\epsilon \equiv 4 - d$, and its mass scale μ. As anticipated, the divergent pieces (corresponding

to subtraction terms in the dispersive representation) can be made to vanish by taking a sufficient number of derivatives with respect to Q^2. This will always be ensured below. Hence the above expressions, together with the prescription (5.7) for the $\Pi^{(i)}_{\mathrm{mod},n}(Q^2, m_{\mathrm{eff}})$, uniquely define our model for the interacting meson correlators.

At this point, it might be useful to emphasize a crucial difference between the resolution-dependent quark masses $m\left(\nu^2\right)$ defined above and the more conventional momentum-dependent self-energies which are encountered, e.g., in quark or instanton-vacuum models. In contrast to the latter, the RDQM does *not* depend on the loop momentum k flowing through the quark propagators, but rather on the overall momentum transfer Q which is assumed to set the resolution scale ν of the constituent quarks. This is analogous to the usual renormalization-group improvement of perturbation theory, where the running RG scale of coupling and mass parameters is similarly identified with the external momentum scale[2].

The identification of the scale ν with the overall momentum Q, i.e. with a variable not associated with the individual quarks but rather with the (channel-dependent) correlator as a whole, raises the crucial issue of channel dependence for the resolution-dependent quark mass.

Representation of input data and matching procedure

Information from several independent sources, including dispersive fits to experimental data in the spin-1 channels, QCD sum rules and lattice simulations of point-to-point correlators, indicate that the detailed structure of the spectral functions $\mathrm{Im}\Pi^{(i)}/\pi$ is strongly channel-dependent [112]. Nevertheless, most channels have two qualitative features in common: (i) only the lowest resonance in a given channel is clearly separated and fully resolved whereas the higher-lying ones increasingly merge with the multi-particle continuum, and (ii) local duality [113] implies that the hadronic continuum, when averaged over suitable invariant-mass intervals, can be approximated by the free-quark continuum in the same channel.

Hence the available experimental and lattice data on the considered meson correlators are (within their partially substantial errors, see below) well described by a parametrization of the spectral functions in terms of a zero-width ground state pole and an effective continuum:

$$\mathrm{Im}\Pi^{(i)}_{data}(s) = \pi\lambda_i^2\delta(s - m_i^2) + \mathrm{Im}\Pi^{(i)}_0(s)\,\theta(s - s_{0,i}). \tag{5.14}$$

This efficient and transparent parametrization, originally designed for QCD sum rules [114], has by now become fairly standard in hadron correlator phenomenology [112]. It depends on only three parameters: the mass m_i and coupling λ_i of the lowest resonance in the meson channel i and the corresponding threshold $s_{0,i}$. Note that local duality implies $s_{0,i} > m_i^2$. The required spectral functions $\mathrm{Im}\Pi^{(i)}_0$ for noninteracting quarks are obtained by analytically

[2]The RDQM approach is restricted to the spacelike momentum region of the correlators.

continuing Eqs. (5.9) - (5.13):

$$\mathrm{Im}\Pi_0^{(s)}(s) = \frac{N_c}{8\pi}\,\theta(s-4m_0^2)\,s\sqrt{\left(\frac{s-4m_0^2}{s}\right)^3}\,, \tag{5.15}$$

$$\mathrm{Im}\Pi_0^{(p)}(s) = \frac{N_c}{8\pi}\,\theta(s-4m_0^2)\,s\sqrt{\frac{s-4m_0^2}{s}}\,, \tag{5.16}$$

$$\mathrm{Im}\Pi_0^{(v)}(s) = \frac{N_c}{12\pi}\,\theta(s-4m_0^2)\,\frac{s+2m_0^2}{s}\sqrt{\frac{s-4m_0^2}{s}}\,, \tag{5.17}$$

$$\mathrm{Im}\Pi_0^{(at)}(s) = \frac{N_c}{12\pi}\,\theta(s-4m_0^2)\sqrt{\left(\frac{s-4m_0^2}{s}\right)^3}\,, \tag{5.18}$$

$$\mathrm{Im}\Pi_0^{(al)}(s) = \frac{N_c}{8\pi}\,\theta(s-4m_0^2)\,\frac{4m_0^2}{s}\sqrt{\frac{s-4m_0^2}{s}}\,. \tag{5.19}$$

Although local duality approximately relates the effective thresholds $s_{0,i}$ to properties of the ground-state resonances via finite-energy sum rules, we prefer to keep them independent in order to achieve a less biased representation of the input data.

We can now determine $m_{\mathrm{eff}}^{(i)}\left(Q^2\right)$ - independently in each channel i - by equating Q^2-derivatives of our model correlator amplitudes, given by Eq. (5.7), to different sets of input data in the above parametrization. Specifically, we will match the second derivatives $\Pi^{(2)}$ since $n = 2$ is the minimal number which renders all free correlators UV-finite and since higher derivatives tend to increasingly impair the numerical analysis[3]. We will refer to this procedure as the (minimal) "RDQM approach". To summarize the above discussion, our resolution-dependent quark masses $m_{\mathrm{eff}}^{(i)}\left(Q^2\right)$ are solutions of the equation

$$\left.\frac{\partial^2\Pi_0^{(i)}(Q^2,m_0)}{\partial\left(Q^2\right)^2}\right|_{m_0\to m_{\mathrm{eff}}^{(i)}(Q^2)} = \frac{2\lambda_i^2}{\left(m_i^2+Q^2\right)^3} + \frac{2}{\pi}\int_{s_{0,i}}^{\infty} ds\,\frac{\mathrm{Im}\Pi_0^{(i)}(s,m_0)}{\left(s+Q^2\right)^3} \tag{5.20}$$

in the channel i. In channels where $m_{\mathrm{eff}}^{(i)}$ reaches zero at a finite Q_c^2 it is assumed to remain zero for all $Q^2 > Q_c^2$ (or, more precisely, for Q^2 larger than the smallest Q_c^2 if there should be more than one, see below).

It remains to fix the three hadronic input parameters on the right-hand side of Eq. (5.20). In the analysis of the vector correlator in Ref. [110] the physical values of m_v and λ_v where used, while $s_{0,v}$ was obtained from a finite-energy sum rule[4]. Since direct experimental data on the momentum dependence of the meson correlators are available in the vector channel only, we have to resort to other sources for determining the parameters m_i, λ_i and $s_{0,i}$ in the other channels. Those will include the phenomenological estimates by Shuryak [112] and two sets of lattice data on point-to-point correlators [11, 115] (both extrapolated to the chiral and continuum limits) which are, at least in principle, free of uncontrolled model assumptions[5].

[3]As in [110], however, one should expect some n-dependence in the resulting $m_{\mathrm{eff}}\left(Q^2\right)$.

[4]The resulting $m\left(Q^2\right)$ of Ref. [110] is to good accuracy (5%) given by the linear parametrization $m\left(Q^2\right) \simeq (0.22\ \mathrm{GeV})\left(1-Q^2/Q_c^2\right)$ with $Q_c^2 = 1.05\ \mathrm{GeV}^2$.

[5]Initially, we had included the cooled lattice data of Ref. [116] in our analysis, in the hope to delineate information about the role of instantons in generating the hadronic input parameters. It turned out, however, that the RDQM method cannot resolve significant differences between the cooled and uncooled data.

The statistical and likely also the systematic errors of the lattice data[6] are still uncomfortably large, however.

The numerical values of m_i, λ_i and $s_{0,i}$ resulting from the different data sets are listed in the left part of Table I. For later use, we note that the correlators calculated in the instanton liquid model (ILM) [118] are also well represented in the pole-duality parametrization, and their predictions for the meson parameters have been included in Table I for comparison. The spacetime correlators corresponding to our input data sets in the respective channels, normalized to the free correlators, are plotted in Fig. 5.1. Most data are available for the vector correlator which has been measured in e^+e^- annihilation experiments and is, at low momenta, dominated by the ρ-meson. The lowest resonance in the transverse axial-vector channel is the heavier a_1 meson. In both channels we use Shuryak's phenomenological analysis of the experimental data [112] and the masses given by the Particle Data Group [58]. The scalar isovector channel is singled out by the absence of an established ground-state resonance. The pseudoscalar channel, on the other hand, is strongly dominated by the pion resonance with its exceptionally small mass and large coupling. For this reason, its ratio with the corresponding free correlator exceeds those in the other meson channels by up to two orders of magnitude.

5.2 QUALITATIVE BEHAVIOR OF THE SCALE-DEPENDENT QUARK MASS

Before embarking on the numerical solution of Eq. (5.20) it will be useful to establish several qualitative properties of the resulting resolution-dependent masses and their channel dependence. Besides providing useful checks and constraints for our subsequent numerical analysis, they will shed light on generic features of the RDQM approach.

Constituent quark masses

To start with, let us consider the $Q^2 \to 0$ limit of Eq. (5.20), which has the analytic solutions

$$m_{\rm eff}^{(s)}(0) = \frac{\sqrt{s_0}}{\sqrt{10}}, \qquad m_{\rm eff}^{(p)}(0) = \frac{\sqrt{s_0}}{\sqrt{6\left(1+\frac{8}{3}\pi^2\alpha_p^2\right)}}, \tag{5.21}$$

$$m_{\rm eff}^{(v)}(0) = \frac{\sqrt{s_0}}{\sqrt[4]{\frac{70}{3}\left(1+8\pi^2\beta_v^2\right)}}, \qquad m_{\rm eff}^{(at)}(0) = \frac{\sqrt{s_0}}{\sqrt[4]{70\left(1+8\pi^2\beta_{at}^2\right)}}. \tag{5.22}$$

The resonance parameters enter these expressions in the combinations

$$\alpha_i \equiv \frac{\sqrt{s_{0,i}}\lambda_i}{m_i^3} \quad \text{(spin-0)}, \qquad \beta_i \equiv \frac{s_{0,i}\,\lambda_i}{m_i^3} \quad \text{(spin-1)}. \tag{5.23}$$

The numerical values of the $m_{\rm eff}^{(i)}(0)$, as obtained from the various input parameter sets, are listed in the fifth column of Table I. With $\sqrt{10} \approx 3.2$ and typical continuum threshold scales $s_{0,i} \approx 1$ GeV one obtains masses of the order $m_{\rm eff}(0) \sim 200 - 350$ MeV - i.e. in the range expected for constituent quarks - in all but the pseudoscalar channel. This holds even in the scalar channel where no resonance is resolved (i.e. $\lambda_s = 0$) in any of the input data sets.

[6] We do not use the recent lattice data [117] from overlap fermions since those are restricted to relatively short distances, lack small-mass extrapolation and might be subject to rather large finite-size corrections.

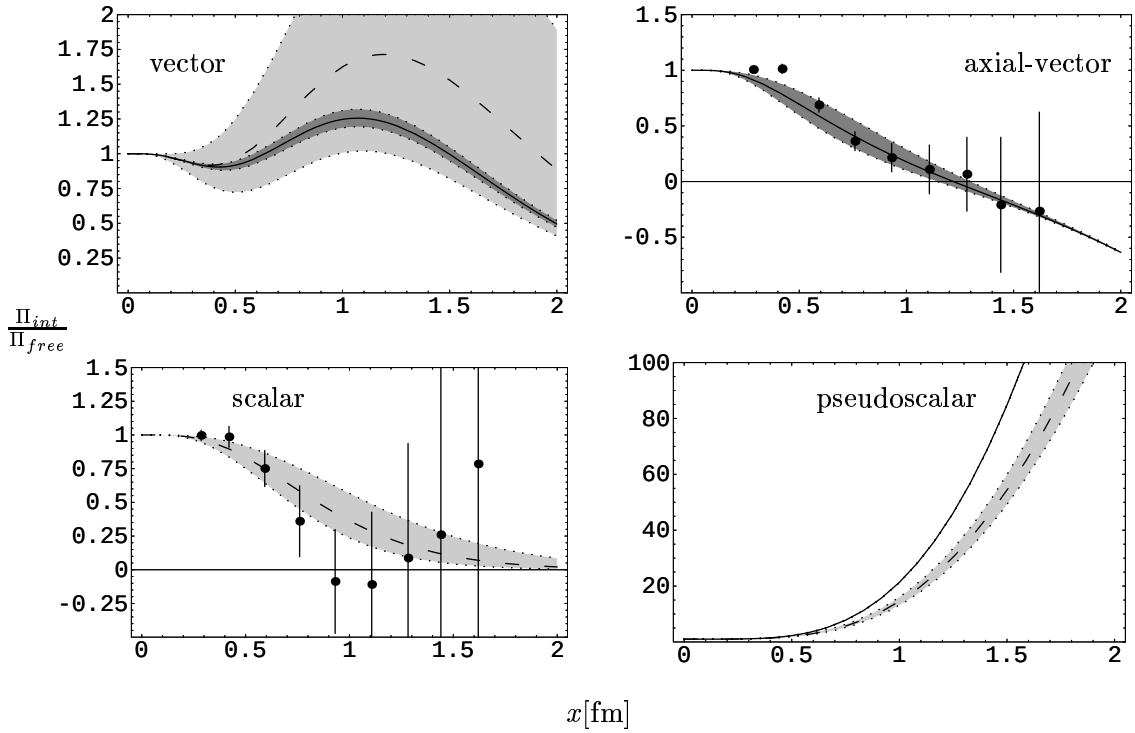

Figure 5.1: The resonance continuum parametrization of the ratio Π_{int}/Π_{free} of interacting and free coordinate space correlators in the channels considered. Solid lines with dark error bands represent the phenomenological correlators [112], whereas dashed lines with brighter (statistical) error bands represent the lattice correlators [11]. In the scalar channel the curve shows our fit to the lattice data (dots), whereas no significant fit to the shown lattice data was possible in axial-vector channel. Note that in the vector channel the error of the given fit is much larger than the error of the original lattice data [11].

The qualitative behavior of the $m_{\text{eff}}^{(i)}(0)$ can be understood by noting that the input values for couplings and continuum thresholds are of comparable size in all channels. Therefore, the resonance masses generate the main distinction between the channels. This is particularly obvious in the pseudoscalar channel where the mass of the resonance is exceptionally small. As a consequence, α_p dominates the denominator of (5.21) and the pseudoscalar constituent quark becomes unrealistically light, of the order of the light current masses: $m_{\text{eff}}^{(p)}(0) \propto m_p^2$. We have thus found first evidence for a strong channel dependence of our RDQM procedure. It does not really come as a surprise, though, because the (quasi-) Goldstone pion cannot be consistently described in the constituent quark model, from which the RDQM approach draws part of its motivation. An artificially small constituent mass is also obtained from the longitudinal part of the axial-vector correlator since partial conservation of the axial-vector current (PCAC) [119] relates it to the pseudoscalar correlator as

$$\Pi^{(al)}\left(Q^2\right) = \frac{4m_0^2}{Q^4}\,\Pi^{(p)}\left(Q^2\right) \ . \tag{5.24}$$

We have therefore not given the corresponding mass formula separately.

Chiral restoration

A characteristic property of resolution-dependent effective quark masses, expected on physical grounds and confirmed in Ref. [110], is that they decrease with growing resolution Q^2. Moreover, the mass of Ref. [110] was found to vanish (for $m_0 = 0$) at a critical scale $Q_c \sim 1$ GeV, in accord with the expectation that the massive "cloud" of a constituent quark disappears when probed hard enough to resolve the massless current quark. The vanishing of m_{eff} has been interpreted as a signature of chiral restoration since constituent quarks owe their mass to spontaneous chiral symmetry breaking and since the "critical momentum" $Q_c \sim 1$ GeV is compatible with the scale $\Lambda_\chi \simeq 4\pi f_\pi \sim 1.2$ GeV around which one expects chiral symmetry to be restored. In the spin-1 channels chiral symmetry even becomes manifest since the noninteracting spin-1 correlators are chirally invariant in the zero-quark-mass limit.

Since chiral symmetry and its spontaneous breaking are determining features of hadron physics one would expect the restoration transition towards $m_{\text{eff}}^{(i)}\left(Q_c^2\right) = 0$ to be a generic and robust property of resolution-dependent constituent masses. In particular, one would hope that the RDQM approach outlined above yields such a behavior in all correlator channels. Below we will establish the conditions under which this is possible. More specifically, we will obtain necessary and sufficient criteria for the existence and number of solutions of Eq. (5.20) at zero quark mass. To this end, we rewrite Eq. (5.20) in the chiral limit by isolating the pole piece on the right-hand side (and multiplying by $\pi/2$). This yields

$$\int_0^{s_0} ds \frac{\text{Im}\Pi_0^{(s/p)}(s, m=0)}{\left(s+Q_c^2\right)^3} = \frac{N_c}{16\pi} \frac{s_0^2}{Q_c^2\left(s_0+Q_c^2\right)^2} = \frac{\pi\lambda_{s/p}^2}{\left(m_{s/p}^2+Q_c^2\right)^3} \tag{5.25}$$

for the spin-0 channels and

$$\int_0^{s_0} ds \frac{\text{Im}\Pi_0^{(v/at)}(s, m=0)}{\left(s+Q_c^2\right)^3} = \frac{N_c}{24\pi} \frac{s_0\left(s_0+2Q_c^2\right)}{Q_c^4\left(s_0+Q_c^2\right)^2} = \frac{\pi\lambda_{v/at}^2}{\left(m_{v/at}^2+Q_c^2\right)^3} \tag{5.26}$$

for the spin-1 channels[7]. If solutions Q_c to these equations exist, the lowest one of them determines the transition point at which the RDQMs vanish. Due to the chiral symmetry of noninteracting, massless quarks the left-hand sides of the above equations are identical for both parities in the spin-0 as well as spin-1 channels.

Although the solutions of Eqs. (5.25) and (5.26) can be obtained analytically, they do not lend themselves easily to a transparent discussion. We therefore extract the required information on existence and number of solutions directly from the equations. Relegating details of the corresponding analysis to the appendix, we just list the main results here. The most general finding is that, independent of the channel, both equations (5.25) and (5.26) can have either zero, one or two solutions Q_c^2, depending on the values of the 3 hadronic parameters m^2, λ^2 and s_0. If two solutions Q_c^2 exist, then by continuity the smaller is the physical one. In the absence of a pole (i.e. for $\lambda_i^2 = 0$), furthermore, the only positive solution is $Q_c^2 = \infty$. In all other cases,Q_c^2 decreases with increasing resonance strength λ_i^2 and with decreasing pole mass m_i. This implies, in particular, that Q_c^2 will be smallest in the pion channel. Several additional properties of the solutions depend on the spin of the underlying correlator:

[7]For transparency of notation we have suppressed the channel labels of $s_{0,i}$ and $Q_{c,i}$.

1. In the spin-0 channels, the further analysis of Eq. (5.25) requires to distinguish the two domains $s_0 \lesseqgtr 3m_{s/p}^2/2$. For $s_0 > 3m_{s/p}^2/2$, which holds naturally in the Goldstone boson channel, and for $s_0^2 < 16\pi^2\lambda_{s/p}^2/N_c$, which is additionally satisfied by the pseudoscalar input parameter sets in Table I, we predict a single solution and find an upper bound on Q_c[8] given by
$$Q_c^2 \leq \frac{s_0 m_{s/p}^2}{2s_0 - 3m_{s/p}^2}. \tag{5.27}$$
(Note that this bound does not apply to our data sets in the scalar channel since m_s^2 cannot be resolved in this case, see below.) Moreover, we note that for the typical $s_{0,p} \sim$ 1 GeV and $m_p \sim 0.14$ GeV found in Table I, the bound (5.27) becomes unrealistically small, $Q_c < 0.1\,\mathrm{GeV}$. In the scalar channel, on the other hand, no pole term can be extracted from the data, i.e. $\lambda_s^2 = 0$. Inspection of Eq. (5.25) immediately shows that the scale-dependent quark mass cannot vanish at any finite resolution in this case. This entails another channel-dependence of the RDQM procedure (if it is not simply a shortcoming of our input data in the scalar channel).

2. In the spin-1 channels, we have again to distinguish between two domains of s_0-values: for $m_{v/at}^2 < s_0 < 2m_{v/at}^2$, which is satisfied by part of our input data in the vector channel and all of them in the axial-vector channel, we find a finite solution for $24\pi^2\lambda_{v/at}^2/N_c > 2s_0$ and none otherwise. For $s_0 > 2m_{v/at}^2$, which is satisfied by the remaining part of our input data in the vector channel, Eq. (5.26) can again have either one or no physical solution, depending on which parameter set in Table I is considered. For $s_0 > 2m_{v/at}^2$ there is an upper bound on Q_c^2 , given by
$$Q_c^2 \leq \frac{s_0}{6\left(2m_{v/at}^2 - s_0\right)}\left[s_0 - 6m_{v/at}^2 - \sqrt{\left(s_0 + 6m_{v/at}^2\right)^2 - 48m_{v/at}^4}\right], \tag{5.28}$$
which can be somewhat sharpened in case of a unique solution (see appendix).

Given an input data set for a correlator with the corresponding values for m, λ and s_0, the above results instantly reveal whether the extracted m_{eff} will vanish at some finite Q_c. With the data in Table I we predict a vanishing effective quark mass in the pseudoscalar channel as well as in the vector channel for the phenomenological, lattice I and II, but not for the ILM data, and no "chiral restoration" in the axial-vector channel (the ILM data in this channel are excluded from this consideration since they do not satisfy $m_{at}^2 < s_0$). These predictions hold for the central values of the input parameter sets and are confirmed by our numerical analysis below. Inside the rather large error range of the input parameter space in the vector channel there are also regions, however, in which no solution for Q_c^2 exists.

Moreover, our above findings show that both the existence and the scale of the "critical momentum" Q_c are rather sensitive to the values of the hadronic input parameters. For $Q_c \gg \Lambda_\chi \sim 1$ GeV, this dependence becomes so strong that details of the input data inside their systematic and statistical error range would contaminate the results. However, critical momenta of such a magnitude well beyond typical hadronic and restoration scales would have to be excluded anyhow on physical grounds, and their occurrence is strongly restricted (for

[8] A somewhat stronger bound, given in the appendix, can be established in the case of a unique solution.

reasonable values of the hadronic parameters) by the bounds (5.27) and (5.28). Finally, the above analysis shows that the RDQM procedure yields a well-defined and, in conjunction with the monotonicity of the $m_{\text{eff}}\left(Q^2\right)$, a unique Q^2-dependence of the resolution-dependent quark masses once the input parameters are fixed.

Generic limitations

A few additional limitations of the RDQM approach can be understood without numerical analysis. First and probably foremost, one should not expect this method to reproduce the exceptional properties of the pseudoscalar correlator, despite our observation that spontaneous chiral symmetry breaking and restoration are to some extent incorporated. We have found above, for example, that the pion pole contribution can only be matched with almost vanishing, i.e. unacceptably small constituent quark masses (cf. Table 5.1). This is consistent with the fact that the RDQM approach derives its main motivation [110] from an analogy with the non-relativistic quark model. Indeed, the latter also fails to describe the pion because it cannot provide the strong binding required by Goldstone's theorem. More generally, one might expect the RDQM approach to be overburdened in channels which contain exceptionally strongly bound states and to be more useful in channels where the lowest-lying resonances are quark-model states (including, e.g., the heavy-quark sector).

Another qualitative limitation of the RDQM approach is related to the channel-dependence of broken internal symmetries. Within the set of channels which we consider in this paper, this is most explicitly demonstrated for isospin symmetry. The underlying assumption of an isospin-symmetric effective mass, together with the isospin invariance of the free correlators, implies that the RDQM approach yields the same correlators in the scalar-isoscalar and scalar-isovector channels[9]. The physical correlators in those two channels, however, differ rather strongly[10]. In fact, lattice and instanton-liquid simulations as well as phenomenological estimates even find them to have opposite signs, indicating a rather strong attraction in the isoscalar and a similarly strong repulsion in the isovector channel [118]. This and other substantial differences cannot be captured by resolution-dependent quark masses *alone*. Even the introduction of an unrealistically large up/down constituent mass difference, at the price of a strong departure from universality and good isospin, would not be able to reproduce, e.g., the sign difference.

5.3 QUANTITATIVE ANALYSIS

In the following section, we discuss the results of determining the resolution-dependent quark masses according to the procedure described in section 5.1, i.e. by solving Eq. (5.20) numerically for $m_{\text{eff}}^{(i)}\left(Q^2\right)$ in the channels i under consideration. Of course, the exact solutions of Eq. (5.20) do constitute neither the most reliable nor the most exhaustive use of the information contained in the input data. In view of the considerable (both statistical and systematic) errors of the latter, an only approximate matching between data and model correlators inside some error margins should result in a better representation of the physics which they contain. Since the implementation of such a procedure would introduce additional ambiguity, however,

[9]Note that isospin-violating disconnected contributions could provide an exception to this rule in channels which carry vacuum quantum numbers.

[10]In the vector channel, the differences between isoscalar and isovector correlators are less pronounced.

we will instead just propagate the error ranges of the input data sets in order to get a measure for the errors of the resulting $m_{\text{eff}}^{(i)}\left(Q^2\right)$.

		m [MeV]	λ [MeV]	$\sqrt{s_0}$ [MeV]	$m_{\text{eff}}(0)$ [MeV]	Q_c^2 [MeV^2]
vector	phen.	780	214±6	1590±20	227±15	1320-318+528
	lat. I	720±60	233±47	1620±230	193±44	464-259+1957
	lat. II	690±170	209±163	1400±400	191±159	531-475+∞
	ILM	950±100	160±38	1500±100	347±92	-
axial-vector	phen.	1230±40	152±22	1600±100	381±42	-
(transverse)	ILM	1132±50	82±15	1100±50	351±27	-
		m [MeV]	$\sqrt{\lambda}$ [MeV]	$\sqrt{s_0}$ [MeV]	$m_{\text{eff}}(0)$ [MeV]	Q_c^2 [MeV^2]
scalar	lat. I	-	-	955±213	338±40	-
pseudoscalar	phen.	138	480	$\approx$ 1600	0.9±0.1	2.5±0.1
	lat. I	156±10	440±10	$<$ 1000	1.6±0.1	7.3±1.0
	ILM	142±14	510±20	1360±100	0.9±0.1	2.3±2.5

Table 5.1: The parameters of the resonance continuum fit to the input meson correlators of Refs. [112], [58] (phenomenological analysis of e^+e^- annihilation and τ-decay data), [11] (lattice simulation I by Chu et al.), [115] (lattice simulation II by Hands et. al.), and finally [118] (random instanton liquid model (ILM)). The phenomenological continuum threshold in the axial vector channel was estimated in [112]. The table also contains our results for the constituent masses and the critical momenta (where they exist). (The infinite upper bound on $Q_{c,v}^2$ from the lattice II data in the vector channel corresponds to the particular parameter combination $s_0 = 2m_v^2$ (cf. Eq. (5.28)) which lies inside the error range of the input data.)

The results of our quantitative analysis are collected in Table 5.1 and in Figs. 5.2-5.4. Besides the values of the critical momenta Q_c^2 (for the parameter sets where they exist) with their error bands, the numerical values of the quark masses at zero momentum transfer are listed in the right part of Table 5.1. As already mentioned, one finds typical constituent quark masses of the order 250 MeV $\lesssim m_{\text{eff}} \lesssim$ 350 MeV in all channels except the pseudoscalar one. The more detailed properties of the resulting $m_{\text{eff}}^{(i)}\left(Q^2\right)$ turn out to be channel-specific:

1. In the pseudoscalar channel we encounter unrealistically small scales for $m_{\text{eff}}^{(p)}$ and Q_c^2, owing to the underrepresentation of Goldstone-mode physics. Even if one would insist on fitting the pseudoscalar correlators by tolerating the necessarily too small $m_{\text{eff}}^{(p)}$, however, the matching would still fail for all $Q^2 > Q_c^2 \sim 5$ MeV^2 since the free, massless correlator cannot reproduce the strong rise found in the input data (cf. Fig. 5.1). This shortcoming acquires additional significance in view of the fact that this rise, and pionic physics in general, is probably underrepresented in the quenched lattice data of [11] and [115] (which yield rather large pion masses). As mentioned above, the relation between pseudoscalar and longitudinal axial-vector correlators (cf. Eq. (5.24)) implies that the latter is beyond the reach of the RDQM approach, too, and does not require independent discussion.

2. In the vector channel, the extracted, resolution-dependent quark masses interpolate

monotonically between reasonable constituent mass values at $Q = 0$ and zero[11] at the "critical" scale Q_c. This general behavior is in accord with the findings of Ref. [110] which were obtained in the same channel. The resulting Q-dependence of $m_{\text{eff}}\left(Q^2\right)$ is closest to the scale dependence of constituent masses which one would expect on the basis of the qualitative arguments given above. It is plotted in Fig. 5.2. As a consequence of our different input data sets and their rather large errors, however, we find a similarly large range of values for Q_c. This is a further indication for the mostly qualitative character of the estimates for m_{eff} which can be obtained from the RDQM approach.

3. The transverse axial-vector channel shares several common features with the vector channel. In particular, both noninteracting amplitudes become equal for zero quark mass. The main difference, at least in the duality-based continuum parametrization of the input data, is the about 60% larger resonance mass. It results in a much smaller (negative) slope of the $m_{\text{eff}}^{(at)}\left(Q^2\right)$, as can be seen from Fig. 5.3. This is the smallest slope found in all considered channels: $m_{\text{eff}}\left(Q^2\right)$ drops from its "constituent" value of about 380 MeV to about 320 MeV at $Q^2 \sim 3$ GeV^2 and saturates there. In particular, m_{eff} does not vanish at any finite Q^2, i.e. there is no indication for chiral restoration in this channel. (In order to obtain a restoration transition, the coupling λ_{at} would have to be about 3 times larger than the phenomenological estimate, i.e. $\lambda_{at} \geq 3\lambda_{a_1}$.) In view of the similarities and the chiral relation with the vector channel, this result might seem surprising. Perhaps it is an indication for the constituent-quark picture to fail at the rather large scales set by the mass of the $a_1\,(1260)$. In any case, the qualitative difference between the behavior of m_{eff} in the vector and axial-vector channels supplies our probably least expected case of channel-dependence in the RDQM approach since, in contrast to the pseudoscalar correlator, both vector and axial-vector resonances are well described by the NRQM.

4. The scalar-isovector channel is singled out by the fact that neither in the lattice nor in the instanton-liquid and phenomenological[12] data the pole of the lowest-lying resonance could be resolved. Our qualitative analysis in section 5.2 established that in this case the effective quark mass cannot vanish, so that their exists no finite Q_c^2 in this channel. This is confirmed by the numerical analysis, as shown in Fig. 5.4. (Unfortunately, lattice data for the scalar-isoscalar point-to-point correlator do not yet exist. This prevents us from studying the isospin-dependence in the scalar channel and in the delineated effective quark masses (cf. section 5.2) quantitatively.)

5.4 CONCLUSION

In our above analysis we have investigated several aspects of resolution-dependent quark masses in hadronic current-current correlation functions. To this end, we have generalized

[11] Note that the resolution-dependent mass extracted from the ILM data does not vanish at any Q^2. This might be related to the significantly larger constituent mass $m_{\text{eff}}^{(v)}(0)$ obtained in the ILM (cf. Table I). Similarly large constituent masses together with the absence of a chiral restoration transition are also found in the axial-vector channel (see below).

[12] The $a_0(980)$ resonance is commonly interpreted as a 4-quark state and therefore not included in the phenomenological analysis of Ref. [112].

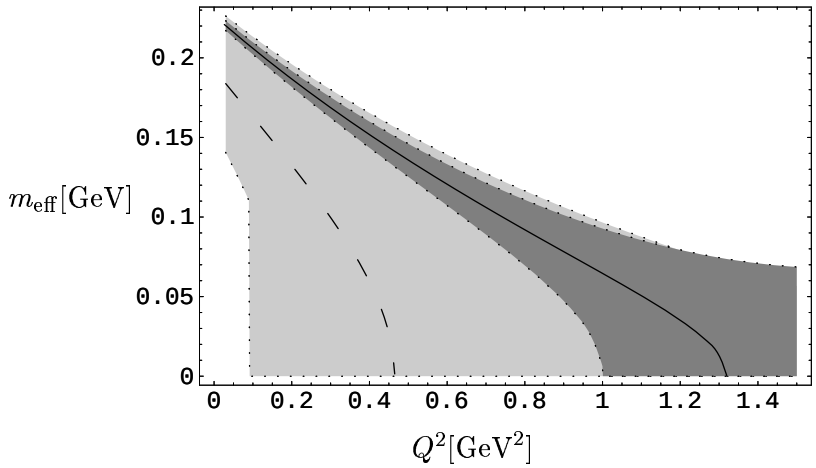

Figure 5.2: The resolution-dependent quark mass as obtained from the vector correlator. The input data are taken from the phenomenological estimate of Ref. [112] (solid with dark error band) and the lattice results of Ref. [11] (dashed with light error band). The error bands represent the propagated uncertainties of the input data (cf. Table I).

the recently proposed RDQM description [110], based on noninteracting mesonic correlators with a resolution-dependent constituent quark mass $m_{\text{eff}}\left(Q^2\right)$, beyond the vector channel. We have determined the resolution-dependent masses by matching the RDQM correlators to the available experimental and lattice data in the light meson channels. This enables us to clarify several virtues and limitations of the RDQM approach by comparison with a larger body of physical information. While the stringency of such comparative tests is limited by the rather large errors of our input data, it is on the other hand enhanced by the rich variety of physics in the different spin-0 and spin-1 meson channels.

Despite this diversity, we find the small-Q^2 behavior of the effective masses to be relatively channel-independent: in all but the pseudoscalar channel we obtain values in the expected range of about 250 - 350 MeV for $m_{\text{eff}}(0)$. The overall description of mesonic correlators in terms of noninteracting correlators with a unique $m_{\text{eff}}\left(Q^2\right)$ and a restoration scale $Q_c^2 \sim \Lambda_\chi^2$, however, does not generalize beyond the vector-meson channel. In fact, we do not find an even approximately universal effective mass: first of all, and as expected, the RDQM method cannot reproduce the pseudoscalar correlator with a physically reasonable constituent mass. Secondly, it also fails to generalize to channels like the axial-vector one whose ground-state resonances are quark-model states. This is more surprising since the approach was conceived in a non-relativistic quark model setting. Furthermore, non-perturbative enhancements of flavor-symmetry breaking, as they manifest themselves e.g. in the substantial differences between the isoscalar and isovector 0^{++} correlators, are not captured. Even the vanishing of m_{eff} at a finite Q_c^2, related to chiral symmetry restoration and thus expected to be a rather robust feature, is realized only in the vector correlator.

The above shortcomings can be traced to essentially one common root: the various correlator channels differ only in the Dirac and flavor structure of their interpolating fields, and consequently all channel dependence of the RDQM correlators is contained exclusively in the weights of chirally even and odd combinations of the *free* Dirac propagators in the spin and flavor traces. The differences between those weights are of order unity and hence cannot gen-

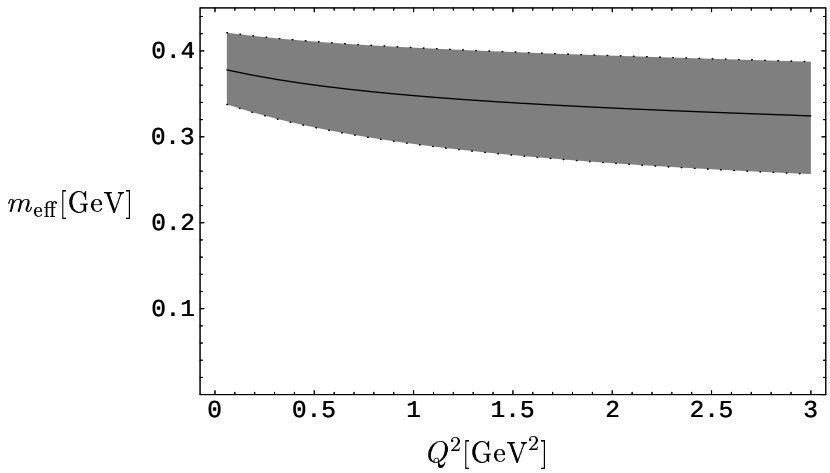

Figure 5.3: The resolution-dependent quark mass as obtained from the transverse axial-vector correlator. The input data are taken from the phenomenological estimate of Ref. [112]. Again, the error bands represent the propagated input uncertainties (cf. Table I).

erate the pronounced channel patterns found in the input data for the interacting correlators. If one nevertheless insists on matching free correlators with Q^2-dependent quark masses to those input data, one is bound to obtain strongly channel-dependent effective masses. Thus the RDQM parametrization is inconsistent with the assumption of the constituent-quark picture that the basic properties of constituent quarks do not depend on the hadron channel in which they are probed. This finding strongly suggests that the minimal RDQM approach, describing all correlators by just a free quark loop with resolution-dependent masses, overburdens those masses with the task of mocking up dynamics which should play itself out elsewhere.

From a microscopic point of view this is not surprising. A consistent RG-treatment of the quark dynamics would generate, besides the explicit interactions, a resolution dependence not only for the quark mass but also for the couplings and interpolating currents. To low orders in the quark-meson interactions, typical corrections due to the exchange of σ- and π-mesons are shown diagrammatically in Fig. 5.5. It is tempting to speculate about their qualitative impact and about whether the absence of such contributions in the minimal RDQM approach might explain some of its shortcomings. The pole diagram (a) contributes only in the pseudoscalar and longitudinal axial-vector channels[13] where a pion is exchanged. Since this contribution is very strongly attractive, it is likely that its neglect prevents a minimal RDQM description of the corresponding correlators with a constituent mass of the typical size. Diagram (b) contributes in the scalar, pseudoscalar, vector and axial-vector channels through vertices with the meson content $\vec{\pi} \times \vec{\pi}$, $\sigma\vec{\pi}$, $\vec{\pi} \times \partial_\mu \vec{\pi}$ and $\sigma\partial_\mu\vec{\pi}$, respectively. The contribution to the vector correlator is therefore mediated solely by Goldstone bosons. Hence the ensuing corrections set in at very low Q^2. In the minimal RDQM correlator, on the other hand, the absence of the corresponding strength can only be compensated by a smaller constituent quark mass $m_{\rm eff}^{(v)}\left(Q^2 \sim 0\right)$. This might explain why we indeed find $m_{\rm eff}^{(v)}(0)$ to be somewhat lower than the typical constituent mass scale. The lighter constituent mass might

[13]Recall that we only consider isovector interpolators.

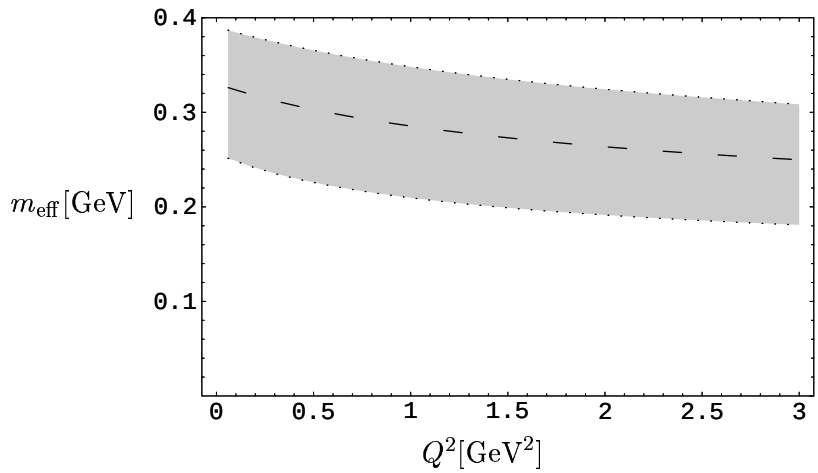

Figure 5.4: The resolution-dependent quark mass as obtained from the scalar correlator. The input data are taken from the lattice [11]. Again, the error bands show the propagated input uncertainties (cf. Table I). The resolution-dependent mass cannot vanish in this channel since no resonance is resolved in the input data.

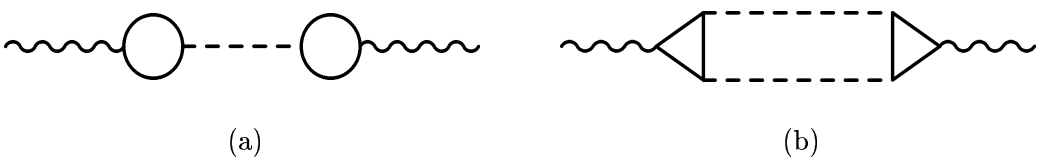

Figure 5.5: Two types of corrections to the hadronic correlators within a chiral quark model. The external currents are represented by wavy, quarks by straight and chiral σ and π mesons by dashed lines.

also facilitate the restoration transition in the vector relative to the transverse axial-vector channel.

In contrast, the corrections of type (b) to the axial-vector channel set in at higher Q^2 since the more massive σ-meson participates. These contributions should be negligible at small Q^2, rendering $m_{\rm eff}^{(at)}(0)$ our perhaps most reliable estimate for the constituent mass. Moreover, since corrections of type (b) with a σ-π pair exchanged can contribute strongly at momenta $Q^2 \sim \Lambda_\chi^2$ close to the typical restoration scale, their neglect may be partially responsible for the absence of a chiral-restoration transition in the transverse axial-vector RDQM correlator. In the scalar channel the situation is less conclusive. Since a pion pair can be exchanged in this channel, too, it is not a priori clear why we obtain a reasonable constituent mass value for $m_{\rm eff}^{(s)}(0)$ although this correction is neglected in the RDQM approach.

The above qualitative arguments, although tentative, give some hints on the possibility to consider such momentum dependent quantities in the RG approach. It suggests, that if in addition to the insufficient momentum dependence of the quark fields discussed in the above approach also the momentum dependence of the bosonic fields is considered this could lead to a reasonable reproduction of the bulk properties of the discussed correlation functions.

Chapter 6

Outlook

The need for an effective theory for the non-perturbative regime of strong interaction that is applicable also at larger scales than the low energy effective theory provided by chiral perturbation theory arises in many fields of strong interaction physics. The efficient description provided by the NJL model is thereby one promising candidate. The improved solution that we have presented could help to understand better to what extend such a simplified description is applicable.

The RG flow equations we have derived in Chapter 3 include so far only a common wavefunction renormalization factor for both chiral modes. It would be very interesting to include the wavefunction renormalization for the radial σ-mode of the bosonic field Φ into the truncation. This would provide a meaningful test on the quality of the description of the low energy regime of strong interaction provided by the NJL model. As discussed in Section 2.2, since chiral symmetry is broken in the ground state, the spectrum should be described by the nonlinear representation of chiral symmetry at low energies and consequently reduce to the "chiral circle". Thereby the σ mode should fully freeze out leaving the pions as the only low energy excitations, reflected by $Z_\sigma \to 0$. In previous approaches only a small reduction compared to the pionic wavefunction renormalization factor has been observed [121, 120], which can not compete against the evolution of the potential to convexity which leads to the inconsistent behavior of a vanishing σ-mass for $k \to 0$ in the chiral limit. The full field dependence included in our approach should include the correct behavior if the NJL model provides a correct decription of the low energy regime. In this case, it should in particular be possible to predict the low energy constants as has been done in [26].

Another extension of our approach would be the inclusion of a continued bosonization [44] of higher order fermionic terms that are generated during the flow. Such an inclusion should yield a better description of the σ-mode at intermediate energies by a partial observance of its bound state substructure and could also lead to an improved low energy behavior.

A very desirable improvement would be the extension of the momentum dependence of

the flow, which is still covered rather crude in our approach. As pointed out [122], it could be possible to include the complete momentum dependence of the wavefunction renormalization factors. This could be established within the used formalism by an additional resumation of derivatives acting on the same field, i.e. for instance in the case of the wavefunction renormalization factor Z_π an additional resumation of terms of the form $\partial^i\Phi\partial^j\Phi$, $\frac{i+j}{2} \in \mathbb{N}$. This would be a clear extension of the derivative expansion, since the "expansion parameter" would not be an external momentum anymore, but rather the configuration of momenta attached to a given graph. The justification for such an expansion is however not fully clear yet.

In addition, the effective action as the generating functional of 1PI diagrams contains a range of physical properties that could be exploited. A challenging but ambitious example would be the computation of correlation functions between physical currents which have been computed in lattice gauge theory [11]. As discussed, to achieve this goal might probably require to extract the scale information inherent in the flow in a well defined way.

The most promising field of applicability for chiral effective field theories like the NJL model, however, is the chiral phase transition at finite temperatures and densities. The study of such systems within the improved approximation scheme presented in this work could bring new insights on the mechanism of the first order transition at finite density which is not fully understood within the NJL model so far due to the rather low transition densities that have been found [28, 92, 98, 38]. As long as lattice gauge theory cannot make predictions on this region, a study of effective models might be the only means to learn about the rich phase structure at high densities that has been found so far [94, 95, 92, 96, 1].

In this respect the inclusion of vector mesons into the description could also have a considerable impact. Namely, the isoscalar ω vector meson condenses at finite density. As has been shown [123], this condensate is relevant for the phase structure and the excitations in the medium. Thereby on could probably also observe the proposed scaling behavior of vector meson masses [124] directly. The behavior of the particles in medium and at finite temperature is very important for an detection of possible new states of matter and would also provide a promissing field for future studies. Moreover, as is currently explored, the thermal flow equation can also be extended in order to include gluonic degrees of freedom in a minimal way to be able to describe the high temperature regime of strong interaction [125].

The derivation of the full set of flow equations for the next to leading order approximation at finite temperature and density is nearly finished. These equations shall be explored as soon as the numerics is stable enough to do this. As discussed this could have a pronounced influence on the first order phase transition due to the proper renormalization of both of the two competing vacua. Thereby, the NJL model could become a more quantitative model for the high density region of strong interaction and provide a better understanding of this physically interesting regime.

The NJL model has also been successfully applied to the weak phase transition in the early universe [126]. Probably also in this field the renormalization group approach to the NJL model could yield a better understanding of the physical processes, as it has done in many studies on the chiral phase transition so far [27, 28, 29, 37, 38].

Finally, a more direct connection of the local fermionic interaction described by the NJL model to the underlying dynamics of QCD which could maybe be established in the context of the renormalization group [45] is still a very desirable goal.

Appendix A

Proper time regularization of the mixed part

The last trace in Eq. (3.17) contains quark bilinears and therefore contributes to the Yukawa coupling and the quark wavefunction renormalization factor. A naive transformation of the logarithm appearing in the last trace of Eq. (3.17) to proper time form would lead to singular results since the momentum structure of the propagators appearing within the logarithm is not accurately regularized this way. Therefore a proper time regularization is possible only after a derivative expansion, signalizing that there may be no regularization of the full effective action at all in this case.
Since the logarithm contains fermionic bilinears, in order to match the considered parametrization of the effective action Eq. (3.2) it can be expanded to first order[1]

$$\Delta\Gamma_M = \frac{1}{2}\int d^4x \int \frac{d^4p}{(2\pi)^4}\,\mathrm{tr}\,\log\Big(1 + \Big(-Z_\Phi\partial^2 + U'' + A - B_\mu\partial_\mu\Big)^{-1} \cdot \big(C - 2\,S_{\bar{q}\Phi^i}D^{-1}S_{\Phi^j q}\big)\Big)\Big|_{\not\partial\to\not\partial+i\not p} \tag{A.1}$$

[1]Note, that as long as no derivatives on bosonic fields are involved, the expansion in fermionic fields could in principle also be carried out to higher orders

Furthermore, due to the parametrization Eq. (3.22) the derivative expansion for this part is has to be performed to first order, which is done by an expansion of the inverses

$$\begin{aligned}\Delta\Gamma_M \approx \tfrac{1}{2}\int d^4x \int \frac{d^4p}{(2\pi)^4}\,\bar{q}\,\mathrm{tr}\Bigg[&\frac{Z_\Phi^{-1}}{p^2+M_\Phi^2}\left(1+\frac{2\,i\,p\cdot\partial}{p^2+M_\Phi^2}\right)\\ &\cdot\Bigg(\left(\frac{\delta^2 g}{\delta\Phi^i\delta\Phi^j}\Sigma+\frac{\delta g}{\delta\Phi^j}e^i+\frac{\delta g}{\delta\Phi^i}e^j+\frac{\delta^2 Z_q}{\delta\Phi^i\delta\Phi^j}\left(\partial\!\!\!/+i p\!\!\!/\right)\right)\\ &-2\left(ge^i+\frac{\delta g}{\delta\Phi^i}\Sigma+\frac{\delta Z_q}{\delta\Phi^i}\left(\partial\!\!\!/+i p\!\!\!/\right)\right)\frac{Z_q^{-1}}{p^2+M_q^2}\left(-\partial\!\!\!/-i p\!\!\!/+\frac{g}{Z_q}\Sigma^\dagger\right)\\ &\cdot\left(1+\frac{2\,i\,p\cdot\partial}{p^2+M_q^2}\right)\left(ge^j+\frac{\delta g}{\delta\Phi^j}\Sigma+\frac{\delta Z_q}{\delta\Phi^j}\left(\partial\!\!\!/+i p\!\!\!/\right)\right)\Bigg)\Bigg]\,q\,, \end{aligned}\tag{A.2}$$

with the abbreviations $M_q^2 = Z_q^{-2}G^2\Phi^2$ and $M_\Phi^2 = Z_\Phi^{-1}U''$. Now it remains to expand out the product, keeping terms in lowest order in derivatives. The appearing propagators can in principle be regularized in proper time form. However, in order to regularize the full momentum structure, it is necessary to remove any momentum dependence from the numerators first by elementary algebraic transformations.

$$\begin{aligned}\Delta\Gamma_M \approx \int d^4x \int \frac{d^4p}{(2\pi)^4}\,\bar{q}\,\mathrm{tr}\Bigg[&\frac{1}{p^2+M_\Phi^2}E_G+\tfrac{1}{2}\frac{1}{p^2+M_\Phi^2}\left(1+\frac{M_\Phi^2}{p^2+M_\Phi^2}\right)E_{Z_q}\\ &+\frac{1}{(p^2+M_q^2)(p^2+M_\Phi^2)}F_G+\tfrac{1}{2}\frac{1}{(p^2+M_q^2)(p^2+M_\Phi^2)}\left(\frac{M_q^2}{p^2+M_q^2}+\frac{M_\Phi^2}{p^2+M_\Phi^2}\right)F_{Z_q}\Bigg]\,q\,, \end{aligned}\tag{A.3}$$

with the abbreviations

$$\begin{aligned}E_G =&\frac{1}{Z_\Phi}\Bigg(\frac{\delta G}{\delta\Phi^2}\left(\delta_{ij}\Sigma+2e^i\Phi^j\right)+2\frac{\delta^2 G}{(\delta\Phi^2)^2}\Phi^i\Phi^j\Sigma\\ &-4\frac{G}{Z_q}\frac{\delta Z_q}{\delta\Phi^2}e^i\Phi^j-8\frac{1}{Z_q}\frac{\delta G}{\delta\Phi^2}\frac{\delta Z_q}{\delta\Phi^2}\Phi^i\Phi^j\Sigma+4\frac{G}{Z_q^2}\left(\frac{\delta Z_q}{\delta\Phi^2}\right)^2\Phi^i\Phi^j\Sigma\Bigg)\\ E_{Z_q} =&\frac{1}{Z_\Phi}\left(\frac{\delta Z_q}{\delta\Phi^2}\delta_{ij}\partial\!\!\!/+2\frac{\delta^2 Z_q}{(\delta\Phi^2)^2}\Phi^i\Phi^j\partial\!\!\!/-4\frac{1}{Z_q}\left(\frac{\delta Z_q}{\delta\Phi^2}\right)^2\Phi^i\Phi^j\partial\!\!\!/\right)\\ F_G =&-\frac{G}{Z_\Phi Z_q^2}\Bigg(G^2e^i\Sigma^\dagger e^j+4G\frac{\delta G}{\delta\Phi^2}\Phi^2e^i\Phi^j+4\left(\frac{\delta G}{\delta\Phi^2}\right)^2\Phi^2\Phi^i\Phi^j\Sigma\\ &-4\frac{G^2}{Z_q}\frac{\delta Z_q}{\delta\Phi^2}\Phi^2e^i\Phi^j-8\frac{G}{Z_q}\frac{\delta G}{\delta\Phi^2}\frac{\delta Z_q}{\delta\Phi^2}\Phi^2\Phi^i\Phi^j\Sigma+4\frac{G^2}{Z_q^2}\left(\frac{\delta Z_q}{\delta\Phi^2}\right)^2\Phi^2\Phi^i\Phi^j\Sigma\Bigg)\\ F_{Z_q} =&\frac{1}{Z_\Phi Z_q}\Bigg(G^2e^i\partial\!\!\!/e^j+4G\frac{\delta G}{\delta\Phi^2}e^i\Phi^j\Sigma^\dagger\partial\!\!\!/+4\left(\frac{\delta G}{\delta\Phi^2}\right)^2\Phi^2\Phi^i\Phi^j\partial\!\!\!/\\ &-4\frac{G^2}{Z_q}\frac{\delta Z_q}{\delta\Phi^2}e^i\Phi^j\Sigma^\dagger\partial\!\!\!/-8\frac{G}{Z_q}\frac{\delta G}{\delta\Phi^2}\frac{\delta Z_q}{\delta\Phi^2}\Phi^2\Phi^i\Phi^j\partial\!\!\!/+4\frac{G^2}{Z_q^2}\left(\frac{\delta Z_q}{\delta\Phi^2}\right)^2\Phi^2\Phi^i\Phi^j\partial\!\!\!/\Bigg)\end{aligned}\tag{A.4}$$

Since the considered proper time representation regularizes only single, isolated poles, the above expression Eq. (A.3) has to be reordered using the identity

$$\frac{1}{q^2+M_q^2}\frac{1}{q^2+M_\Phi^2} = \frac{1}{M_q^2-M_\Phi^2}\left(\frac{1}{q^2+M_\Phi^2}-\frac{1}{q^2+M_q^2}\right) \tag{A.5}$$

to finally obtain the proper time regularizable form Eq. (3.18).

Appendix B

The derivative expansion for the bosonized NJL-model

Although this work is mainly concerned with the linear σ-model with a $SU(2)_L \otimes SU(2)_R \sim O(4)$ symmetry in four dimensions, because of the importance of the $O(N)$ model for various applications, we rather immediately perform the computation for general $O(N)$ symmetry in d dimensions as has been analyzed in [39].

B.1 Expansion and Resumation

As one of the great advantages of the SPT formalism, the actual derivative expansion in this scheme is just as simple as developing an exponential and keeping the terms compatible with the regarded truncation. To achieve this goal for the considered approximation Eq. (3.2) it is essential to consider and resum the commuting, derivative-free parts in Eq. (3.19). In the fermionic contribution this part is given by $\Pi_q \equiv Z_q^2 p^2 + G^2\Phi^2$ and in NLO derivative expansion the truncated 1-loop (T1L) correction takes the form

$$\Delta\Gamma_F^{T1L} \approx \tfrac{1}{2}\int d^dx \int \frac{d\tau}{\tau}\int \frac{d^dp}{(2\pi)^d}\,\mathrm{tr}\left[\sum_{n=0}^{\infty}\frac{(-\tau)^n}{n!}\Pi_q^n \right. \tag{B.1}$$

$$+\sum_{n=2}^{\infty}\frac{(-\tau)^n}{n!}\binom{n}{2}\Pi_q^{n-2}Z_q^2\left(\not\partial\left(G\Sigma^\dagger\right)\right)^2 - \sum_{n=2}^{\infty}\frac{(-\tau)^n}{n!}\sum_{k=0}^{n-2}\Pi_q^k\left(Z_q^2\partial^2 + Z_q\left(\not\partial Z_q\right)\not\partial\right)\Pi_q^{n-k-1}$$

$$\left. -p_\mu p_\nu \sum_{n=2}^{\infty}\frac{(-\tau)^n}{n!}\sum_{j=0}^{n-2}\Pi_q^j\left(2Z_q^2\partial_\mu + Z_q\left(\not\partial Z_q\right)\gamma_\mu\right)\sum_{k=0}^{n-2-j}\Pi_q^k\left(2Z_q^2\partial_\nu + Z_q\left(\not\partial Z_q\right)\gamma_\nu\right)\Pi_q^{n-j-k-2}\right],$$

whereas in the bosonic case $\Pi_\Phi \equiv Z_\Phi p^2 + U''$ has to be resumed to all orders, yielding

$$\begin{aligned}\Delta\Gamma_B^{T1L} \approx -\tfrac{1}{2}\int d^dx \int\frac{d\tau}{\tau}\int\frac{d^dp}{(2\pi)^d}\,\mathrm{tr}\Bigg[&\sum_{n=0}^{\infty}\frac{(-\tau)^n}{n!}\Pi_\Phi^n \\ &+\sum_{n=1}^{\infty}\frac{(-\tau)^n}{n!}n\Pi_\Phi^{n-1}A-\sum_{n=2}^{\infty}\frac{(-\tau)^n}{n!}\sum_{k=0}^{n-2}\Pi_\Phi^k\left(Z_\Phi\partial^2+B_\mu\partial_\mu\right)\Pi_\Phi^{n-k-1} \\ &-p_\mu p_\nu\sum_{n=2}^{\infty}\frac{(-\tau)^n}{n!}\sum_{j=0}^{n-2}\Pi_\Phi^j\left(2Z_\Phi\partial_\mu+B_\mu\right)\sum_{k=0}^{n-2-j}\Pi_\Phi^k B_\nu\Pi_\Phi^{n-j-k-2} \\ &-2p_\mu p_\nu\sum_{n=3}^{\infty}\frac{(-\tau)^n}{n!}\sum_{j=0}^{n-3}\Pi_\Phi^j\left(2Z_\Phi\partial_\mu+B_\mu\right)\sum_{k=0}^{n-j-3}\Pi_\Phi^k Z_\Phi\partial_\nu\Pi_\Phi^{n-j-k-2}\Bigg]\,.\end{aligned} \tag{B.2}$$

Here, the first term in each case which does not contain derivatives renormalizes the effective potential, whereas all other terms contain derivatives on bosonic fields and contribute to the bosonic wavefunction renormalization. These arise both from fermion and boson loop fluctuations. On the other hand, the very last term, containing quark fields, arises from both bosonic and mixed fluctuations and yields the renormalization of the quark wavefunction and the Yukawa coupling. The task, which will be discussed in this appendix, is then to resum the truncated expansions (B.1,B.2) to get a closed expression for the effective action. In order to achieve this, the first step is to perform the unsaturated derivatives using Leibniz's rule. This results in quite lengthy expressions. For instance the most complicated part in (B.2) containing two terms $\propto Z_\Phi p_\mu\partial_\mu$ involves

$$\begin{aligned}&\sum_{n=3}^{\infty}\frac{(-\tau)^n}{n!}\sum_{j=0}^{n-3}\Pi_\Phi^j Z_\Phi\partial_\mu\sum_{k=0}^{n-j-3}\Pi_\Phi^k Z_\Phi\partial_\nu(\Pi_\Phi)^{n-j-k-2} \\ &=\sum_{n=4}^{\infty}\frac{(-\tau)^n}{n!}\sum_{j=0}^{n-4}\Pi_\Phi^j\sum_{k=0}^{n-4-j}\sum_{l=0}^{n-4-j-k}\Bigg(\sum_{m=0}^{k}\Pi_\Phi^m Z_\Phi(\partial_\mu\Pi_\Phi)\Pi_\Phi^{k+l-m}Z_\Phi(\partial_\nu\Pi_\Phi)\Pi_\Phi^{n-4-j-k-l} \\ &\qquad+\Pi_\Phi^k\sum_{m=0}^{l}\Pi_\Phi^m Z_\Phi(\partial_\mu\Pi_\Phi)\Pi_\Phi^{l-m}Z_\Phi(\partial_\nu\Pi_\Phi)\Pi_\Phi^{n-4-j-k-l} \\ &\qquad+\Pi_\Phi^{k+l}Z_\Phi^2(\partial_\nu\Pi_\Phi)\sum_{m=0}^{n-4-j-k-l}\Pi_\Phi^m(\partial_\mu\Pi_\Phi)\Pi_\Phi^{n-4-j-k-l-m}\Bigg) \\ &\quad+\text{ terms}\propto Z_\Phi\partial_\mu Z_\Phi\partial_\nu\Pi_\Phi\,.\end{aligned} \tag{B.3}$$

The main difficulty at this point is that the matrices Π_Φ, Z_Φ, B_μ, and their derivatives do not commute in $O(N)$-space. Therefore, in order to resum the appearing sums it is necessary to reorder them. In most cases this can be done by shifting summation variables and the use of the simple reordering formula

$$\sum_{a=0}^{b}\sum_{c=0}^{a}f(a,b,c)=\sum_{c=0}^{b}\sum_{a=c}^{b}f(a,b,c)\,. \tag{B.4}$$

Again, the most complicated part comes from expression (B.3) which after shifting integration indices and using the cyclicity of the trace leaves the following five-fold sum

$$\begin{aligned}
&\sum_{n=4}^{\infty}\frac{(-\tau)^n}{n!}\sum_{j=0}^{n-4}\sum_{k=0}^{j}\sum_{l=0}^{k}\left(\left(\sum_{m=l}^{j-k+l}+\sum_{m=0}^{l}\right)\Pi_\Phi^m Z_\Phi(\partial_\mu\Pi_\Phi)\Pi_\Phi^{n-4-m}Z_\Phi(\partial_\nu\Pi_\Phi)\right.\\
&\qquad\left.+\sum_{m=0}^{l}\Pi_\Phi^{n-4-m}Z_\Phi^2(\partial_\nu\Pi_\Phi)\Pi_\Phi^m(\partial_\mu\Pi_\Phi)\right)\\
&=\sum_{n=4}^{\infty}\frac{(-\tau)^n}{n!}\sum_{m=0}^{n-4}\left(\left(n\binom{m+2}{2}-2\binom{m+3}{3}\right)\Pi_\Phi^m Z_\Phi(\partial_\mu\Pi_\Phi)\Pi_\Phi^{n-4-m}Z_\Phi(\partial_\nu\Pi_\Phi)\right.\\
&\qquad\left.+\binom{m+3}{3}\Pi_\Phi^m Z_\Phi^2(\partial_\nu\Pi_\Phi)\Pi_\Phi^{n-4-m}(\partial_\mu\Pi_\Phi)\right)\,,
\end{aligned}\tag{B.5}$$

where the partially resumed result is obtained in a sumptuary computation. In the reordered form most of the sums have been successively performed using the binomial sum identity

$$\sum_{a=c}^{b}\binom{a}{c}=\binom{b+1}{c+1}\,,\tag{B.6}$$

The fermionic contribution can be resumed directly, whereas the bosonic correction is only partly resumed so far

$$\begin{aligned}
\Delta\Gamma_B^{T1L}=&-\tfrac{1}{2}\int d^dx\int\frac{d\tau}{\tau}\int\frac{d^dp}{(2\pi)^d}\,\mathrm{tr}\Bigg[\\
&\left(1-\frac{\tau^2}{2}Z_\Phi(\partial^2\Pi_\Phi)-\tau A+p_\mu p_\nu Z_\Phi\left(\frac{2\tau^3}{3}(\partial_\mu(Z_\Phi\partial_\nu\Pi_\Phi))-\tau^2(\partial_\mu B_\mu)\right)\right)e^{-\tau\Pi_\Phi}\\
&-2\sum_{n=3}^{\infty}\frac{(-\tau)^n}{n!}\sum_{m=0}^{n-3}\binom{m+2}{2}(\Pi_\Phi)^m Z_\Phi(\partial_\mu\Pi_\Phi)(\Pi_\Phi)^{n-3-m}(\partial_\mu\Pi_\Phi)\\
&-4p_\mu p_\nu\sum_{n=4}^{\infty}\frac{(-\tau)^n}{n!}\sum_{m=0}^{n-4}\left(\left(n\binom{m+2}{2}-2\binom{m+3}{3}\right)\Pi_\Phi^m Z_\Phi(\partial_\mu\Pi_\Phi)\Pi_\Phi^{n-4-m}Z_\Phi(\partial_\nu\Pi_\Phi)\right.\\
&\qquad\left.+\binom{m+3}{3}\Pi_\Phi^m Z_\Phi^2(\partial_\nu\Pi_\Phi)\Pi_\Phi^{n-4-m}(\partial_\mu\Pi_\Phi)\right)\\
&-\sum_{n=2}^{\infty}\frac{(-\tau)^n}{n!}\sum_{m=0}^{n-2}\binom{m+1}{1}\Pi_\Phi^m B_\mu\Pi_\Phi^{n-2-m}\left((\partial_\mu\Pi_\Phi)+p_\mu p_\nu B_\nu\right)\\
&-2p_\mu p_\nu\sum_{n=3}^{\infty}\frac{(-\tau)^n}{n!}\sum_{m=0}^{n-3}\left(\left(n\binom{m+1}{1}-2\binom{m+2}{2}\right)\Pi_\Phi^{n-3-m}B_\mu\Pi_\Phi^m Z_\Phi(\partial_\nu\Pi_\Phi)\right.\\
&\qquad\left.+\binom{m+2}{2}\left(\Pi_\Phi^m B_\nu\Pi_\Phi^{n-3-m}Z_\Phi(\partial_\mu\Pi_\Phi)-\Pi_\Phi^{n-3-m}Z_\Phi B_\nu\Pi_\Phi^m(\partial_\mu\Pi_\Phi)\right)\right)\Bigg]\,.
\end{aligned}\tag{B.7}$$

In order to perform the remaining sums and the $O(N)$-traces it is necessary to decompose the wavefunction-matrix Z_Φ and mass-matrix U'' into their radial (σ) and spherical (π) parts

in $O(4)$ space using the projectors (3.21)

$$(\Pi_\Phi)_{ij} = (Z_\Phi)_{ij}\, p^2 + \frac{\delta^2 U}{\delta\phi_i \delta\phi_j} = (Z_\Phi)_{ij}\, p^2 + \left(4\frac{\delta^2 U}{(\delta\phi^2)^2}\phi_i\phi_j + 2\frac{\delta U}{\delta\phi^2}\delta_{ij}\right) \tag{B.8}$$
$$= \left(Z_\sigma\, p^2 + 2\frac{\delta U}{\delta\phi^2} + 4\phi^2\frac{\delta^2 U}{(\delta\phi^2)^2}\right)(X_\sigma)_{ij} + \left(Z_\pi p^2 + 2\frac{\delta U}{\delta\phi^2}\right)(X_\pi)_{ij} \equiv \Pi_\sigma\,(X_\sigma)_{ij} + \Pi_\pi\,(X_\pi)_{ij}\ .$$

Due to these projectors, powers of Π_Φ are easily computed

$$(\Pi_\Phi)^n = \sum_{m=0}^{n}\binom{n}{m}(\Pi_\sigma X_\sigma)^m\,(\Pi_\pi X_\pi)^{n-m} = \Pi_\sigma^n X_\sigma + \Pi_\pi^n X_\pi\ . \tag{B.9}$$

For instance, the part (B.5) takes the form

$$\sum_{i,j\in\{\sigma,\pi\}}\sum_{n=0}^{\infty}\frac{(-\tau)^{n+4}}{(n+4)!}\Pi_j^{2n}\sum_{m=0}^{n}\left((n+4)\binom{m+2}{2} - \binom{m+3}{3}\right)\left(\frac{\Pi_i^2}{\Pi_j^2}\right)^m X_i(\partial_\mu\Pi_\Phi)X_j(\partial_\nu\Pi_\Phi)\ .$$

Expressions for the remaining sums (over the index m) can be obtained from derivatives of a finite geometrical sum

$$\sum_{a=0}^{b}\binom{a}{c}x^a = \frac{1}{c!}\frac{d^c}{dx^c}\sum_{a=0}^{b}x^a = \frac{1}{c!}\frac{d^c}{dx^c}\left(\frac{1-x^{b+c+1}}{1-x}\right)\ . \tag{B.10}$$

B.2 TRACES

The fermionic traces are given by the standard results for Euclidian γ-matrices

$$\begin{aligned}\mathrm{tr}\,[\mathbb{I}] &= 4N_cN_f\\ \mathrm{tr}\,[\gamma_\mu\gamma_\nu] &= 4N_cN_f\,\delta_{\mu\nu}\ .\end{aligned} \tag{B.11}$$

where N_c and N_f denote the numbers of colors and flavors, respectively. The appearing bosonic traces are much more involved. Nevertheless, they can be obtained in a lengthy but straightforward computation.

The full set of traces reads

$$
\begin{aligned}
\mathrm{tr}\left[X_\sigma\right] &= 1 \\
\mathrm{tr}\left[X_\pi\right] &= N-1 \\
\mathrm{tr}\left[X_\sigma(\partial^2\Pi_\Phi)\right] &= -\,2\,\frac{\Pi_\sigma-\Pi_\pi}{\Phi^2}\left((\partial\Phi)^2-\frac{(\Phi\cdot\partial\Phi)^2}{\Phi^2}\right)+\left(\partial^2\Pi_\sigma\right) \\
\mathrm{tr}\left[X_\pi(\partial^2\Pi_\Phi)\right] &= 2\,\frac{\Pi_\sigma-\Pi_\pi}{\Phi^2}\left((\partial\Phi)^2-\frac{(\Phi\cdot\partial\Phi)^2}{\Phi^2}\right)+(N-1)\left(\partial^2\Pi_\pi\right) \\
\mathrm{tr}\left[X_\sigma(\partial\Pi_\Phi)X_\sigma(\partial\Pi_\Phi)\right] &= (\partial\Pi_\sigma)^2 \\
\mathrm{tr}\left[X_\pi(\partial\Pi_\Phi)X_\pi(\partial\Pi_\Phi)\right] &= (N-1)\,(\partial\Pi_\pi)^2 \\
\mathrm{tr}\left[X_\sigma(\partial\Pi_\Phi)X_\pi(\partial\Pi_\Phi)\right] &= \frac{(\Pi_\sigma-\Pi_\pi)^2}{\Phi^2}\left((\partial\Phi)^2-\frac{(\Phi\cdot\partial\Phi)^2}{\Phi^2}\right) \\
\mathrm{tr}\left[X_\sigma(\partial Z_\Phi)(\partial\Pi_\Phi)\right] &= -\,(Z_\pi-Z_\sigma)\,\frac{\Pi_\sigma-\Pi_\pi}{\Phi^2}\left((\partial\Phi)^2-\frac{(\Phi\cdot\partial\Phi)^2}{\Phi^2}\right)+(\partial Z_\sigma)\,(\partial\Pi_\sigma) \\
\mathrm{tr}\left[X_\pi(\partial Z_\Phi)(\partial\Pi_\Phi)\right] &= -\,(Z_\pi-Z_\sigma)\,\frac{\Pi_\sigma-\Pi_\pi}{\Phi^2}\left((\partial\Phi)^2-\frac{(\Phi\cdot\partial\Phi)^2}{\Phi^2}\right)+(N-1)\,(\partial Z_\pi)\,(\partial\Pi_\pi) \\
\mathrm{tr}\left[X_\sigma A\right] &= -\,\frac{Z_\pi-Z_\sigma}{\Phi^2}\left((\partial\Phi)^2-\frac{(\Phi\cdot\partial\Phi)^2}{\Phi^2}\right) \\
\mathrm{tr}\left[X_\pi A\right] &= (N-1)\,\frac{Z_\pi-Z_\sigma}{\Phi^2}\left(\left((\partial\Phi)^2-\frac{(\Phi\cdot\partial\Phi)^2}{\Phi^2}\right)+\left(\Phi\cdot\partial^2\Phi\right)\right) \\
\mathrm{tr}\left[X_\sigma\,(\partial B)\right] &= 2\,\frac{Z_\pi-Z_\sigma}{\Phi^2}\left((\partial\Phi)^2-\frac{(\Phi\cdot\partial\Phi)^2}{\Phi^2}\right)+\left(\partial^2 Z_\sigma\right) \\
\mathrm{tr}\left[X_\pi\,(\partial B)\right] &= -\,2\,\frac{Z_\pi-Z_\sigma}{\Phi^2}\left((\partial\Phi)^2-\frac{(\Phi\cdot\partial\Phi)^2}{\Phi^2}\right)+(N-1)\left(\partial^2 Z_\pi\right) \\
\mathrm{tr}\left[X_\sigma B X_\sigma B\right] &= (\partial Z_\sigma)^2 \\
\mathrm{tr}\left[X_\pi B X_\pi B\right] &= (N-1)\,(\partial Z_\pi)^2 \\
\mathrm{tr}\left[X_\sigma B X_\pi B\right] &= 0 \\
\mathrm{tr}\left[X_\sigma B X_\sigma(\partial\Pi_\Phi)\right] &= (\partial Z_\sigma)\,(\partial\Pi_\sigma) \\
\mathrm{tr}\left[X_\pi B X_\pi(\partial\Pi_\Phi)\right] &= (N-1)\,(\partial Z_\pi)\,(\partial\Pi_\pi) \\
\mathrm{tr}\left[X_\sigma B X_\pi(\partial\Pi_\Phi)\right] &= -\,2\,(Z_\pi-Z_\sigma)\,\frac{\Pi_\sigma-\Pi_\pi}{\Phi^2}\left((\partial\Phi)^2-\frac{(\Phi\cdot\partial\Phi)^2}{\Phi^2}\right) \\
\mathrm{tr}\left[X_\pi B X_\sigma(\partial\Pi_\Phi)\right] &= 0\,.
\end{aligned}
\tag{B.12}
$$

Here, N denotes the dimension of the $O(N)$-space over which the trace is taken and takes $N=4$ for the chiral $SU(2)_L \otimes SU(2)_R$ symmetry.
In the computation of the $O(4)$-traces for the mixed part it can be used that the τ- and

γ-matrices obey a Clifford algebra in 3 and 5 dimensions respectively. These traces result in

$$\begin{aligned}
\mathrm{tr}\left[X_\sigma e^i \Sigma^\dagger e^i\right] &= \Sigma \\
\mathrm{tr}\left[X_\pi e^i \Sigma^\dagger e^i\right] &= -3\Sigma \\
\mathrm{tr}\left[X_\sigma e^i \partial\!\!\!/ e^i\right] &= \partial\!\!\!/ \\
\mathrm{tr}\left[X_\pi e^i \partial\!\!\!/ e^i\right] &= 3\partial\!\!\!/ \\
\mathrm{tr}\left[X_\sigma \Phi^i e^j\right] = \mathrm{tr}\left[X_\sigma \Phi^j e^i\right] &= \Sigma \\
\mathrm{tr}\left[X_\pi \Phi^i e^j\right] = \mathrm{tr}\left[X_\pi \Phi^j e^i\right] &= 0
\end{aligned} \tag{B.13}$$

B.3 INTEGRATIONS AND TRANSFORMATION TO RENORMALIZED FORM

Since some of these traces involve terms $\propto \Phi\cdot\partial^2\Phi$ and $\propto \partial^2\Pi_i^2$ it is necessary to perform partial integrations, where the surface terms vanish in the infinite volume limit

$$\begin{aligned}
0 &= \int d^dx\, \partial\left(\mathrm{e}^{-\tau\Pi_i^2}\frac{\Phi\cdot\partial\Phi}{\Phi^2}\right) = \int d^dx \frac{\mathrm{e}^{-\tau\Pi_i^2}}{\Phi^2}\left(\Phi\cdot\partial^2\Phi + (\partial\Phi)^2 - 2\frac{(\Phi\cdot\partial\Phi)^2}{\Phi^2} - 2\tau\frac{\delta\Pi_i^2}{\delta\Phi^2}(\Phi\cdot\partial\Phi)^2\right) \\
0 &= \int d^dx\, \partial\left(\mathrm{e}^{-\tau\Pi_i}\partial\Pi_i\right) = \int d^dx\, \mathrm{e}^{-\tau\Pi_i}\left(\partial^2\Pi_i - \tau\left(\partial\Pi_i\right)^2\right) \quad , \quad i\in\{\sigma,\pi,q\}\,.
\end{aligned} \tag{B.14}$$

The momentum integrations can be performed using the general Gaussian expression

$$\int \frac{d^dp}{(2\pi)^d}\,\mathrm{e}^{-cp^2}\,p_{\mu_1}p_{\mu_2}\cdots p_{\mu_{2m}} = \frac{2^{-m}}{(4\pi)^{\frac{d}{2}}}\,c^{-(m+2)}\sum_{\mathcal{P}\{\mu_1,\mu_2,\cdots,\mu_{2m}\}}\delta_{\mu_1\mu_2}\cdots\delta_{\mu_{2m-1}\mu_{2m}}\,. \tag{B.15}$$

One last, but important step in the derivation of the one loop effective action is the partial renormalization of the expression by the introduction of renormalized effective masses. Consider for instance the fermionic correction to the effective potential, which takes the form

$$\Delta U_F \propto \int_0^\infty \frac{d\tau}{\tau}\exp\left(-\tau G^2\Phi^2\right) \tag{B.16}$$

In the case of a constant wavefunction renormalization factor Z_q at a fixed vacuum Φ_0, it is possible to scale the proper time variable τ in the integral via $\tau\to\tau' = Z_q^2\tau$ in order to absorb the constant wavefunction renormalization factors and obtain a renormalized mass $m_q = \frac{g^2}{Z_q^2}\Phi_0^2$ in the proper time expression. However, since in our improved approximation all quantities are Φ-dependent, it is necessary that the effective masses are renormalized quantities at each given vacuum value Φ. This can be established if the exponential is expanded in some complete set of functions[1] in Φ^2. Due to the linearity of the integral, the proper time variables in each separate integration over individual terms of the expansion can be scaled correspondingly to absorb the full Φ-dependent wavefunction renormalization factors and establish renormalized effective masses Eq. (3.27) in the final expression for the one loop effective action. Due to this procedure we do not need any wavefunction renormalization factors in our cutoff functions as applied in previous works [37, 39], but they depend only on a unique renormalized scale

[1] Since the flow variables are analytic functions, a local power series expansion would be possible for instance.

parameter k. Such an appearance of Φ-dependent Z-factors in the cutoff function would have been hard to justify in our case.
Finally, one can introduce the effective four-boson coupling Λ Eq. (3.31) and the effective pion decay constant F_π Eq. (3.30) in the uniform wavefunction approximation using the identity,

$$M_\sigma^2 - M_\pi^2 = \frac{2}{Z_\phi}\left(\frac{\delta U}{\delta\Phi^2} + 2\frac{\delta^2 U}{(\delta\Phi^2)^2}\Phi^2\right) - \frac{2}{Z_\phi}\frac{\delta U}{\delta\Phi^2} \quad \Rightarrow \quad 1 = \frac{2\,F_\pi^2\,\Lambda}{M_\sigma^2 - M_\pi^2}\,, \tag{B.17}$$

and one arrives at the result for the effective action (3.22) with parameters given by (3.23-3.26), whereas the respective couplings for the general $O(N)$-model in d dimensions take the exceptionally short form

$$U(\Phi^2) = U^{\rm uv} - \frac{1}{2\,(4\pi)^{\frac{d}{2}}}\int\frac{d\tau}{\tau^{\frac{d}{2}+1}}\left((N-1)\,e^{-\tau M_\pi^2} + e^{-\tau M_\sigma^2}\right) \tag{B.18}$$

$$Z_\phi(\Phi^2) = Z_\phi^{\rm uv} + \frac{4\,Z_\phi\,F_\pi\,\Lambda^2}{(4\pi)^{\frac{d}{2}}}\int\frac{d\tau}{\tau^{\frac{d}{2}}}\left(\frac{e^{-\tau M_\pi^2} + e^{-\tau M_\sigma^2}}{(M_\sigma^2 - M_\pi^2)^2} - \frac{2}{\tau}\,\frac{e^{-\tau M_\pi^2} - e^{-\tau M_\sigma^2}}{(M_\sigma^2 - M_\pi^2)^3}\right) \tag{B.19}$$

Appendix C

Proper time regularization

Schwinger's proper-time representation [33] of the logarithm of an operator O is given by

$$\log O = -\lim_{\Lambda\to\infty,\kappa\to 0}\int_{\frac{1}{\Lambda^2}}^{\frac{1}{\kappa^2}}\frac{d\tau}{\tau}\,\mathrm{e}^{-\tau O}\,. \tag{C.1}$$

This expression results from the $\Lambda \to \infty$ limit of the series expansion of the generalized Γ-function given by

$$-\Gamma\left[0,\tfrac{O}{\Lambda^2}\right] = -\int_{\frac{1}{\Lambda^2}}^{\infty}\frac{d\tau}{\tau}\,e^{-\tau O} = C + \ln(O) - \ln(-\Lambda^2) + \frac{1}{1\cdot 1!}\frac{O}{\Lambda^2} + \frac{1}{2\cdot 2!}\left(\frac{O}{\Lambda^2}\right)^2 + \dots\,, \tag{C.2}$$

where C is the Euler constant. Taking derivatives on both sides of Eq. (C.1) gives expressions for inverse powers

$$\frac{1}{O^n} = \lim_{\Lambda\to\infty,\kappa\to 0}\frac{1}{\Gamma(n)}\int_{\frac{1}{\Lambda^2}}^{\frac{1}{\kappa^2}} d\tau\,\tau^{n-1}\,\mathrm{e}^{-\tau O}\,. \tag{C.3}$$

Keeping κ and/or Λ finite in the proper time integral, they act as an IR cutoff κ and an UV cutoff Λ in the encompassing trace respectively and provide the desired regularization for physical n-point functions.
For the derivation of flow equations an explicit UV cutoff is not necessary, since such a cutoff is implicit in the initial conditions of the flow. The infrared regularization is done in this case by a smooth cutoff function $f(\tau k^2)$ in the proper time integral, that depends on a infrared scale k. The heat kernel cutoff function has to satisfy the following conditions

$$f(x\to 0) = 1 \tag{C.4}$$

$$f(x\to\infty) = 0 \tag{C.5}$$

$$f'(x) = -x^2 g(x)\,. \tag{C.6}$$

Condition (C.4) is required since the action Γ_k should become the full effective action Γ at $k = 0$ (in the limit $k \to 0$ the infrared cutoff is therefore removed). Condition (C.5) suppresses modes with fixed "virtuality" k for large τ. Condition (C.6) assures that the renormalization group equation for the k-dependent effective action is ultraviolet finite. The function $g(x)$ is a generic regular function in the vicinity of the origin.
A general set of functions respecting the above conditions, which has been used in the literature [35, 37], is given by the functions[1] $f^{(a)}$, where

$$f^{(a)}(x) = \frac{\Gamma(a,x)}{\Gamma(a)} \,. \tag{C.7}$$

with standard incomplete Γ-functions depending on a general real parameter a. In order to derive renormalization group equations, the derivative of this cutoff with respect to the cutoff function is the relevant quantity given by

$$k\frac{\partial f^{(a)}(k^2\tau)}{\partial k} = -\frac{2}{\Gamma(a+1)}(k^2\tau)^{a+1}\,\mathrm{e}^{-\tau k^2} \,. \tag{C.8}$$

In the special case of an integer parameter $a = n \in \mathbb{N}$ these functions, which have been used for several applications [37, 38, 39, 127], take the form[2]

$$f^{(n)}(x) = \mathrm{e}^{-x}\sum_{j=0}^{n}\frac{x^j}{j!} \,, \tag{C.9}$$

which enables an analytic integration of the occurring integrals and a closed form of the vacuum flow equations.
In this work we additionally apply the set of cutoff functions with a half integer parameter $a = \alpha + \frac{3}{2}$, $\alpha \in \mathbb{N}$. Due to the broken Lorentz invariance such a half integer cutoff is much better suited for thermal systems and leads to analytic flow equations in this case.

[1] As shown in [39], the ideal cutoff function can depend on the dimension of the system in question.

[2] In [127] it has been proposed to use the $n \to \infty$ of these cutoff function in order to derive a flow equation that improves the computation of universal quantities. However, in the non-universal regime covered in this work this limit seems not well defined due to the presence of explicit scales.

Appendix D

Numerical analysis

The considered renormalization group flow equations are a coupled set of nonlinear partial differential equations of the generalized parabolic type posed as an initial value problem in the flow parameter $k \in [0, \Lambda]$ and as a boundary value problem in the field parameter $\rho \in [0, \rho_{max}]$. These evolution equations for the "couplings" C_i have the generic form

$$\frac{\partial C_i(k,\rho)}{\partial k} = f_i\left(k, \rho, C_j(k,\rho), \frac{\partial C_j(k,\rho)}{\partial \rho}, \frac{\partial^2 C_j(k,\rho)}{(\partial \rho)^2}\right) . \tag{D.1}$$

There are mainly two different solution schemes[1] to solve the occurring renormalization group flow equations, namely the local series expansion around the vacuum expectation value ρ_0 and the discretization in the field variable ρ on a grid.

D.1 Series expansion

The series expansion method can only be applied in the case of a unique vacuum[2] but it is numerically much less demanding than the second one. Since it covers only the physically relevant region with high resolution it yields accurate results and has a good convergence with the expansion order [63, 128].
In this method both the couplings and the right hand sides of the flow equations (D.1) are

[1] In principle there is also the possibility to expand the system globally in a complete set of functions. In this case the difficulty is to find a set of functions defined on a appropriate domain, that suites the form of the considered couplings. In the case of the effective potential such a set seems to be given by Chebyshev polynomials. Nevertheless, the coupled set of equations becomes quite complicated and the respective numerical analysis unfortunately turned out to be too unstable for quantitative predictability.

[2] An expansion around each one of two competing minima, occurring in the case of a first order phase transition, is not possible since one of the stationary points becomes a maximum during the evolution and the respective flow becomes unstable.

expanded in a local power series around the k-dependent vacuum expectation value $\rho_0(k)$ given by the minimum of the effective potential $U \equiv C_1$ (i.e. correspondingly $c_1^{(1)} = 0$)

$$C_i(k,\rho) = \sum_{j=0}^{n} c_i^{(j)}(k)(\rho - \rho_0(k))^j \quad , \quad f_i(\cdots) = \sum_{j=0}^{n} f_i^{(j)}(\rho - \rho_0(k))^j \,. \tag{D.2}$$

Comparing coefficients on both sides yields a set of coupled ordinary differential equations for the expansion coefficients

$$\frac{\partial \rho_0(k)}{\partial k} = -\frac{1}{2c_1^{(2)}} f_1^{(1)} \,, \tag{D.3}$$

$$\frac{\partial c_i^{(j)}(k)}{\partial k} = f_i^{(j)} + (1-\delta_{jn})(j+1)\frac{\partial \rho_0}{\partial k} c_i^{(j+1)}(k) \,. \tag{D.4}$$

The convergence radius of the power series tends to zero[3] in the limit $k \to 0$, which reflects the fact that the effective potential becomes convex in this limit [22] and in this case the expansion around the physical vacuum would be just at the kink, where the potential starts to rise.

D.2 DISCRETIZATION

The other numerical solution method for the partial differential equations by discretization on a grid is more flexible than the expansion technique just discussed. It can also cover situations, where there are two competing vacua or a large explicit symmetry breaking.
The ρ-variable is discretized on a grid with sites ρ_i and the derivatives of the couplings are replaced by finite differences at the respective grid sites. This couples the ordinary differential equations at each grid sites only locally with the equations at neighboring grid sites and transforms the system of partial differential equations in a much larger system of ordinary differential equations.
Due to the strong nonlinearities in the considered set of flow equations a direct replacement of the derivatives by finite differences faces instabilities since errors from the difference scheme propagate nonlinear. Similar to previously proposed methods [129], the chosen way to circumvent this is to discretize and evolve not only the couplings C_i but also there ρ-derivatives as far as they enter the equations. In this case finite differences only appear linearly in the equation for the highest ρ-derivative and stable error propagation is ensured.
This scheme faces the question of boundary conditions for the equations Eq. (D.1) at the borders $\rho = 0$ and $\rho = \rho_{max}$ of the grid , which are mathematically required for a problem of the given kind. At the right boundary, one can exploit the specific form of the flow equations, which guarantees that the couplings do not change with k at asymptotically large ρ. At the left boundary, however, there is no real boundary condition since ρ is a radial variable and so $\rho = 0$ is actually not a boundary point. There is merely a regularity condition, which yields

[3]For the considered flow equations, the convergence radius - which is approximately defined by the value where the contribution from the highest monomial exceeds the others - goes like $\Delta\rho(k) \sim k^2 \log(k)$ in the limit $k \to 0$.

the following set of conditions

$$\lim_{\rho\to\infty} \frac{\partial C_i(k,\rho)}{\partial k} = 0\,, \tag{D.5}$$

$$\lim_{\rho\to 0} \rho\, C_i(k,\rho) = 0\,. \tag{D.6}$$

Although mathematically correct, these conditions do not lend themselves very well to numerical computations due to their limiting nature[4]. Instead it has proven to be a good approximation [129, 39] to adopt "free" boundary conditions and use asymmetric differences at the boundary points which only rely on points in the interior. Nevertheless Eq. (D.5) suggests that the right boundary should be chosen rather large $\rho_{max} >> \rho_0$ in order to minimize numerical errors produced at the boundary.

D.3 NUMERICAL IMPLEMENTATION

All numerical computations in this work have been done within the Mathematica [64] environment. They have been performed on grids with 50 to 100 sites and finite differences computed from 3 to 7 sites. The grid has been chosen nonuniform in order to cover the physically interesting region in an optimal way and nonetheless to be sufficiently far away from the right boundary of the grid. Furthermore, the method discussed above, by integrating the flow for the derivatives of the couplings has been implemented and improves the numerical accuracy considerably.
In the first order region at large chemical potential the demands on the numerical accuracy are particularly high, since the Fermi edge involves discontinuities during the flow. These discontinuities affect different grid ranges during the evolution. In particular, the above discussed "derivative method" is not directly applicable in this case since the discontinuities are especially pronounced in the derivatives.
The developed computer code has been designed in a fully scalable manner in order to control all relevant approximation parameters and to be able to extend the system of equations and solve renormalization group flow equations for other systems in this environment. This would especially enable to computed the evolution for the full set of flow equations in next to leading order in the derivative expansion at finite temperature and density within this program. As soon as the numerics is sufficiently enhanced this could allow to explore also the interesting first order region in this scheme.

[4]In case of Eq. (D.6) it does not help to pose the whole flow for the variables $C_i'(k,\rho) = \rho\, C_i(k,\rho)$ since this introduces new instabilities in the equations.

Bibliography

[1] K. Rajagopal and F. Wilczek, arXiv:hep-ph/0011333.

[2] S. Weinberg, "The Quantum Theory of Fields I & II", Cambridge University Press (1995).

[3] H. Fritzsch, M. Gell-Mann and H. Leutwyler, Phys. Lett. B **47** (1973) 365.

[4] J. Zinn-Justin, arXiv:hep-th/0201220.

[5] C. Vafa and E. Witten, Nucl. Phys. B **234** (1984) 173.

[6] D. Diakonov and . V. Polyakov, Nucl. Phys. B **389** (1993) 109.

[7] J. Gasser and H. Leutwyler, Annals Phys. **158** (1984) 142. J. Gasser and H. Leutwyler, Nucl. Phys. B **250** (1985) 465.

[8] S. Scherer, arXiv:hep-ph/0210398.

[9] J. I. Kapusta, "Finite temperature field theory", Cambridge University Press (1989).

[10] U. J. Wiese, Lecture presented at the Graduiertenkolleg at Heidelberg University.

[11] M. C. Chu, J. M. Grandy, S. Huang and J. W. Negele, Phys. Rev. D **48** (1993) 3340 [arXiv:hep-lat/9306002].

[12] G. Boyd, J. Engels, F. Karsch, E. Laermann, C. Legeland, M. Lutgemeier and B. Petersson, Nucl. Phys. B **469** (1996) 419 [arXiv:hep-lat/9602007].

[13] F. Karsch, E. Laermann and A. Peikert, Phys. Lett. B **478** (2000) 447 [arXiv:hep-lat/0002003].

[14] F. Karsch, E. Laermann and A. Peikert, Nucl. Phys. B **605** (2001) 579 [arXiv:hep-lat/0012023].

[15] J. Zinn-Justin, "Quantum field theory and critical phenomena", Oxford 1989.

[16] L. H. Chan, Phys. Rev. Lett. **54** (1985) 1222.

[17] I. J. Aitchison and C. M. Fraser, Phys. Rev. D **31** (1985) 2605.

[18] J. A. Zuk, Phys. Rev. D **32** (1985) 2653; J. A. Zuk, Phys. Rev. D **33** (1986) 3645.

[19] K. G. Wilson, Phys. Rev. D **3** (1971) 1818; K. G. Wilson, Phys. Rev. B **4** (1971) 3174; K. G. Wilson, Phys. Rev. B **4** (1971) 3184; K. G. Wilson and J. B. Kogut, Phys. Rept. **12** (1974) 75.

[20] F. J. Wegner and A. Houghton, Phys. Rev. A **8** (1973) 401.

[21] C. Wetterich, Phys. Lett. B **301** (1993) 90.

[22] J. Berges, N. Tetradis and C. Wetterich, Phys. Rept. **363** (2002) 223 [arXiv:hep-ph/0005122].

[23] D. U. Jungnickel and C. Wetterich, Phys. Rev. D **53** (1996) 5142 [arXiv:hep-ph/9505267].

[24] D. U. Jungnickel and C. Wetterich, Eur. Phys. J. C **1** (1998) 669 [arXiv:hep-ph/9606483].

[25] D. U. Jungnickel and C. Wetterich, Phys. Lett. B **389** (1996) 600 [arXiv:hep-ph/9607411].

[26] D. U. Jungnickel and C. Wetterich, Eur. Phys. J. C **2** (1998) 557 [arXiv:hep-ph/9704345].

[27] J. Berges, D. U. Jungnickel and C. Wetterich, Phys. Rev. D **59** (1999) 034010 [arXiv:hep-ph/9705474].

[28] J. Berges, D. U. Jungnickel and C. Wetterich, Eur. Phys. J. C **13** (2000) 323 [arXiv:hep-ph/9811347].

[29] J. Berges, D. U. Jungnickel and C. Wetterich, arXiv:hep-ph/9811387.

[30] D. F. Litim and J. M. Pawlowski, Phys. Rev. D **65** (2002) 081701 [arXiv:hep-th/0111191].

[31] D. F. Litim and J. M. Pawlowski, Phys. Lett. B **516** (2001) 197 [arXiv:hep-th/0107020].

[32] D. F. Litim and J. M. Pawlowski, Phys. Rev. D **66** (2002) 025030 [arXiv:hep-th/0202188].

[33] J. S. Schwinger, Phys. Rev. **82** (1951) 664.

[34] M. Oleszczuk, Z. Phys. C **64** (1994) 533.

[35] S. B. Liao, Phys. Rev. D **53** (1996) 2020 [arXiv:hep-th/9501124].

[36] B. J. Schaefer and H. J. Pirner, Nucl. Phys. A **627** (1997) 481 [arXiv:hep-ph/9706258].

[37] B. J. Schaefer and H. J. Pirner, Nucl. Phys. A **660** (1999) 439 [arXiv:nucl-th/9903003].

[38] J. Meyer, G. Papp, H. J. Pirner and T. Kunihiro, Phys. Rev. C **61** (2000) 035202 [arXiv:nucl-th/9908019].

[39] O. Bohr, B. J. Schaefer and J. Wambach, Int. J. Mod. Phys. A **16** (2001) 3823 [arXiv:hep-ph/0007098].

[40] M. E. Peskin and D. V. Schroeder, "Introduction to Quantum Field Theory", Addison Wesley (1995).

[41] J. Polchinski, arXiv:hep-th/9210046.

[42] J. Polchinski, Nucl. Phys. B **231** (1984) 269.

[43] S. Arnone, A. Gatti and T. R. Morris, Phys. Rev. D **67** (2003) 085003 [arXiv:hep-th/0209162].

[44] H. Gies, Phys. Rev. D **66** (2002) 025006 [arXiv:hep-th/0202207]. H. Gies and C. Wetterich, arXiv:hep-th/0209183.

[45] E. Meggiolaro and C. Wetterich, Nucl. Phys. B **606** (2001) 337, hep-ph/0012081.

[46] T. Schafer and E. V. Shuryak, Rev. Mod. Phys. **70** (1998) 323 [arXiv:hep-ph/9610451].

[47] H. Forkel, arXiv:hep-ph/0009136.

[48] S. Weinberg, Phys. Rev. Lett. **19** (1967) 1264.

[49] Y. Nambu and G. Jona-Lasinio, Phys. Rev. **122** (1961) 345; Y. Nambu and G. Jona-Lasinio, Phys. Rev. **124** (1961) 246.

[50] S. P. Klevansky, Rev. Mod. Phys. **64** (1992) 649.

[51] T. Hatsuda and T. Kunihiro, Phys. Rept. **247** (1994) 221 [arXiv:hep-ph/9401310].

[52] J. Jaeckel and C. Wetterich, arXiv:hep-ph/0207094.

[53] V. Branchina, Phys. Lett. B **549** (2002) 260 [arXiv:hep-ph/0101157].

[54] G. Ripka, "Quarks bound by chiral fields", Oxford University Press (1997).

[55] H. Gies and C. Wetterich, Phys. Rev. D **65** (2002) 065001 [arXiv:hep-th/0107221].

[56] M. Gell-Mann and M. Levy, Nuovo Cim. **16** (1960) 705.

[57] B. W. Lee, Nucl. Phys. B **9** (1969) 649. J. L. Gervais and B. W. Lee, Nucl. Phys. B **12** (1969) 627.

[58] K. Hagiwara *et al.* [Particle Data Group Collaboration], Phys. Rev. D **66** (2002) 010001.

[59] T. Kunihiro, S. Muroya, A. Nakamura, C. Nonaka, M. Sekiguchi and H. Wada [SCALAR Collaboration], arXiv:hep-lat/0210012.

[60] A. Bonanno and D. Zappala, Phys. Rev. D **57** (1998) 7383 [arXiv:hep-th/9712038].

[61] G. 't Hooft, Nucl. Phys. B **72** (1974) 461.

[62] E. Witten, HUTP-79/A078.

[63] G. Papp, B. J. Schaefer, H. J. Pirner and J. Wambach, Phys. Rev. D **61** (2000) 096002 [arXiv:hep-ph/9909246].

[64] S. Wolfram, "Mathematica, 5th Edition", Wolfram Media (2003).

[65] T. Spitzenberg, K. Schwenzer and H. J. Pirner, Phys. Rev. D **65** (2002) 074017 [arXiv:hep-ph/0201095].

[66] P. M. Fishbane, R. E. Norton and T. N. Truong, Phys. Rev. D **46** (1992) 1768.

[67] J. Gasser and H. Leutwyler, Phys. Rept. **87** (1982) 77.

[68] V. Dmitrasinovic, H. J. Schulze, R. Tegen and R. H. Lemmer, Annals Phys. **238** (1995) 332.

[69] M. Oertel, M. Buballa and J. Wambach, Phys. Lett. B **477** (2000) 77 [arXiv:hep-ph/9908475]; M. Oertel, M. Buballa and J. Wambach, Nucl. Phys. A **676** (2000) 247 [arXiv:hep-ph/0001239].

[70] J. Meyer, PhD Thesis (in German), University Heidelberg (2001).

[71] L. Giusti, F. Rapuano, M. Talevi and A. Vladikas, Nucl. Phys. B **538** (1999) 249 [arXiv:hep-lat/9807014].

[72] J. D. Walecka, "Theoretical Nuclear and Subnuclear Physics", Oxford University Press (1995).

[73] T. Banks and A. Casher, Nucl. Phys. B **169**, 103 (1980).

[74] A. V. Smilga and J. Stern, Phys. Lett. B **318**, 531 (1993).

[75] J. J. Verbaarschot and T. Wettig, Ann. Rev. Nucl. Part. Sci. **50**, 343 (2000), hep-ph/0003017.

[76] M. E. Berbenni-Bitsch, S. Meyer, A. Schafer, J. J. Verbaarschot and T. Wettig, Phys. Rev. Lett. **80**, 1146 (1998) hep-lat/9704018.

[77] P. H. Damgaard, hep-lat/0110192.

[78] J. C. Osborn, D. Toublan and J. J. Verbaarschot, Nucl. Phys. B **540**, 317 (1999) hep-th/9806110.

[79] M. A. Stephanov, Nucl. Phys. Proc. Suppl. **53**, 469 (1997) hep-lat/9607060.

[80] K. B. Efetov, Phys. Rev. B **56** (1997) 9630.

[81] P. H. Damgaard, Nucl. Phys. B **608** (2001) 162, hep-lat/0105010.

[82] C.-Y. Wong, "Introduction to High-Energy Heavy-Ion Collisions", World Scientific (1994)

[83] P. F. Kolb and U. Heinz, arXiv:nucl-th/0305084.

[84] P. Braun-Munzinger, J. Stachel, J. P. Wessels and N. Xu, Phys. Lett. B **344** (1995) 43 [arXiv:nucl-th/9410026]; P. Braun-Munzinger, J. Stachel, J. P. Wessels and N. Xu, Phys. Lett. B **365** (1996) 1 [arXiv:nucl-th/9508020]. P. Braun-Munzinger, I. Heppe and J. Stachel, Phys. Lett. B **465** (1999) 15 [arXiv:nucl-th/9903010]; P. Braun-Munzinger, D. Magestro, K. Redlich and J. Stachel, Phys. Lett. B **518** (2001) 41 [arXiv:hep-ph/0105229]; P. Braun-Munzinger, K. Redlich and J. Stachel, arXiv:nucl-th/0304013.

[85] L. G. Yaffe and B. Svetitsky, Phys. Rev. D **26** (1982) 963. B. Svetitsky and L. G. Yaffe, Nucl. Phys. B **210** (1982) 423.

[86] J. B. Kogut, M. Stone, H. W. Wyld, W. R. Gibbs, J. Shigemitsu, S. H. Shenker and D. K. Sinclair, Phys. Rev. Lett. **50** (1983) 393.

[87] R. D. Pisarski and F. Wilczek, Phys. Rev. D **29** (1984) 338.

[88] C. R. Allton *et al.*, Phys. Rev. D **66** (2002) 074507 [arXiv:hep-lat/0204010].

[89] Z. Fodor and S. D. Katz, Phys. Lett. B **534** (2002) 87 [arXiv:hep-lat/0104001].

[90] S. Chandrasekharan and U. J. Wiese, Phys. Rev. Lett. **83** (1999) 3116 [arXiv:cond-mat/9902128].

[91] A. Rebhan, arXiv:hep-ph/0111341.

[92] J. Berges and K. Rajagopal, Nucl. Phys. B **538** (1999) 215 [arXiv:hep-ph/9804233].

[93] D. Bailin and A. Love, Phys. Rept. **107** (1984) 325.

[94] M. G. Alford, K. Rajagopal and F. Wilczek, Phys. Lett. B **422** (1998) 247 [arXiv:hep-ph/9711395].

[95] R. Rapp, T. Schafer, E. V. Shuryak and M. Velkovsky, Phys. Rev. Lett. **81** (1998) 53 [arXiv:hep-ph/9711396].

[96] M. G. Alford, K. Rajagopal and F. Wilczek, Nucl. Phys. B **537** (1999) 443 [arXiv:hep-ph/9804403].

[97] M. A. Halasz, A. D. Jackson, R. E. Shrock, M. A. Stephanov and J. J. Verbaarschot, Phys. Rev. D **58** (1998) 096007 [arXiv:hep-ph/9804290].

[98] T. M. Schwarz, S. P. Klevansky and G. Papp, Phys. Rev. C **60** (1999) 055205 [arXiv:nucl-th/9903048].

[99] M. A. Stephanov, K. Rajagopal and E. V. Shuryak, Phys. Rev. Lett. **81** (1998) 4816 [arXiv:hep-ph/9806219].

[100] Z. Fodor and S. D. Katz, JHEP **0203** (2002) 014 [arXiv:hep-lat/0106002].

[101] F. Karsch, E. Laermann and C. Schmidt, Phys. Lett. B **520** (2001) 41 [arXiv:hep-lat/0107020].

[102] I. S. Gradstein and I. M. Ryshik, "Tables of Integrals, Series and Products", Academic Press (1994)

[103] K. Schwenzer, Diploma thesis (in German), University Heidelberg (2000).

[104] M. Asakawa and K. Yazaki, Nucl. Phys. A **504** (1989) 668.

[105] Z. Fodor, S. D. Katz and K. K. Szabo, arXiv:hep-lat/0208078.

[106] Z. Fodor, Nucl. Phys. A **715** (2003) 319 [arXiv:hep-lat/0209101].

[107] C. R. Allton, S. Ejiri, S. J. Hands, O. Kaczmarek, F. Karsch, E. Laermann and C. Schmidt, arXiv:hep-lat/0305007.

[108] J. Alexandre, V. Branchina and J. Polonyi, Phys. Lett. B **445** (1999) 351 [arXiv:cond-mat/9803007].

[109] D. J. Gross and F. Wilczek, Phys. Rev. Lett. **30** (1973) 1343.

[110] H. G. Dosch, T. Gousset and H. J. Pirner, Phys. Rev. D **57**(1998) 1666 [arXiv:hep-ph/9707264].

[111] V.A. Novikov, M.A. Shifman, A.I. Vainsthein, and V.I. Zakharov, Nucl. Phys. B **191** (1981) 301.

[112] E. V. Shuryak, Rev. Mod. Phys. **65**(1993) 1.

[113] M. Shifman, hep-ph/0009131, in M. Shifman (ed.): *At the frontier of particle physics/ Handbook of QCD*, vol. 3, p. 1447-1494 (World Scientific, Singapore, 2001).

[114] M.A. Shifman, A.I. Vainsthein, and V.I. Zakharov, Nucl. Phys. B **147** (1979) 385.

[115] S. J. Hands, P. W. Stephenson and A. McKerrell [UKQCD Collaboration], Phys. Rev. D **51**(1995) 6394 [arXiv:hep-lat/9412065].

[116] M. C. Chu, J. M. Grandy, S. Huang and J. W. Negele, Phys. Rev. D **49** (1994) 6039 [arXiv:hep-lat/9312071].

[117] T. DeGrand, Phys. Rev. D **64** (2001) 094508 [arXiv:hep-lat/0106001].

[118] E. V. Shuryak and J. J. Verbaarschot, Nucl. Phys. B **410**(1993) 55 [arXiv:hep-ph/9302239].

[119] S. Coleman, *Aspects of Symmetry*, Cambridge University Press 1988.

[120] H. Lamecker, Diploma thesis, University Heidelberg (2000).

[121] A. Bonanno and D. Zappala, Nucl. Phys. A **681** (2001) 108 [arXiv:hep-ph/0006169].

[122] N. Tetradis and C. Wetterich, Nucl. Phys. B **422** (1994) 541 [arXiv:hep-ph/9308214].

[123] D. Ebert, Y. L. Kalinovsky, L. Munchow and M. K. Volkov, Int. J. Mod. Phys. A **8**, 1295 (1993).

[124] G. E. Brown and M. Rho, Phys. Rev. Lett. **66** (1991) 2720.

[125] J. Braun, K. Schwenzer and H.-J. Pirner, in preparation

[126] W. A. Bardeen, C. T. Hill and M. Lindner, Phys. Rev. D **41** (1990) 1647.

[127] M. Mazza and D. Zappala, Phys. Rev. D **64** (2001) 105013 [arXiv:hep-th/0106230].

[128] J. Meyer, K. Schwenzer, H. J. Pirner and A. Deandrea, Phys. Lett. B **526** (2002) 79 [arXiv:hep-ph/0110279].

[129] J. Adams, J. Berges, S. Bornholdt, F. Freire, N. Tetradis and C. Wetterich, Mod. Phys. Lett. A **10** (1995) 2367 [arXiv:hep-th/9507093].

Thanks!

I am very grateful to Hans-Jürgen Pirner for his continuous support during the long time we worked together. I enjoyed the numerous interesting discussions, his direct approach to physical problems and the friendly atmosphere in his group.

Many thanks to Jürgen Berges for his attendance to referee my thesis. The discussions with him and his advice concerning my future plans have been extremely helpful.

Thomas Spitzenberg earns a special thank because he proofread most of this thesis and helped me a lot by many insightful discussions. I also appreciated very much to share an office with him during his stay in Heidelberg. The same holds for my current "roommates" Jens Braun and Lars Jendges.

I would like to thank Hilmar Forkel, Jochen Meyer and Thomas Spitzenberg for fruitful collaboration. Furthermore, I appreciated very much the helpful discussions with Alberto Accardi, Holger Gies, Jörg Jäckel, Boris Kerbikov, Daniel Litim, Stephane Munier, Christian Nowak, Gabor Papp, Bernd-Jochen Schäfer and Arif Shoshi.

I would like to express my gratitude to Jörg Hüfner and Christoph Wetterich for their letters of recommendation and Jörg Hüfner also for the nice tradition of Friday's tea time.

Thanks to Yuri Ivanov for the excellent management of the computer system and to the secretariat for their great cooperativeness. I am also grateful to Sonja Bartsch and Kai Müller for reading part of this thesis.

I am indebted to the Graduiertenkolleg for the rewarding seminars, lectures and workshops and to the Landesgraduiertenförderung Baden Württemberg for their financial support.

Finally I want to thank the people at the Institute for Theoretical Physics that made this beautiful building also to a nice place.

And last but not least I want to thank my family for their support over all these years - I hope I will have the possibility to spend more time with you than I could in the last months.